Biophysical Studies of Processes Involved in Acanthamoeba Infections: Contact Lens Contamination, Adhesion, and Intracellular Dynamics

Dissertation

zur Erlangung des akademischen Grades Doktor der Ingenieurswissenschaften
(Dr. Ing.)
der Technischen Fakultät
der Christian-Albrechts-Universität zu Kiel

vorgelegt von
Julia Franziska Reverey

Kiel 2014

Dissertation vorgelegt am: 17.02.2014
Termin der Disputation: 21.03.2014
Druckreife erteilt: 07.04.2014

Erstgutachterin: Prof. Dr. Christine Selhuber-Unkel

Zweitgutachter: Prof. Dr. Eckhard Quandt

"Wenn man nicht versucht, etwas zu tun, was jenseits des bereits Gemeisterten liegt, dann wird man nicht wachsen."

Ralph Waldo Emerson

Erklärung

Hiermit erkläre ich, dass die beigefügte Dissertation, abgesehen von der Beratung durch die Betreuerin, nach Inhalt und Form meine eigene Arbeit ist.

Die Arbeit, ganz oder zum Teil, wurde nie schon einer anderen Stelle im Rahmen eines Prüfungsverfahrens vorgelegt und ist nie veröffentlicht worden oder zur Veröffentlichung vorgelegt worden.

Außerdem ist die Arbeit unter Einhaltung der Regeln guter wissenschaftlicher Praxis der Deutschen Forschungsgemeinschaft entstanden.

Kiel, den 11.04.2014

Abstract

Acanthamoeba castellanii can cause a severe and painful, acanthamoeba keratitis. In this disease, the acanthamoebae reach the eye via contaminated contact lenses. In the eye, they invade cornea cells and kill them. The first step in this process is the formation of a close contact between the acanthamoeba and the target-cell. This contact is mainly mediated by mannose. Subsequently, cytolytic factors move to the contact site and are released leading to the death of the target-cell. The single steps involved in the infection pathway, namely contact lens contamination, carbohydrate-mediated acanthamoeba adhesion, and intracellular transport were investigated in this thesis.

As the use of contact lenses is a main risk factor in the infection process, in the first part of this thesis different silicone hydrogel and hydrogel materials were investigated for their potential to be contaminated with *A. castellanii*. Furthermore, influences of standard contact lens cleaning procedures on the adhesion and proliferation of *A. castellanii* were evaluated. It was observed that *A. castellanii* preferentially adhered to lenses with high water content (>60 %). Furthermore, while multipurpose and peroxide solution reduced adhesion of acanthamoeba significantly, only the peroxide solution was able to kill all *A. castellanii* effectively.

If contaminated contact lenses are inserted into the eye, acanthamoebae reach the cornea, move through the epithelial tissue of the cornea and kill target-cells in the underlying cell layers. Thus, in the second part of this thesis interactions of acanthamoebae with proteins in the extracellular matrix, as well as the carbohydrate-mediated adhesion to target-cells were investigated. In order to mimic the extracellular matrix, glass slides were coated with proteins and the number of adhering acanthamoebae was evaluated. Compared to the glass, increased adhesion was observed on matrigel followed by fibronectin. This increase in number of adhering acanthamoeba was presumably mediated by mannose present in the protein coatings. In order to investigate the initial adhesion of acanthamoebae to target-cells, quasi-hexagonally arranged patterns of gold nanodots with different interparticle distances were produced by diblock copolymer micelle nanolithography and functionalized with mannose or glucose, respectively. By passivating the areas between the dots with polyethylene glycol (PEG), unspecific adhesion of the acanthamoebae in the inter-particle space was reduced and therefore only the biofunctionalized gold dots served as anchoring points for the adhesion. The evaluation of the number and the spreading area of *A. castellanii* showed that already relatively low densities of mannose lead to stable adhesion of the acanthamoebae and that mannose as single ligand is sufficient for adhesion. In order to quantify forces of the binding of *A. castellanii* to carbohydrate-functionalized surfaces, force spectroscopic measurements were carried out by atomic force microscopy (AFM). The measurements showed that with increasing contact time of acantameobae to mannose coated AFM cantilevers the maximum adhesion force and the adhesion energy increase.

After initial adhesion of acanthamoeba to the target-cell, cytolytic factors, move to the contact site, are released and lead to target-cell death. Thus intracellular transport of vesicles was investigated in the last part of this thesis. In order to examine the

intracellular dynamics, the transport processes of particles inside acanthamoebae were evaluated and compared after addition of filament depolymerizing substances and molecular-motor inhibiting substances. The intracellular space in *A. castellanii* is extremely crowded, and most particles were moving actively. This was also the case after the different treatments, which inhibited the motion of the whole amoebae, but not of the intracellular particles.

Zusammenfassung

Acanthamoeba castellanii können eine schmerzhafte, das Sehvermögen beeinträchtigende Acanthamöbenkeratitis verursachen. Dabei gelangen die Acanthamöben häufig über kontaminierte Kontaktlinsen oder Kontaktlinsenbehälter in das Auge. Dort dringen sie in die Hornhaut ein und töten Zielzellen ab. Dieser Mechanismus wird über die Ausbildung eines engen Kontakts zur Zielzelle initiiert. Die Kontaktbildung selbst wird hauptsächlich durch das Kohlenhydrat Mannose vermittelt. Nach Kontaktbildung bewegen sich zytolytische Faktoren in der Amöbe zur Kontaktstelle und werden dort freigegeben. Dies führt zum Tod der Zielzelle. In dieser Arbeit wurden drei relevante Phasen der Infektion untersucht: Kontamination von Kontaktlinsen mit Amöben, Kohlenhydrat-basierte Kontaktbildung zwischen Acanthamöbe und Zielzelle, sowie intrazellulärer Transport.

Da Kontaktlinsen einen Hauptrisikofaktor in der Infektion darstellen, wurden im ersten Teil dieser Arbeit verschiedene Kontaktlinsenmaterialien (Siliconhydrogele sowie Hydrogele) auf ihr Kontaminationspotential untersucht. Zudem wurde der Einfluss von gängigen Reinigungsmethoden auf die Anhaftung und das Überleben der Acanthamöbe geprüft. Es zeigte sich, dass *A. castellanii* bevorzugt an Kontaktlinsen mit hohem Wassergehalt haften (> 60 %). Sowohl Pflegelösung als auch Peroxidlösung reduzierten die Adhäsion der Acanthamöben, wobei jedoch nur die Peroxidlösung die Zellen vollständig abtötete.

Werden kontaminierte Kontaktlinsen ins Auge eingesetzt, erreichen die Amöben die Hornhaut, durchdringen das Epithelgewebe und töten Zellen in den darunterliegenden Zellschichten ab. Daher wurden im zweiten Teil Wechselwirkungen zwischen Acanthamöben und extrazellulärer Matrix, sowie die durch Kohlenhydrate vermittelte Anhaftung von Acanthamöben an Zielzellen untersucht. Um die extrazelluläre Matrix zu imitieren, wurden Deckgläser mit Proteinen beschichtet und die Anzahl anhaftender Acanthamöben bestimmt. Der Vergleich zur unbeschichteten Kontrolle ergab eine erhöhte Adhäsion von Acanthamöben auf Matrigel gefolgt von Fibronektin. Zur Untersuchung der initialen Anhaftung von Acanthamöben an Zielzellen, wurden Substrate mit quasi-hexagonal angeordneten Goldnanopunkten mit unterschiedlichen Abständen hergestellt und mit Mannose bzw. Glucose funktionalisiert. Unspezifische Anhaftung der Acanthamöben zwischen Goldpunkten wurde durch Passivierung dieser Bereiche mit Polyethylenglykol (PEG) verhindert, sodass ausschließlich funktionalisierte Goldpunkte als Haftstellen für Acanthamöben dienten. Die Analyse von Zellzahl und Zellfläche ergaben, dass bereits geringe Dichten des Kohlehydrats Mannose zu stabiler Adhäsion der Acanthamöben führten, wobei Mannose als einzelner Ligand ausreichte. Das kurzzeitige Anhaftungsverhalten an Kohlenhydrat-beschichtete Oberflächen sowie die Adhäsionskraft von Acanthamöben wurden erstmals mittels kraftspektroskopischer Untersuchungen am Rasterkraftmikroskop (AFM) quantifiziert. Die Messungen ergaben eine deutliche Zunahme von maximaler Adhäsionskraft und Adhäsionsenergie mit ansteigender Kontaktzeit zwischen Acanthamöbe und Mannose-beschichteter Oberfläche.

Das initiale Anhaften der Acanthamöbe an die Zielzelle bewirkt eine Migration von in Vesikeln eingeschlossenen zytolytischen Faktoren zur Kontaktstelle. Daher wurde im letzten Teil dieser Arbeit der intrazelluläre Transport von Vesikeln näher untersucht.

Dazu wurden Vesikeltrajektorien analysiert und einzelne zelluläre Transportstrukturen gezielt mittels Zugabe von Filament-depolymerisierenden Substanzen sowie Substanzen zur Inaktivierung molekularer Motoren gestört. Es wurden überwiegend aktive Bewegungen von intrazellulären Vesikeln beobachtet. Die verschiedenen Substanzen stoppten zwar nahezu die Bewegung der gesamten Zellen, inhibierten jedoch nicht den Transport der Vesikel in der Acanthamöbe.

Contents

1. Introduction

The genus *Acanthamoeba spp*. are free-living acanthamoebae existing in a variety of air, water and natural environments [1]. Pathogenic acanthamoebae like *Acanthamoeba castellanii* (*A. castellanii*) can cause severe diseases such as granulomatous amoebic encephalitis and acanthamoeba keratitis. Especially contact lens users are at risk to contract acanthamoeba keratitis, when coming into contact with acanthamoebae via contaminated solutions and contact lens storage cases [2]. But also non-contact lens users can be infected with acanthamoeba keratitis (~10 %) [3]. In this case the infection is related to an injury of the corneal epithelium. Due to their ubiquitous nature humans come into contact with acanthamoebae during their everyday life, for example during swimming in lakes or even when washing hands with tap water [4]. Acanthamoebae reach the eye either via contaminated water or contact lenses and start to kill target-cells in a contact dependent process. Their adhesion to the target-cells is mediated by a mannose binding protein (MBP) [5-7], which causes the pathogenic potential of different species of acanthamoebae, such as *A. castellanii* [8]. After adhesion to corneal epithelial cells, acanthamoebae penetrate the cornea e.g. via injuries of the epithelial barrier. Such injuries increase the risk of an infection also for non-contact users [9]. This may be connected to a higher mannose content in this area [10]. After penetrating the cornea acanthamoebae invade the underlying cell layers leading to an inflammatory response [3, 11-12]. Symptoms of acanthamoeba keratitis are photophobia, redness, tearing, and corneal opacity [13-14]. Acanthamoeba keratitis can lead to blindness and due to invasion of the corneal nerves causes severe pain to the patient [14]. The pathogenic potential of acanthamoebae can even increase as they can be hosts for endosymbionts (potential human pathogenic viruses, bacteria or yeast such as *Legionella pneumophila*), which leads to an increased risk of other infections e.g. legionnaires' disease or lung inflammation [13, 15-16]. This chapter provides the biological background of acanthamoeba and closes the loop between acanthamoeba infections and materials science. First, the organisation of acanthamoeba is described starting with biological basics of proteins and single cells. Next, cell dynamics, acanthamoeba-cell interactions, and the target-cell killing process are introduced.

1.1. Biological Background of Acanthamoeba

1.1.1. Proteins

The basic building stone of all living systems are proteins, i.e. large hydrophobic molecule chains, which consist of many amino acids ordered in a defined way. Typically they consist of 50 to 200 amino acids [17], which are connected by a peptide bond.

All amino acids are essentially based on one polypeptide backbone, -NH-(CHR)-CO-, where R denotes the unique side chain that determines the type and properties of the respective amino acid. There are 20 proteinogenic amino acids, out of which naturally occurring proteins are composed. The order and number of the amino acids lead to certain protein structures of the protein. The amino acid chains fold in an energetically efficient manner. The structure of a protein can be classified into the primary structure, i.e. the amino acid sequence, the secondary structure, which determines the folding of the peptide chain into alpha helix and beta sheets, and the ternary structure, the stable three dimensional organization of the protein. Mainly weak bonds like van der Waals forces, hydrogen bonds and electrostatic interactions cause the folding of the protein. Although these bonds are relatively weak compared to a covalent bond, the linkage between two parts of the peptide chain can be very strong, as there are many weak bonds adding up to a strong binding [17].

Very large proteins consist of protein domains that may have different tasks [17]. The functions and properties of a protein are determined by its shape and by interactions with other molecules. Typical functions of proteins include signaling, immune defense, enzymatic functions, or transport within the cell. So called transmembrane proteins connect the cell to the extracellular matrix, and transmit environmental changes to the cell. For specific cell adhesion so called receptor-ligand bonds are very important.

The bond between the receptor protein and the ligand is commonly very specific, and based on molecular recognition [18]. In Figure 1-1, a schematic view of a typical receptor-ligand bond is shown. In case of cell adhesion, the cellular membrane contains proteins, acting as receptors for certain molecules (ligands), to which the cell can specifically bind. The forces of the single non-covalent bonds, which are involved in the binding, are much weaker than the overall binding constant. One of the strongest known receptor-ligand bonds is the biotin-streptavidin bond with a binding constant of 88 kJ / mol [19]. Overall receptor-ligand bonds are relatively weak bonds, which are very important for cells as they allow highly dynamic and adaptive binding of the cell. In case of acanthamoebae this is very important as acanthamoebae are highly flexible and mobile cells, which act like an intelligent, adaptive material. During their movement they react flexibly and quickly on different surface properties.

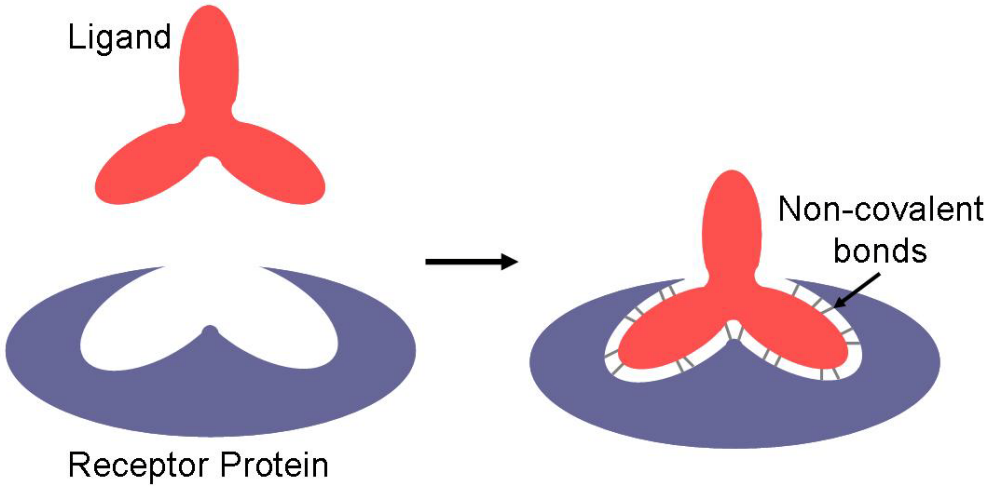

Figure 1-1 Receptor-ligand bond. The ligand structurally fits into the binding pocket of the receptor. The receptor and the ligand bind to each other by non-covalent bonds such as van-der-Waals or hydrogen bonds. Compared to the single non-convalent bonds involved in the receptor-ligand binding, the overall binding force is drastically increased due to the large number of bonds. Nevertheless, the receptor-ligand binding is not very strong, but very important for cell mobility and adaptive adhesion as the bonds are highly dynamic.

1.1.2. Acanthamoeba as Eukaryotic Protozoa

Cells can be divided into three domains Bacteria, Archaea and Eukaryotes. Bacteria and archaea are prokaryotes, which neither have a nucleus nor a cytoskeleton [17, 20]. All multicellular organisms, such as animals, plants and fungi consist of eukaryotic cells, which contain a nucleus. On the other hand, there are also free-living unicellular organisms (protozoa) such as acanthamoeba, which are also eukaryotes but cannot be classified into one of the eukaryotic groups mentioned above [14]. The endosymbiotic theory states that eukaryotes originated by symbioses of free-living bacteria that now constitute cellular organelles including the characteristic membrane enclosed nucleus, where all genetic information of the cell is stored. The outer border of the eukaryote is a plasma membrane that consists of a lipid double layer mainly comprised of phospholipids. Lipid molecules are amphiphils having one polar, hydrophilic end and one non-polar, hydrophobic end. The hydrophilic head groups are located outside and inside the cell; the hydrophobic tails are in between (Figure 1-2 up right). Besides phospholipids, a multitude of different proteins with various functions (e.g. receptors, transport proteins, enzymes, and cell adhesion proteins) are attached to or embedded in the plasma membrane [17]. In Figure 1-2 a schematic acanthamoeba is depicted.

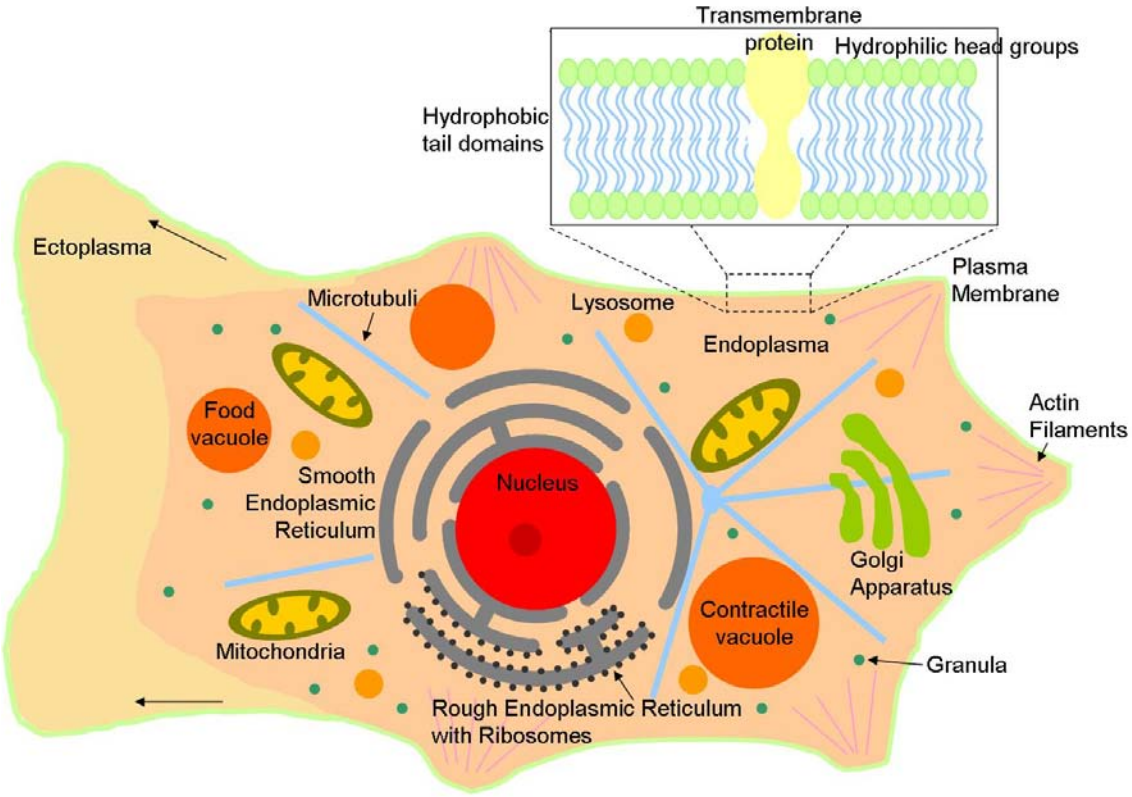

Figure 1-2 Schematic view of an eukaryotic cell (acanthamoeba) and the plasma membrane. The different organelles of the cell have distinct tasks in the metabolism. In the nucleus the genetic information is stored. Mitochondria are cellular power plants, which generate most of the needed energy. The endoplasmic reticulum produces lipids, phospholipids and steroids, serves as Ca^{2+} storage and is responsible for folding of proteins. The products of the endoplasmic reticulum are transported to the golgi, where they are modified, packed into vesicles and transported to other organelles.

Apart from the nucleus eukaryotic cells as acanthamoeba contain a number of organelles, which are surrounded by a membrane, e.g. the endoplasmic reticulum , the golgi apparatus, and mitochondria. They have different metabolic functions. The endoplasmic reticulum has various functions in the production of lipids and steroids. Together with ribosomes, which translate the genetic code into proteins. Recently synthesized proteins are directly transported into the endoplasmic reticulum for folding, "quality control" and first steps of processing. The products from the endoplasmic reticulum are then transported to the golgi apparatus. Here lipids and proteins are further modified with mainly carbohydrates. The golgi also functions as the cellular post office. Lipids and proteins are depending on their destination packed into vesicles and lysosomes and transported to the target structure. [17]. For the osmotic regulation acanthamoebae have a contractile vacuole, by which excess water can be stored, released into the cell by contraction or transported to the cell membrane and released outside of the acanthamoebae. Moreover a number of food vacuoles, in which food particles are digested, and lipid and protein containing granules are present in acanthamoebae.

The cytoskeleton of acanthamoebae consists of different protein filaments and determines shape and mobility of the cell. It consists of microtubules, actin and intermediate filaments, to form a flexible three dimensional network within the cell, which allows continuous remodeling of the cell shape.

Acanthamoebae are eukaryotic cells with a rather viscous cell wall, and a very dynamic cytoskeleton. This allows fast movement and quick changes in shape, e.g. to flow around small particles or bacteria, and to form large membrane invaginations to take up food particles or liquid. The leading edge of the acanthamoebae consists of the so called ectoplasma and no cell organelles are present in this area. The aspect of intracellular dynamics will be further described section 1.1.3 and in chapter 5.

1.1.3. Cytoskeleton and Intracellular Dynamics

The cytoskeleton is composed of microtubuli, intermediate, and actin filaments. Microtubuli are protein chains with a diameter of about 25 nm consisting of tubulin monomers. They spread out from the centrosome, which is an organelle located near the cell nucleus and which is also known as microtubule organizing center [17, 21]. Intermediate filaments consist of different intermediate filament proteins and have a diameter of about 10 nm. Actin, however, is present in cells as a free monomer in a globular (G-actin) and as a polymerized, filamentous form (F-actin). G-actin is composed out of 374 amino acids and has a molecular weight of 41 kDa [22]. F-actin is a double stranded helical protein consisting of actin monomers with a diameter between 5 and 9 nm. Actin filaments can be found within the whole cell, but they are concentrated at dynamic structures, by which the cell is moving forward, primarily near the plasma membrane, in focal contacts and in pseudopodia [23-24].

Actin filaments and microtubuli are involved in cell contraction and movement, and serve as transport routes within the cell. Molecular motor proteins walk along these tracks by converting energy into motion by hydrolysis of adenosine triphosphate (ATP) (Figure 1-3).

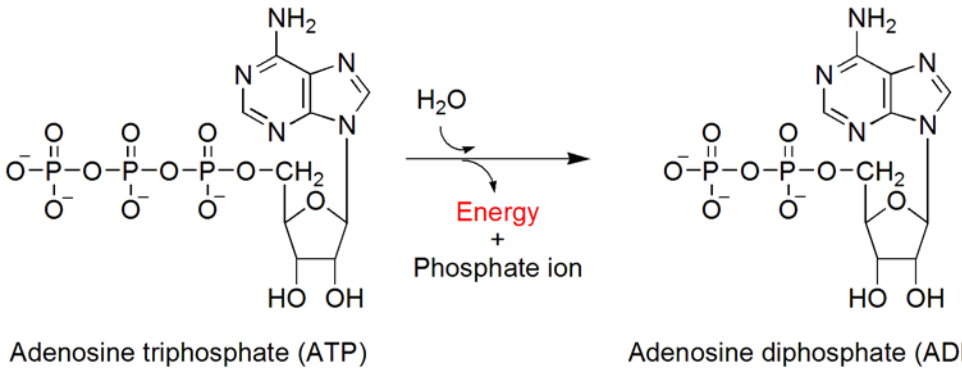

Figure 1-3 ATP Hydrolysis reaction. The hydrolysis of the ATP leads to the release of free energy, which is used for active processes within cells, e.g. transport. The products are adenosine diphosphate and inorganic phosphate.

Typically, molecular motors play a key role in the intracellular transport of materials, which is needed for essential processes as cell adhesion, movement, cell division and phagocytosis [17].
Molecular motors are divided into different families, myosin, kinesin and dynein. The important parts of molecular motors are the cargo binding tail region and the motor head, which binds to the transport routes. The composition of the motor head is essential for the classification of these proteins as it specifically binds either to actin filaments or to microtubuli. Within the families of molecular motors, there are big differences in the conformation of the single motors concerning the structure of the protein [17].
Myosins are molecular motor proteins, which are found on actin filaments, while kinesin and dynein are motors walking along microtubuli. The way the molecular motors move along their routes is very different. While the motion of kinesins is like a walking movement, myosin attaches to the actin filament, exerts forces on the filament, and detaches again [25]. In very dynamic cells such as acanthamoebae, large amounts of actin with corresponding myosin are present. For that reason many studies about myosin were conducted by using actin and myosin isolated from acanthamoeba [26-28].

1.1.4. Extracellular Matrix and Cell Adhesion

Most biological tissues such as the connective tissue are organized in an extracellular matrix (ECM), a three dimensional network consisting of glycoproteins, proteins, and polysaccharides, that are produced and secreted by the cells themselves. Large parts of the body consists of ECM and for that reason every cell, and therefore also pathogenic acanthamoebae, which move through the connective tissue of the host, have to adhere to the ECM components. The ECM can be divided into fibrous parts, amorphous matrix, extracellular liquid, and cross-linking proteins [17]. The fibrous parts mainly consist of collagen and other elastic fibers like elastin and microfibrils. Collagen is produced for example by fibroblasts in the connective tissue and various different types are present nearly in the whole body. The distinct collagens can be very elastic or rather stiff, which leads to different properties of the tissue. For example cartilage and bone are mainly made up of fibrous collagen of either type I or II, while organs as the kidney or the intestine mainly consist of reticular fibrils of collagen III [17]. The amorphous matrix is built up by glycosaminoglycans and proteoglycans, which bind water, carbohydrates, lipids and albumin and interact with other macromolecules. The ECM furthermore contains many growth factors, enzymes, chemokines, and cytokines, whose activity and availability is modulated by proteins in the ECM, which bind to these molecules. Besides this, the proteins in the ECM influence cell adhesion and migration by interaction with cell surface receptors [29]. Typically, cellular adhesion is not mediated by single bindings but by huge clusters of adhesion molecules [30-31]. During adhesion of cells to ECM molecules molecular clustering is e.g. essential for the formation of focal contacts, which are

stable adhesion sites [32-33]. In the ECM many important adhesion molecules for cells are present, which allows stable adhesion of diverse cell types [34]. For acanthamoebae, the adhesion to ECM components is important as they have to move through the tissue in order to reach their target-cells. Furthermore, for the extracellular target-cell killing the adhesion to the target-cell is essential.

A very prominent and important glycoprotein in the ECM is fibronectin. It crosslinks the different macromolecules in the ECM, and is involved in nearly all cellular processes such as growth, differentiation, adhesion, and motility [35]. In tissue culture and research, it is used to improve adhesion of cells to surfaces. Another protein mixture, which resembles the ECM and is widely used, is matrigel. It is a gelatinous protein mixture, which is secreted and extracted from Engelbreth-Holm-Swarm mouse sarcoma cells and mainly consists of collagen, laminin and entactin [36].

1.1.5. A Cell as a Complex, Adaptive, and Dynamic Biomaterial

In general, cells can be regarded as viscoelastic, adaptive materials with advanced mechanical properties. The intracellular space of acanthamoebae is very densely packed, but still highly flexible and dynamic. A fluid-like endoplasm and a more gelatinous ectoplasm allow for quick changes in the movement. For example, parts of the cell can change from fluid like to more viscous during movement [37]. These parts are mainly dynamic structures such as pseudopodia, by which the acanthamoeba is adhering to the surface. The cell plasma stays fluid like, such that the amoebae can flow around small particles to phagocytose them. When exposed to stress, parts of the cell, e.g. the focal contacts become stiffer and the elastic properties in different cell regions change [38]. This shows that cells can intelligently adapt their viscoelastic properties according to the actual situation. Besides viscoelastic properties, cells can also dynamically adapt their adhesion as well as intracellular transport routes [17]. The latter is particularly amazing as cells are often densely packed systems. This shows that cells have optimized complex processes, which can serve as inspiration for novel artificial materials.

1.2. *Acanthamoeba spp*.

The different species of *Acanthamoeba spp*. can roughly be devided into pathogenic and non-pathogenic acanthamoebae. An example for a non-pathogenic acanthamoeba is *Acanthamoeba comandoni* (*A. comandoni*, ATCC® 30135), which was isolated from garden humus and is harmless to other organisms. Pathogenic acanthamoebae such as *Acanthamoeba castellanii* (*A. castellanii*, ATCC® 30234, derived from ATCC® 30011), which was isolated from yeast culture, can cause severe diseases such as amoebic keratitis and chronic granulomatous amoebic encephalitis. Patients

suffering from amoebic encephalitis are mostly immunocompromised, e.g. AIDS patients or people dealing with other autoimmune diseases, such as diabetes [39]. The first case of amoebic encephalitis of an AIDS infected patient was reported in 1986 [40], and the number of amoebic encephalitis diagnosed AIDS patients increased notably in the following years [1]. The first case of acanthamoeba keratitis became known in 1973, and here, too, the number of cases increased rapidly [14]. Infections with acanthamoeba keratitis were found to be closely related to the use of contact lenses [41], where lack in contact lens hygiene or deficient contact lens care have been identified as causes of infections. As nowadays more and more people are using contact lenses, the importance of understanding the mechanisms involved in infections with acanthamoebae has been growing.

Acanthamoebae are also referred to as the trojan horses of the microbial world. Besides the potential to cause acanthamoeba keratitis and granulomatous amoebic encephalitis, acanthamoebae are a risk for human health as they can be carriers of human pathogenic endosymbionts, such as viruses, yeast or bacteria. *Legionella pneumofila* are an example for pathogenic bacteria, which grow inside acanthamoebae and which can cause severe lung inflammation [1, 42-44].

1.2.1. Acanthamoeba Trophozoites and Cysts

Acanthamoebae are widely distributed in the environment [1, 14]. A reason for their ubiquitous nature is that they have two stages in their life cycle: one active trophozoite state and one dormant cyst state. Acanthamoeba trophozoites have a size between 25 and 40 µm, in the cyst state the size ranges from 10 to 25 µm [1]. Under unfavourable condititions (overcrowding, lack of nutrients, extreme temperatures, extreme pH) the active trophozoites are able to rapidly encyst. In this state the acanthamoebae are protected from the environmental influences by a double walled membrane, which mainly consists of cellulose and chitin. In this robust encapsulation the organism can withstand immunological attacks and even survive high doses of gamma and UV-radiation [45]. In the cyst state acanthamoebae are furthermore protected from medication, which leads to drug resistances [46]. In an appropriate environment with nutrients, adequate temperature and pH, the cysts are able to transform back to the trophozoite stage. Acanthamoeba trophozoites show a characteristic shape with small pseudopodia called acanthopodia [47], temporary projections, by which the acanthamoebae move forward. These acanthopodia play an important role in the amoebic adhesion and in the motility of acanthamoebae [6].

In our lab we have cultures of non-pathogenic *A. comandoni* as well as of pathogenic *A. castellanii*. Light microscopy observations (Figure 1-4) of trophozoites and cysts of both species show that the sizes of the trophozoites and cysts differ strongly. *A. castellanii* (B and D) are much smaller than the trophozoites of *A. comandoni* (A and C). Also the cysts of different species of acanthamoebae can vary in shape; the cysts of *A. comandoni* are rather round, while those of *A. castellanii* can have varying shapes. In both cases the characteristic double walled membrane is clearly visible.

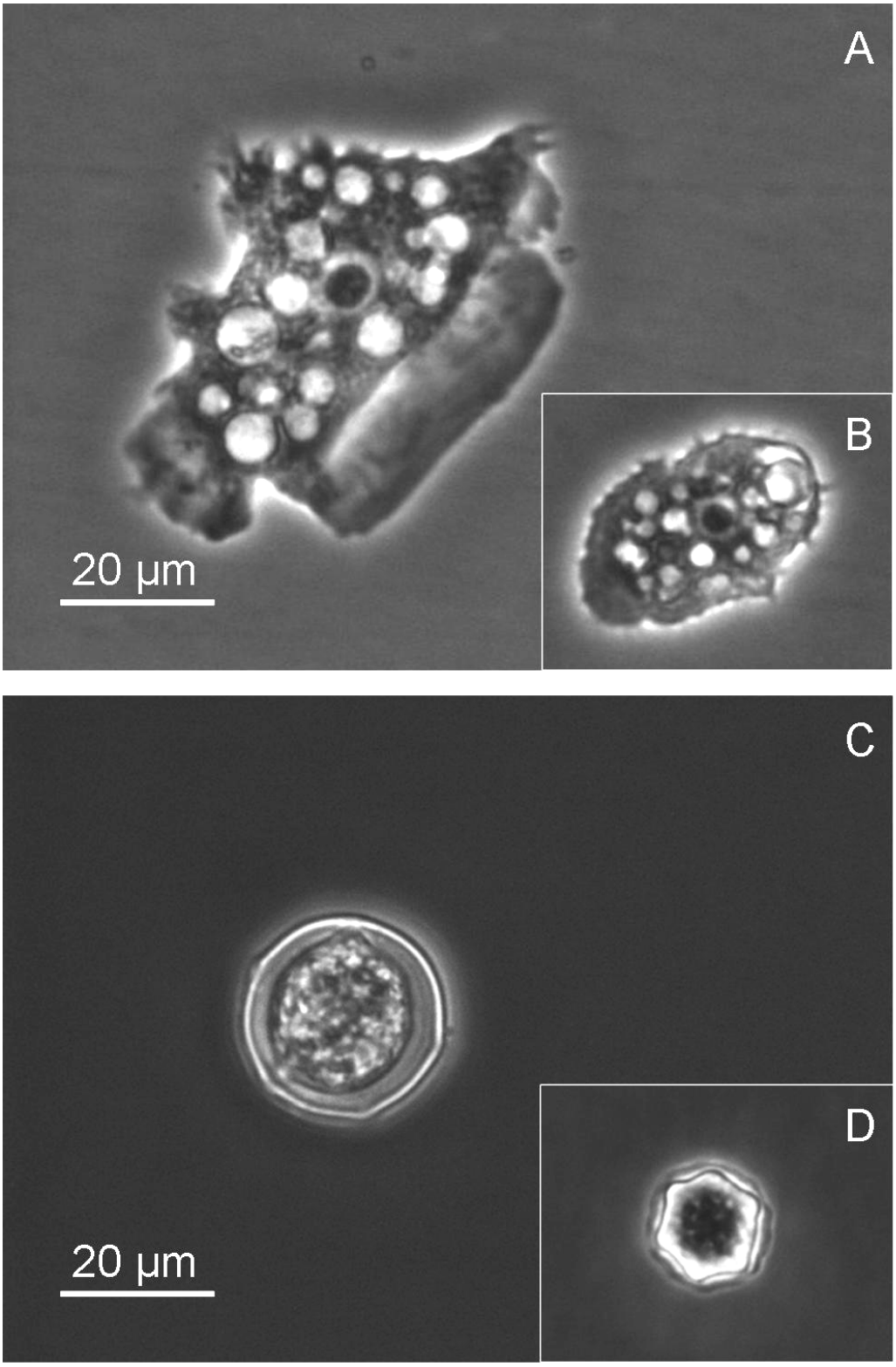

Figure 1-4 Trophozoites (top) and cysts (bottom) of *A. comandoni* (A and C), and *A. castellanii* (B and D). It becomes obvious that the trophozoites as well as the cysts of *A. castellanii* are smaller than those of *A. comandoni*.

Trophozoites (greek: trophe – nourishment) feed on yeast, bacteria, small particles and other cells [1]. Furthermore, they can endocytose large amounts of liquid (pinocytosis) in non-selective way by engulfment [48]. Specific uptake of particles is done via phagocytosis, a mechanism that is activated by receptors at the contact site. The size of the membrane invagination during this process depends on the size of the object, which is ingested. These food containing vesicles, called phagosomes, fuse with the digestion enzyme containing lysosomes and are finally transferred back to the membrane, where non-digested food rests are exocytosed. For phagocytosis and pinocytosis acanthamoebae can form large membrane invaginations, the so called food cups [1, 49].

Figure 1-5 A shows a swimming *A. comandoni* trophozoite forming such a food cup. The *A. castellanii* depicted in Figure 1-5 B took up large amounts of stained medium by food cup formation. The medium was stained by a membrane-impermeable fluorescent dye (AlexaFluor 488 Hydrazide salt, Life Technologies GmbH, Darmstadt, Germany). Moreover small red fluorescent beads (Polysciences Europe GmbH, Eppelheim, Germany) were taken up, which were added to the medium. This image was recorded in a confocal microscope such that the cross-section of only one layer of the cell is represented.

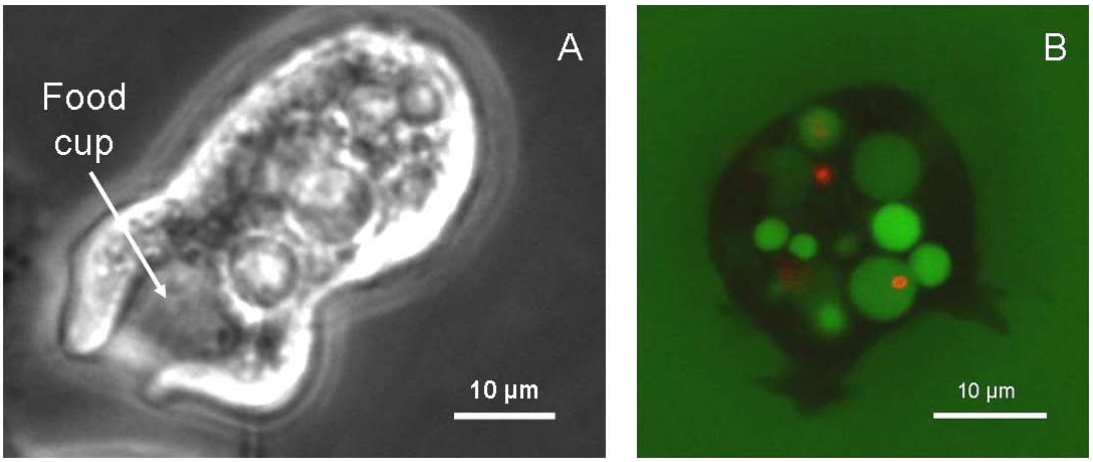

Figure 1-5 Swimming *A. comandoni* forming a food cup to take up large amounts of liquid (A). The liquid taken up by the formation food cups is stored in large vacuoles, which can be observed in case of the *A. castellanii* trophozoite depicted in (B). In this case the culture medium was stained by a membrane impermeable dye (AlexaFluor 488 Hydrazide Salt). In the medium red fluorescent beads were floating, which were also taken up by the amoeba (small red dots). The image was recorded using a confocal microscope, by which images of single layers of cells can be recorded.

1.2.2. Acanthamoeba Adhesion and Dynamics

Concerning adhesion, intracellular and extracellular dynamics, acanthamoebae cannot be compared to tissue cells like fibroblasts or endothelial cells. Acanthamoebae are

more motile and migrate much faster compared to other cells [14]. They are able to move in a crawling-like motion on stiff surfaces as well as on water air interfaces. It has been observed, that acanthamoebae form protean platforms on the ventral surface, the so called "associated contact" [37]. Between the rest of the cell and the substrate a small gap is present. For forward movement, pseudopod-like structures develop subtended to the associated contact and build focal contacts. These focal contacts are stable in their position. As the acanthamoebae have an outer gelatinous ectoplasm and an inner more fluid like endoplasm, they can move forward by fluid flow of endoplasm to the adhesion point in the front, where it coagulates into more stiff ectoplasm. At the rear the ectoplasm changes into fluid like endoplasm, the focal adhesions detach and endoplasm streams forward [37]. The strength of amoebic adhesion depends on the electrolyte concentration in the surrounding liquid. At high electrolyte concentrations the gap between substrate and cell body is relatively small compared to low electrolyte concentrations. This leads to an increased motility and also to stronger adhesion at higher electrolyte concentrations [37].
In the microscope differences between swimming and adherent acanthamoebae are clearly visible (Figure 1-6).

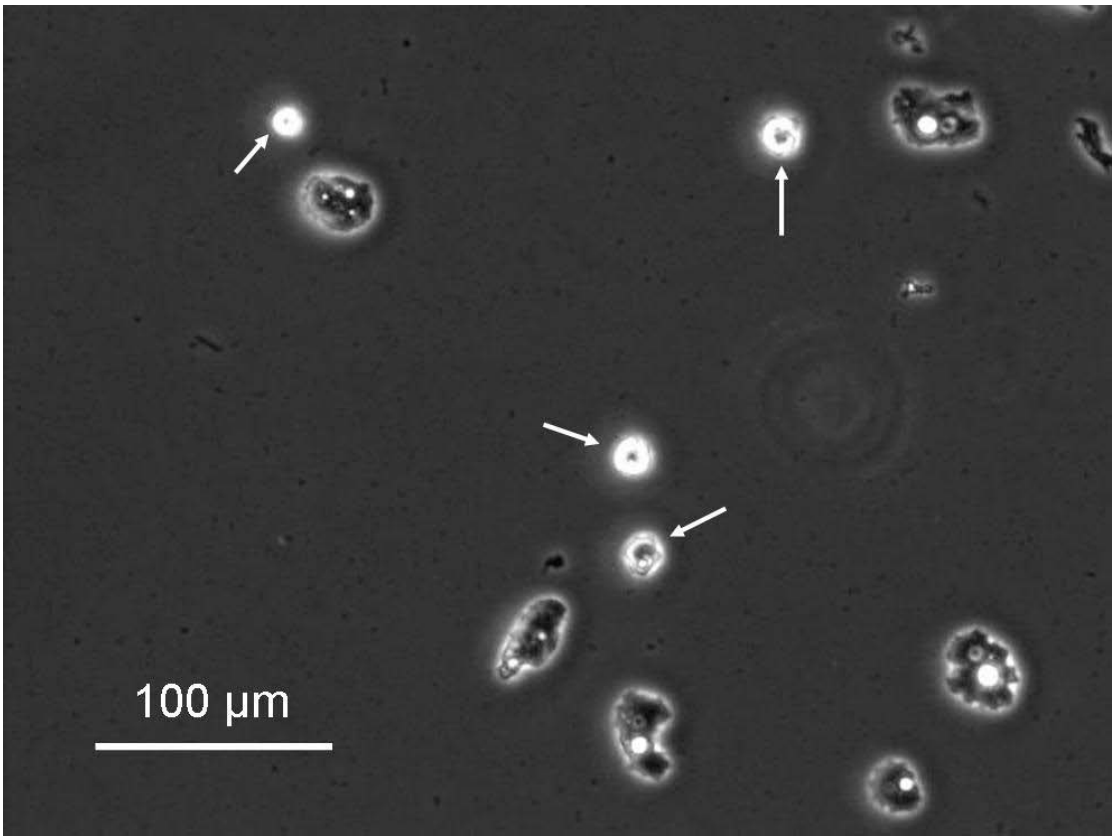

Figure 1-6 *A. castellanii* on glass substrate. Some of the acanthamoebae are adhering well to the surface, while some are floating (white arrows). The floating amoebae are much smaller and appear round leading to a larger thickness and therefore to an increased brightness in the phase contrast image compared to the adherent acanthamoebae.

In general, swimming acanthamoebae appear smaller than adherent ones as they round up (Figure 1-6, arrows). Due to their increased thickness, swimming acanthamoebae in phase contrast microscopy appear much brighter than the adherent ones, which flatten and spread on the surface.

1.2.3. Acanthamoeba Target-cell Killing Mechanism

Acanthamoebae naturally phagocytose yeast, fungi or bacteria. Moreover pathogenic acanthamoebae can kill target-cells in the human body by a contact dependent extracellular killing mechanism (Figure 1-7). Adhesion to target-cells is an essential step in the infection with acanthamoebae, and depends on a mannose binding protein (MBP), that can be found in pathogenic isolates, but is only present in low amounts in non-pathogenic acanthamoebae [8]. MBP is a transmembrane protein, which consists of 833 amino acids and can be divided into a large extracellular domain, a transmembrane domain and a short cytoplasmic domain. [5, 50].

Most mammalian and animal cells have a cell surface coat on the plasma membrane composed out of different oligo- and polysaccharides. These polysaccharides consist of different carbohydrates such as fucose, glucose, and mannose and are bound to membrane proteins (glycoproteins) and lipids (glycolipids). The MBP in the membrane of *A. castellanii* bind to mannose on the cell coat of their target-cells, and adhere specifically to them. By addition of mannose to the medium the specific adhesion could be inhibited as the MBPs are saturated by free mannose. This was shown *in vitro* in experiments with cocultures of acanthamoebae and chinese hamster corneal epithelial cells [51]. Besides the adhesion, mannose was furthermore found to induce the release of cytolytic factors [51-53]. Those are contact dependent metalloproteinases, which lead to programmed cell death (apoptosis) of the target-cell. In addition *A. castellanii* also releases contact independent proteinases and a mannose-induced protein (MIP-133), which potentially lead to contact-independent cell death [6, 53]. If mannose is added, for example, to culture media of pathogenic acanthamoebae, they release cytolytic factors and target-cells can be killed also without direct contact [51-53]. Besides this, in *A. culbertsoni* recently a pore-forming protein was identified, which is involved in the target-cell killing [54]. Similar proteins might also be involved in other pathogenic acanthamoebae such as *A. castellanii*, but have so far not been identified. For the release of the metalloproteinases as well as of the pore-forming proteins, active and passive transport mechanisms to the contact site seem to be necessary in order to release cytolytic factors at the right position.

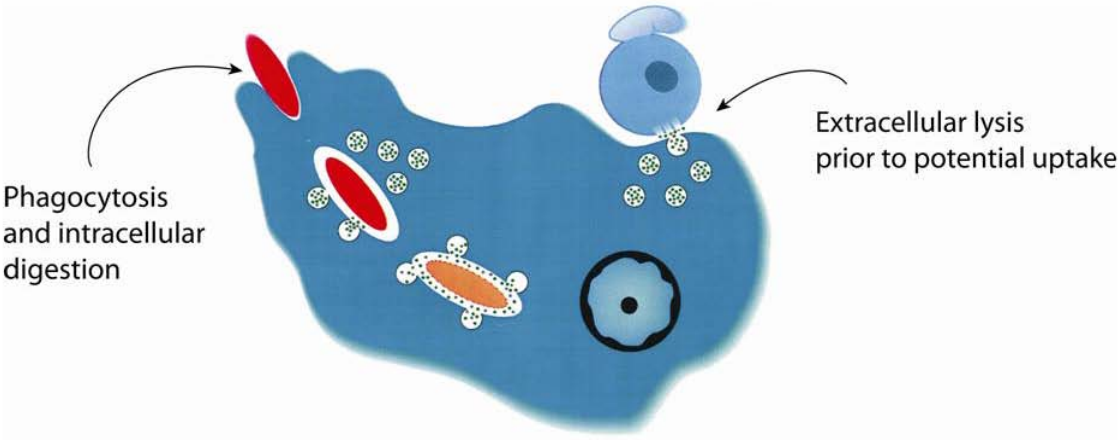

Figure 1-7 Schematic illustration of target-cell killing mechanisms. Acanthamoeba can kill target-cells intra- (left) or extracellularly (right). In case of intracellular target-cell killing, the acanthamoebae kill the target-cells after phagocytosis. For extracellular target-cell killing, specific adhesion of acanthamoeba to target-cells is mediated by mannose, a carbohydrate present in the cell coat of the target-cells. After contact formation granules move to the contact site and the acanthamoebae release contact-dependent metalloproteinases and other proteinases, which lead to target-cell death. For *A. culbertsoni* furthermore a pore-forming protein was identified, which is involved in the target-cell killing. Modified from [55].

This indicates that the intracellular movements of vacuoles and granules are an important prerequisite for the pathogenicity of acanthamoebae. The intracellular space of acanthamoebae is very crowded and for that reason many different transport mechanisms might be involved that according to current knowledge have not been investigated and understood yet. For the pathogenic potential furthermore it was observed that the number of acanthopodia plays a crucial role - pathogenic species show more acanthopodia than non-pathogenic ones [6].

Besides acanthamoebae there are other pathogenic amoebae such as *Entamoeba histolytica*, which cause human amoebiasis by a comparable, contact dependent target-cell killing process [56]. Every year more than 100000 humans die from amoebiasis, a highly infectious disease of the intestine [57]. For *Entamoeba histolytica* as well as for acanthamoebae the processes involved in the infection pathway are not fully understood yet.

1.2.4. Status quo and aim of the thesis

In the past years several studies revealed the ubiquitous distribution of acanthamoebae all over the world [58-62]. Acanthamoebae were isolated from swimming pools [61], air conditioning systems [58-59] and several other environments. The evaluation of several cases in Thailand of acanthamoeba keratitis showed that not only contact lens users are affected. Here the majority of the cases was found in non-contact lens users [63]. In India between 1993 and 2002 there was an epidemy of keratitis cases, where less than 1 % of the patients were contact lens users [64]. These studies show that the risk of acanthamoeba infections is omnipresent. But nevertheless, the overall risk of

acanthamoeba keratitis infections is increased for contact lens users [3]. In the USA there was an outbreak of acanthamoeba keratitis. This was related to a contact lens care solution, which promoted the growth of acanthamoebae, and was recalled [65]. In order to avoid infections it is necessary to understand, which parameters are involved in the contamination of contact lenses with acanthamoebae. New cleaning disinfecting solutions should be tested for the potential of acanthamoebae contaminations.

In recent years high efforts were made in order to improve medication strategies and treatments against acanthamoeba infections. Nevertheless, the mechanisms involved in the infection pathway remain not fully understood.

One step in the infection pathway that is known to be essential for the pathogenesis is the contact formation of acanthamoebae to their target-cells by the mannose-binding protein (MBP). In recent studies the influence of mannose on target-cell adhesion, cytotoxicity, and phygocytosis has been examined by genetically modifying the acanthamoebae and applying mannose to the mutants for some cell cycles [66-67]. This treatment affected the MBP of the acanthamoebae in such a way that the mannose selected amoebae showed reduced adhesion to target-cells, and a reduced cytotoxicity compared to the wild type cells [66-67]. In a recent study it has been discovered that actin is involved in the contact formation of acanthamoebae to their target-cells. The researchers treated acanthamoebae with actin depolymerizing substances and detected a reduced adhesion to target-cells [68]. As actin is mainly present in dynamic structures such as acanthopodia, the reduced adhesion to target-cells is quite logic as by applying depolymerizing substances the formation of such dynamic structures, which are needed for adhesion, is drastically reduced.

A further aspect involved in the cytotoxicity of acanthamoeba is the intracellular transport during the target-cell killing process. Cytolytic factors such as the recently indentified pore-forming protein in *A. culbertsoni* [54], have to be transported to the contact site between acanthamoeba and target-cell. For *Entamoeba histolytica* first transport mechanisms could recently be identified [69]. So far the aspect of intracellular transport processes, according to current knowledge, for acanthamoebae was not investigated yet.

Most of the recent studies on acanthamoebae were biological and biochemical studies. The aim of this thesis was to receive a comprehensive picture of processes involved in acanthamoeba infections by using biophysical and material scientific approaches.

As acanthamoebae are often associated with contact lens usage, the aim of the first part was to investigate acanthamoebae adhesion on commercial contact lens materials. When investigating the contamination of contact lenses with acanthamoebae, interesting questions are: Are material properties of the contact lenses influencing acanthamoebae adhesion? How do cleaning and disinfection of contact lenses influence the adhesion and the survival of acanthamoebae?

A further step was to investigate adhesion of acanthamoebae on artificial carbohydrate-functionalized materials. Here, yet not answered questions, which are of

great importance, are: Do pathogenic and non-pathogenic acanthamoebae show strong differences in the carbohydrate-specific adhesion? How do acanthamoebae adhere to extracellular matrix proteins and is specific binding involved? Is there a critical density of MBP adhesion sites, which is needed for stable adhesion of acanthamoebae? Is mannose as a ligand sufficient for acanthamoebae adhesion to target-cells?

As intracellular transport of granules is essential for target-cell killing, a prerequisite for understanding contact-dependent intracellular dynamics is to analyze native transport mechanisms inside acanthamoebae. In particular, the aim of the last part was to examine, which transport mechanisms are involved in intracellular dynamics.

In the following chapters experiments answering these questions are presented and discussed in detail. All experiments were conducted with acanthamoebae in the trophozoite stage.

2. Experimental techniques

The smallest objects visible to the unaided human eye are in the range of 100 µm. The sizes of acanthamoebae typically range from 10 to 50 µm, making it impossible to investigate any process at the cellular level with the naked eye. In order to observe intracellular dynamics and adhesion processes, techniques to visualize those processes are needed. Thus, in order to understand processes at the cellular level, it is necessary to apply microscopic techniques, which make the dimensions of cells and their organelles visible. Examples include light microscopy, fluorescence microscopy, scanning electron microscopy (SEM) and atomic force microscopy (AFM). AFM is a technique to not only record surface topography but also to measure small forces down to the piconewton regime in so called force spectroscopy measurements [70-71]. Another novel technique capable of the acquisition of three dimensional images of cells without the need of complicated staining protocols is the use of surface contrast microscopy (SCM) using photonic crystal slabs (PCS) [72].

In this part light microscopy as well as AFM are introduced. To investigate cell adhesion behavior furthermore adhesion platforms with well-controlled chemistry are required. Therefore, the technique of diblock copolymer micelle nanolithography [73] is described, which is used for preparing gold nanostructures for biofunctionalization.

2.1. Light Microscopy

The first microscope (greek micros = small, skopein = to see) was built over 400 years ago, most probably by Galileo Galilei.

The resolution (d) of a microscope is restricted by the wavelength λ of the used light and the numerical aperture (NA) of the objective.

$$d = \lambda/(2\,NA) \qquad (1)$$

NA=n sinα, n=refractive index of medium between cover slip and lens of objective, α=half opening angle of objective.

Visible light consists of electromagnetic waves, which have wavelengths ranging from 400 nm to 750 nm in the visible regime. Thus the resolution of a conventional light microscope is limited to ~ 200 nm.

In the light microscope the essential parts for the magnification are on the one hand the objective and the tube lens and on the other hand the ocular. When imaging objects with a camera, the magnification by the ocular does not account for the overall magnification. The magnification (m) in the objective and the tube lens of the microscope is given by the focal length (f) of the tube lens and of the objective [74].

$$m = f_{\text{tube lens}} / f_{\text{objective}} \qquad (2)$$

Imaging of cells is very special due to the nearly transparent nature of the cells. For that reason techniques such as phase contrast microscopy as well as fluorescence microscopy are the most commonly used ones. Phase contrast microscopy was

discovered by Frits Zernike [75-76], who won the Nobel Prize in 1953. The technique is used to make transparent objects, so called phase objects (e.g. cells), visible under the microscope. Depending on the thickness and the refractive index of the object, the phase of incoming light is changed. If the refractive index of the object is lower than that of the surrounding medium, the phase is increased, if the refractive index of the object is larger, the phase is decreased. These phase shifts normally are not visible for the eye. In the phase contrast microscope, the light path of the diffracted light, which passes the phase object is different than that of the direct light.

Incoming light passes an annular ring in the back focal plane of the condensor and is focussed onto the sample. A part of the light is diffracted at the transparent object, while another part passes the image plane without diffraction (direct light). The direct light passes the back focal plane of the objective at the so called phase ring, where the intensity of the light is decreased and where the phase is increased by ¼ of the wavelength. The phase of the light, which passes the phase object (cells), is changed depending on thickness and refractive index of the object and passes arbitrary positions on the back focal plane of the objective.

Changes in phase at the sample and the increase in phase at the annular ring lead to phase differences of the diffracted and the direct light and consequently to interference [75-76]. The interference leads to changes in amplitude, which can be observed as dark (destructive interference, ideally total phase shift of 1/2 λ) or bright structures (constructive interference, ideally no phase shift). Because of different refractive indices of the organelles, it can be observed that in acanthamoeba there are bright and dark organelles (Figure 2-1 A).

Structures, which are thicker than 10 µm, appear with a bright halo due to diffraction of the direct light at the edges. This effect can also be observed when imaging the acanthamoebae (Figure 2-1 A), while fibroblasts are flatter and therefore can be imaged without a bright halo (B).

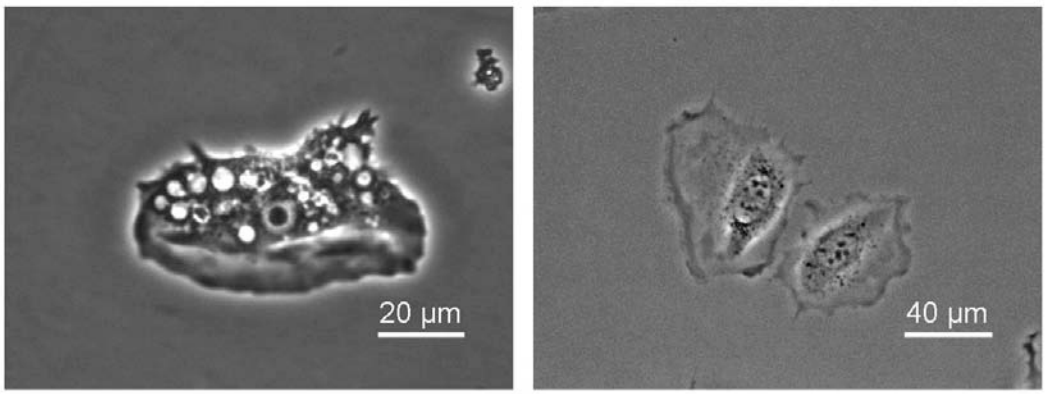

Figure 2-1 Phase contrast image of *A. comandoni* trophozoite (left) and Fibroblasts (REF52wt) (right). It becomes obvious that with phase contrast thick transparent objects such as the acanthamoebae appear with a bright halo around the cell. Intracellular structures are well visible. Fibroblasts are flatter and therefore no halo around the cell is visible.

In this work mainly a CKX41 phase contrast microscope (Olympus GmbH, Hamburg, Germany) with 10 × objective, and Hamamatsu camera of the type C9300 was used. The image size of 640×480 pixel gives a resolution of 1 pixel is ~0.7 µm. When calculated according to equation (1), with $NA = 0.25$ for the 10 × objective the resolution is $d = 1$ µm. With a 60 × objective 1 pixel is ~0.18 µm in size, while the resolution according to (1) with $NA = 1.35$ is $d = 0.185$ µm.
In order to obtain information about intracellular processes besides the contrast of the image, the velocity of the recording of the sequence is important. As the motion inside acanthamoebae can be very fast, the used camera has been chosen such that frame rates of up to 150 Hz at full image size are possible.

2.1.1. Fluorescence Microscopy

Fluorescence microscopy is a label-based contrast enhancement method. For experiments on cells, parts of the cell such as the nucleus or the actin filaments can be stained by fluorescent dyes or cells can be genetically modified. Fluorescent stains contain certain molecules, the fluorophores, which after excitation with light of a specific wavelength, emit light of another wavelength. The emitted wavelength is larger than the excitation wavelength, and the difference between these two is called Stoke's shift. In order to record fluorescence images, the microscope has to be equipped with excitation, and emission filters, as well as a dichroic mirror matching to the distinct wavelengths. Only light of the excitation wavelength can pass the excitation filter. The filtered light hits the dichroic mirror, is directed to the sample and activates the fluorophores. The sample emits light of another wavelength, which is reflected through the dichroic mirror and the excitation filter onto a detector. By using different dyes and filter combinations, different organelles in cells can be stained and differentiated in the recorded images.
In case of acanthamoebae the staining of the amoebic membrane and cell organelles appeared to be very difficult as the buildup of the membrane seems to be different than that of mammalian cells. For this reason the standard staining protocols, which are used for other cell lines cannot be directly applied for acanthamoebae. Besides the staining of the acanthamoebae also their genetic modification with fluorescent markers for our lab bears inaccessible differences to mammalian cells, and could not be successfully applied by using standard protocols. For these reasons, nearly all experiments in this thesis were conducted with phase contrast microscopy.

2.1.2. Surface Contrast Microscopy

A label-free technique for imaging surface near objects such as cells is the use of photonic crystal slabs as substrate for cell samples. This technique is called surface contrast microscopy (SCM) [72] and can be used for fixed cells under liquid free conditions. A detailed description of the technique is given in [72]. The advantage of this technique in comparison to phase contrast microscopy is the enhanced contrast

without a halo effect at the edge of the cell. For this reason the cell size can be determined more precisely. In Figure 2-2 a surface contrast image of *A. castellanii* on a Photonic Crystal Slab (PCS) is shown. Furthermore, an evaluation of the thickness of surface-near objects is possible with this technique [77]. A disadvantage of surface contrast microscopy is that the contrast inside the cell is reduced such that the intracellular organelles are not well visible anymore. Furthermore, the technique can only be applied to fixed cells and not for life cell experiments, because the surface has to be dried for the measurements. For those reasons in the experiments conducted in this thesis surface contrast microscopy was not applicable as living acanthamoebae in liquid environment were needed.

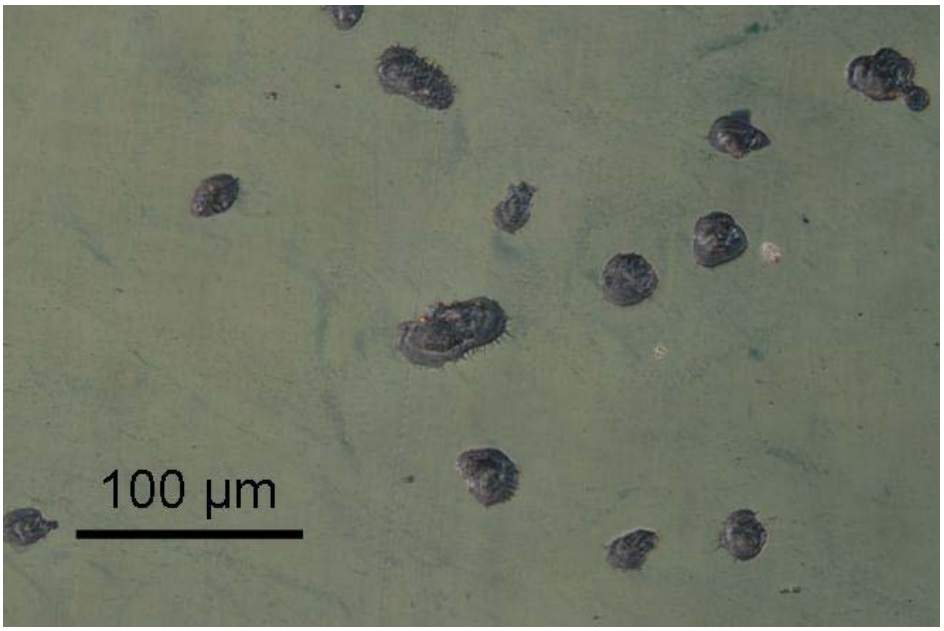

Figure 2-2 Surface Contrast Microscopy image of glutaraldeyhyde (1 %) fixed *A. castellanii* in dry conditions on a Photonic Crystal Slab. The area of the cells is well visible without a bright halo compared to phase contrast microscopy.

2.2. AFM

After the invention of the Atomic Force Microscope (AFM) in the late 1980th [78], it has become a versatile tool to study specimen properties in various fields of science [79-81]. It is a highly precise instrument for imaging of surfaces in order to determine roughness and topography from the micrometer down to the sub nanometer range. Furthermore, AFM can be used for force spectroscopic measurements of protein-protein interactions and even of cell-surface interactions with piconewton sensitivity [82-83]. Such measurements can also provide important information about cell-material interactions with implant materials. AFM can be used with *A. castellanii*, in

order to study their contact formation to target-cells in detail. For this purpose, the target molecule for adhesion is presented at the cantilever and forces between cell and cantilever can be measured by approaching it to the acanthamoeba trophozoite and retracting it after a certain contact time at the amoeba.
A schematic drawing of the main functional parts of the AFM is given in Figure 2-3.

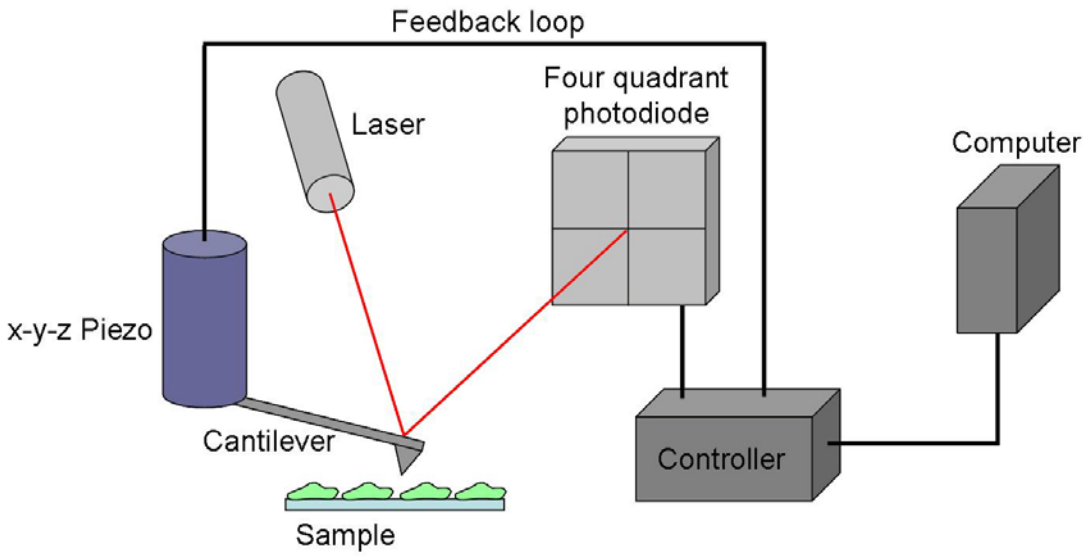

Figure 2-3 Functional parts of the atomic force microscope. A cantilever with a sharp tip is scanned laterally over the surface of the sample. A laser is reflected at the back side of the cantilever onto a four quadrant photodiode. Due to attractive or repulsive interactions between cantilever and sample, the cantilever bends upwards or downwards and the laser signal on the photodiode changes. A feedback loop recalculates the signal changes and accordingly adapts the extension of the piezo in z-direction.

The central part of the AFM is a cantilever, which is typically equipped with a sharp tip. During imaging, the tip is laterally scanned line by line over the surface of the sample. A laser is positioned on the front edge of the cantilever and reflected into a four-segment photodiode. Attractive or repulsive interactions between the sample surface and the cantilever cause a bending of the cantilever towards or away from the surface. This leads to a change of the position of the laser on the photodiode. In constant force mode these changes of the photodiode output signal are transferred to a feedback loop, which is responsible for keeping the signal at the photodiode and therefore the distance between tip and sample constant. It controls the movement of the piezo by applying a voltage leading to either extension or compression of the piezo depending on the cantilever deflection. The cantilever or the sample is connected to the piezo and therefore the position is changed accordingly. In this way, the surface topography is reconstructed from the movement of the x-y-z piezo and topographical images of the sample surface can be created [78].

Besides imaging of surfaces, as mentioned before, AFM can be used for force spectroscopy measurements in order to investigate forces acting between single molecules [84] or between cells and surfaces [85].
In order to investigate binding processes between cells the involved molecules can be isolated from cells and purified in order to functionalize the cantilever with the molecule. The functionalized cantilever then is approached to a differently functionalized surface until a certain force is reached, is kept at this force for a defined time and retracted at a constant speed (Figure 2-4 A) [86]. If molecules, which cannot be easily isolated from the cell, are involved, another possibility is to functionalize the cantilever with adhesive molecules such as certain proteins to stably trap the cell on the cantilever. In this case tipless cantilevers are utilized in order to avoid damaging of the cell [87]. In case of measurements with mammalian cells heatable stages can be used to keep the temperature constant at 37°C. For the cantilever functionalization in case of mammalian cells typically a sandwich functionalization with concanavalin A and biotin-streptavidin is carried out. In order to functionalize the cantilever here the receptor-ligand bond of biotin and streptavidin is utilized. First a BSA-biotin layer is adsorbed on the cantilever surface, in the next step a streptavidin layer is deposited followed by a layer of biotin-concanavalin A [88]. Another possibility is to glue the cell to the cantilever by using Cell-Tak™, an adhesive for cells and tissue, which has been shown to stably fix also weakly adhering cells to the cantilever [89]. The trapped cell is then approached to a biofunctionalized surface (Figure 2-4 B) or to another cell (Figure 2-4 C) [85, 90]. By this approach cell mechanics can be measured [91-92] and furthermore, these measurements can give information about adhesion cluster formation [93].

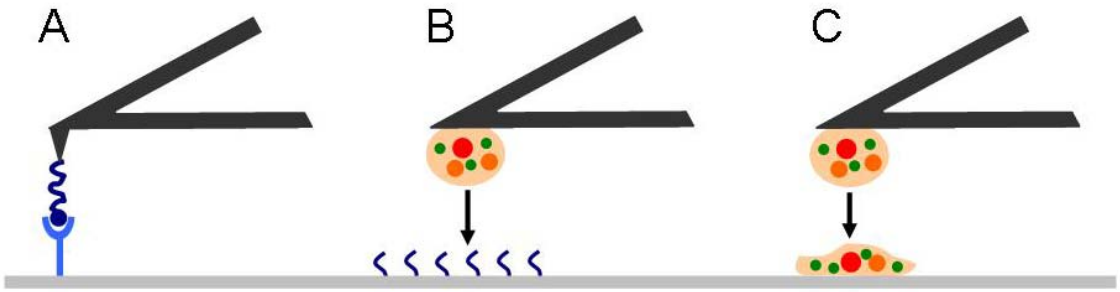

Figure 2-4 Examples for configuration of force spectroscopy measurements with AFM. Either molecules are isolated from cells and the cantilever is functionalized with such molecules and brought into contact with a differently functionalized surface (A) or a cell is stably fixed to the cantilever and approached to a functionalized surface (B) or to an adhering cell on a surface (C).

In case of *A. castellanii* none of the standard procedures, neither concanavalin A functionalization nor Cell-Tak™ functionalization could stably trap the trophozoite on the cantilever. With concanavalin A the trophozoite did not even attach to the

cantilever, while with Cell-Tak™ the acanthamoeba attached to the cantilever but started to crawl along it (sequence Figure 2-5). For that reason, instead of gluing the acanthamoebae to the surface, a carbohydrate-functionalized cantilever was approached to trophozoites adhering in a petri dish.

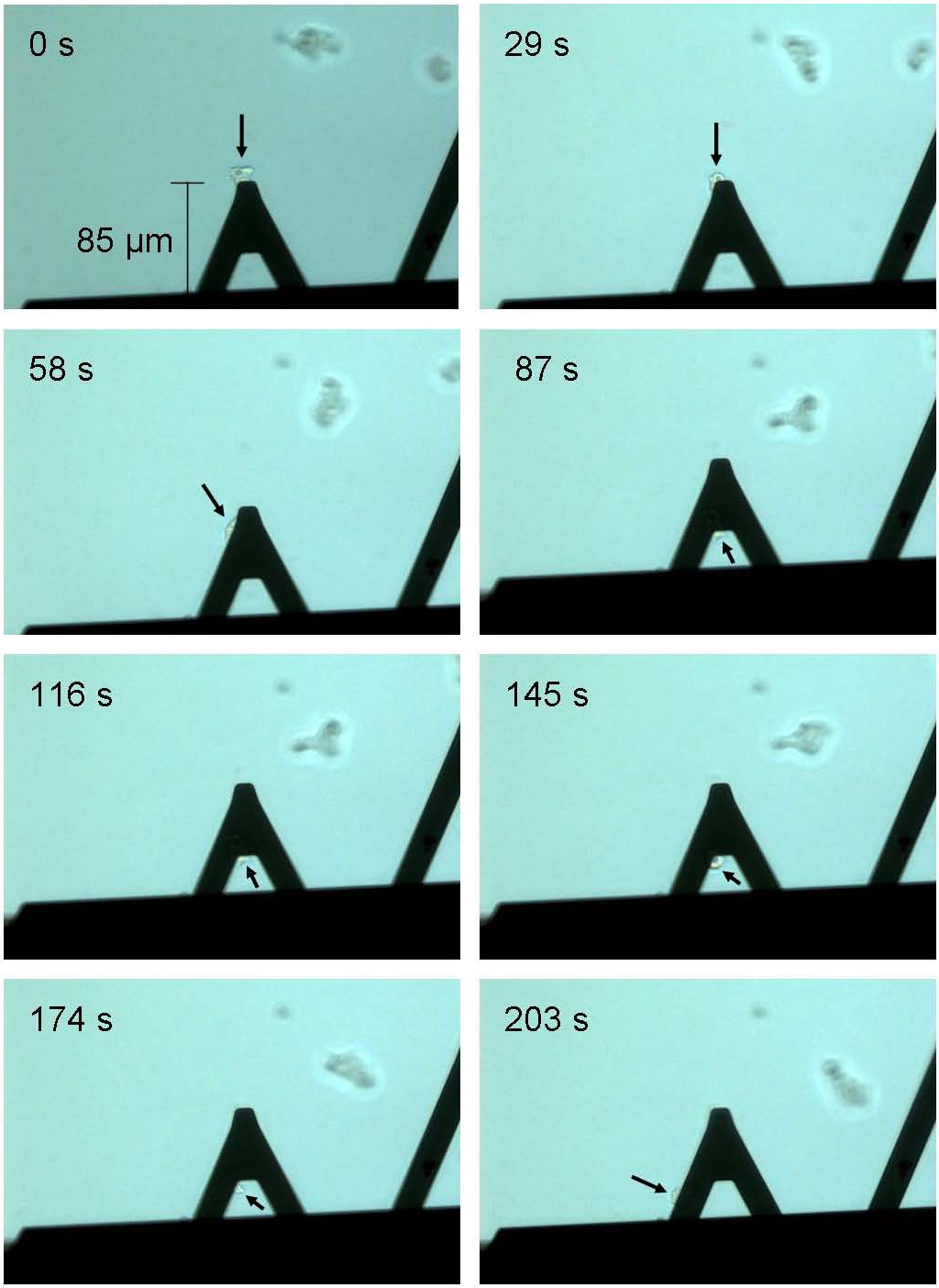

Figure 2-5 *A. castellanii* crawling on a Cell-Tak™ functionalized cantilever. The acanthamoeba adhered to the cantilever, but could not be fixed to the very end of the cantilever. Arrows mark the position of the acanthamoeba on the cantilever.

During such measurements, force distance curves (Figure 2-6A) are recorded, in which unbinding events can be detected. Furthermore, the maximum adhesion force and the adhesion energy can be calculated from such curves. In order to understand, which interactions occur between the functionalized tip and the surface, the force distance curves have to be analyzed. The individual steps of a force distance curve are schematically shown in Figure 2-6 B.

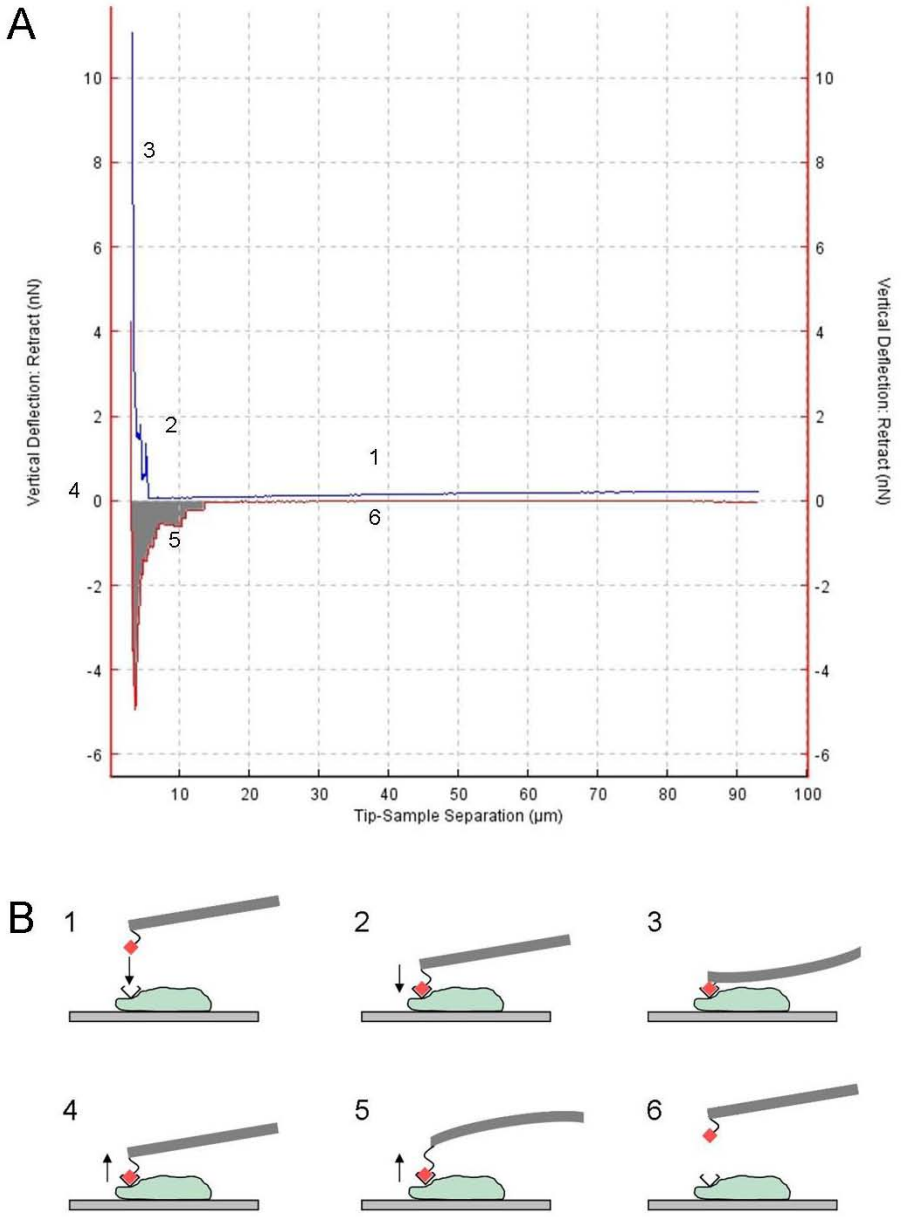

Figure 2-6 A Force distance curve recorded during force spectroscopic measurement with a mannose-functionalized cantilever on an adhering *A. castellanii*. B Cantilever behavior during measurement. The cantilever is being approached to the adhering cell (1), comes into contact (2) and is kept at a certain force for a distinct time (3). The cantilever is retracted and bends downwards due to interactions between the functionalized cantilever and surface proteins of the cell (5). After rupture of the bindings the cantilever is retracted until its original position is reached again (6).

When the tip is approached to the surface the force acting on the cantilever stays zero and therefore the deflection is also zero (1+2). As soon as the cantilever comes into contact with the surface, it bends upwards, which leads to a linear increase of the force on the sample (3). During the retraction of the cantilever, the bending of the cantilever is reduced until the repulsive force becomes zero again (4). In case of interactions between cantilever and surface/cell, the cantilever bends downwards due to attractive interactions (5) until a certain force is reached, which is needed for rupture of a bond (unbinding force). The minimum point of the curve gives the maximum adhesion force, while the area below the curve (grey area in Figure 2-6 A) is the adhesion energy.

2.3. Diblock Copolymer Micelle Nanolithography

Diblock copolymer micelle nanolithography is a self assembly-based technique for fabricating quasi-hexagonally arranged patterns of gold nanodots. For the preparation of such patterns, a polymer solution containing a solvent (here: toluene), and an amphiphilic diblock copolymer is produced. The copolymer consists of a hydrophobic polystyrene (PS) part and a hydrophilic poly-2-vinylpyridine (P2VP) part. Its concentration in the solvent has to be above the critical micelle concentration (cmc) in order to ensure, that micelles are formed. In these micelles the PS part is in contact with the toluene and the P2VP part is oriented towards the center of the sphere. In the next step, hydrogen tetrachloroauretate(III)trihydrate ($HAuCl_4$) is added to the solution and is concentrated at the center of the spherical micelles due to polar interactions with the P2VP and because of a low solubility in toluene [73].
As a substrate for the gold nanostructures here mainly glass cover slips are used, which had been cleaned with piranha solution (sulfuric acid + hydrogen peroxide) before deposition of the micelle solution. The process is shown in Figure 2-7.
In order to produce a self assembled monolayer of the gold dots, the glass slides are covered with the copolymer solution by spin coating or dip coating. The micelles with the gold salt self-assemble on the surface in a hexagonally arranged pattern. After deposition the coated glass slides are plasma treated in a hydrogen / argon plasma in order to remove the polymers on the surface and to reduce the gold ions to elemental gold [94]. Figure 2-8 shows a scanning electron microscopy image of gold nanoparticles assembled in a quasi-hexagonal way on a glass substrate. In order to investigate the influence of carbohydrates or proteins on the adhesion properties of cells, the gold nanostructures need to be functionalized to serve as contact sites for the cells.

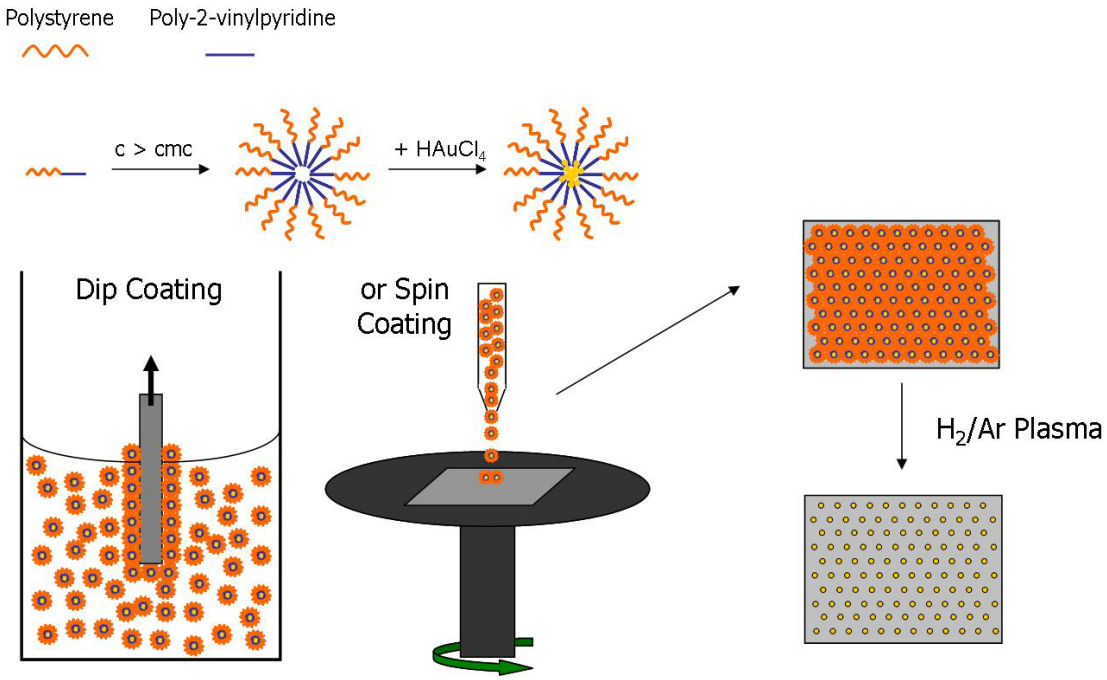

Figure 2-7 Schematic view on diblock copolymer micelle nanolithography. At first, a micellar solution containing polystyrene and poly-2-vinylpyridine at concentrations above the critical micelle concentration (cmc) are produced with toluene. Subsequently gold salt is added, which agglomerates in the middle of the micelles. Substrates are either spin or dip coated and treated with a H_2/Ar Plasma to remove the polymer and to reduce the gold salt to elemental gold.

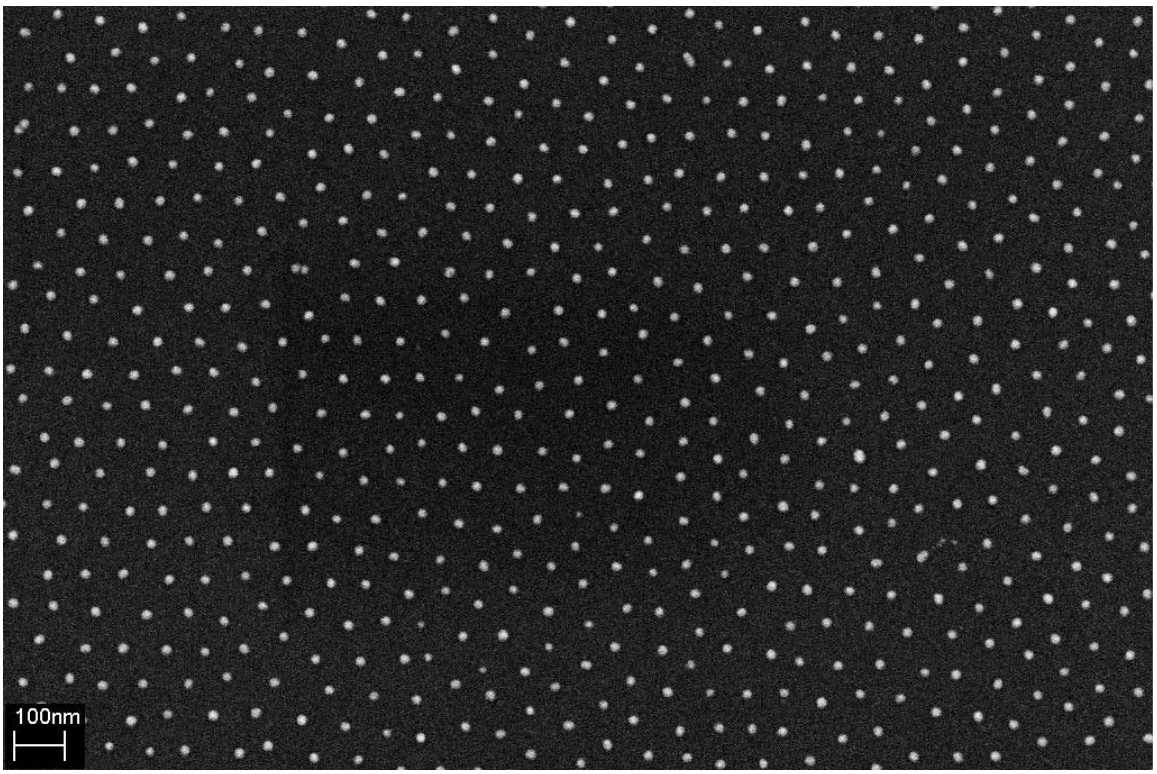

Figure 2-8 Scanning electron microscopy image of a gold nanostructured surface produced by diblock copolymer micelle nanolithography. The gold dots are arranged in a quasi hexagonal pattern and can be functionalized, e.g. by proteins or carbohydrates, which serve as anchoring points for cell adhesion.

In the case of wild type rat embryonic fibroblasts (REF52wt), which are cells of the connective tissue, the gold nanostructures can be functionalized by a RGD peptide (c(RDGfK)), to which the $\alpha_v\beta_3$ integrin in the REF52wt cell binds with high affinity [95]. To avoid binding of cells to the space between the single gold nanoparticles, the surfaces are passivated using a polyethylene glycol (PEG), which is known to prevent cell adhesion [96].

For REF52wt, it has been shown that for mimicking the RGD peptide in the ECM the spacing between the gold dots plays an important role in cell adhesion [93, 97]. It was observed that the distance between the single functionalized gold nanodots should not be larger than 58 nm as these cells need a certain distance between the anchoring sites for adhesion [97]. If the spacing between the gold nanodots of the nanostructures is small enough the fibroblasts can build focal contacts and focal adhesions and spread well on the surface. Above 58 nm, the fibroblasts cannot build stable focal adhesions leading to unstable adhesion and after a while to cell death [97]. Also for other cells, as for example osteoblasts, similar results have been found. In integrin $\alpha_v\beta_3$-RGD mediated adhesion, the inter-particle distances (IPD) should range between 58 nm and 73 nm in order to ensure stable adhesion [95]. Furthermore, it was found, that also the adhesion strength depends on the inter-particle spacing and thus the density of the functionalization sites [93]. In case of acanthamoebae such experiments were not conducted yet. In single experiments we could find, that *A. castellanii* does not bind to RGD peptides like the REF52wt cells (own data, not shown here). This fact and the differences between acanthamoebae and other cells concerning motility, adhesion and metabolism lead to the conclusion, that acanthamoebae can not be compared to cells in the body and that adhesion experiments with acanthamoebae require suitable adjustments to existing experimental protocols. Adhesion of acanthamoebae to target-cells, as well as acanthamoebae pathogenicity have frequently been reported to be mannose dependent [6-8, 51-53, 98-100]. In order to investigate the influence of mannose on the adhesion of acanthamoebae to host cells, gold nanostructured surfaces can be used to mimic the glycocalyx of target-cells. By applying diblock copolymer micelle nanolithography, it becomes possible to investigate, whether mannose as single ligand is sufficient or if other binding molecules (carbohydrates or proteins) are needed for stable adhesion. Furthermore, by this technique critical ligand densities or distances for stable adhesion can be determined. The influence of the distance of ligands (e.g. mannose) on the adhesion properties, such as cell spreading area or adhesion quantity, can also be explored.

3. Acanthamoeba Adhesion to Soft Contact Lenses and Influence of Cleaning Procedures

Infections with acanthamoeba keratitis stand in close correlation with the use of contact lenses. By adhering to the contact lenses, acanthamoebae obtain the path to get into the eye, where they cause this inflammatory disease [101]. As the contamination of the contact lenses is essential in the infection process, studies on adhesion of *A. castellanii* to different soft contact lenses are presented in this chapter, and possible influences of material properties on the amoebic adhesion are evaluated. In this context the non-specific adhesion, independent of carbohydrates or proteins, is evaluated. Furthermore, the influence of contact lens care solutions and contact lens disinfection procedures on the survival and proliferation of *A. castellanii* are treated here. The results of this chapter are summarized in a paper that has been published in Contact Lens & Anterior Eye [102].

3.1. Acanthamoeba and Contact Lenses - an Overview

The risk of an infection with acanthamoeba keratitis is significantly higher for contact lens users than for non-contact lens users [41]. Bad contact lens hygiene causes a main risk in the infection with pathogenic acanthamoeba species, such as *A. castellanii*. Most of the patients suffering from acanthamoeba keratitis did not follow the cleaning instructions of the manufacturers. For example, lenses are cleaned in home-made cleaning solutions containing tap water, or, disinfection and cleaning is carried out less frequently than recommended [103]. Either of these above mentioned careless cleaning procedures can cause contaminated contact lenses and storage cases [2-3], consequently acanthamoebae are transferred to the cornea, leading to sight-threatening keratitis [14]. In the infected eye the acanthamoebae are able to encyst, which protects from medication, and gives rise to drug resistances [46]. In the cyst state the acanthamoeba can survive in the eye for several moths and after decrease of the symptoms and stopping of medication, the acanthamoebae transfer back to the trophozoite state leading to recurring inflammation [104].

Contamination of contact lenses with pathogenic acanthamoebae depends on various factors. Material properties, including ionic properties [105-106], silicone content [107-108], and water content [105-106], influence the adhesion of acanthamoebae. In previous studies it has been shown that with increasing water content the number of acanthamoebae on the lenses increases. Furthermore, ionic lenses were found to have a higher risk of contamination with acanthamoebae than non-ionic lenses [105-106]; silicone hydrogel lenses exhibit higher contamination levels than those without silicone in first generation silicone hydrogels [107]. Rather, for second generation silicone hydrogels no influence of the silicone content on acanthamoeba contamination could be observed [108]. In general, the risk of contamination with acanthamoebae for worn contact lenses is higher than for unworn lenses [109]. For

example, lenses contaminated with bacteria showed more adherent acanthamoebae compared to fresh lenses [108].

A further issue, which might influence the contamination of contact lenses with acanthamoebae, is meachnosensing. Mechanosensing is the phenomenon, that cells respond to the mechanical properties of their environment, which is well known for mammalian cells [110] and where indications were found for the social amoeba *Dictiostelium discoideum* [111-112]. For acanthamoebae so far mechanosensing was not investigated.

Besides the pure material properties of contact lenses, the applied cleaning solutions and procedures play an essential role in the infection process with acanthamoebae. It was shown, that some cleaning solutions promote the encystment of the acanthamoebae, while others influence the adhesion and viability of the acanthamoebae [45, 113]. Also the cleaning procedure influences the survival of acanthamoebae on the lenses. If a rub and rinse procedure is used, the cleaning is more effective than rinsing without rubbing [114].

Furthermore, the disinfection procedure also influences the survival of acanthamoebae on contact lenses and in storage cases. Different peroxide treatments have different effects on the survival of trophozoites and cysts. While in most cases trophozoites are killed by peroxide solution, this is not always the case for cysts [115]. The efficacy of disinfection solutions can also vary between distinct species of acanthamoebae [116].

3.2. Materials and Methods

3.2.1. Cell Culture of Acanthamoeba

A. castellanii (ATTC 30234) were cultured in Peptone Yeast Glucose (PYG) Medium 712 (20 g proteose peptone (BD, Sparks, USA), 1 g yeast extract (BD, Sparks, USA), 950 ml distilled water, 10 ml 0.4 M $MgSO_4 * 7H_2O$ (AppliChem GmbH, Darmstadt, Germany), 8 ml 0.05 M $CaCl_2$ (AppliChem GmbH, Darmstadt, Germany), 34 ml 0.1 M sodium citrate $* 2H_2O$ (Merck KGaA, Darmstadt, Germany), 10 ml 0.005 M $Fe(NH_4)_2(SO_4)_2 * 6 H_2O$ (AppliChem GmbH, Darmstadt, Germany), 10 ml 0.25 M $Na_2HPO_4 * 7H_2O$ (Carl Roth GmbH & Co. KG, Karlsruhe, Germany), 10 ml 0.25 M KH_2PO_4 (Carl Roth GmbH & Co. KG, Karlsruhe, Germany), 50 ml 2 M glucose (Sigma-Aldrich Chemie GmbH, Munich, Germany)) at room temperature (RT) in tissue culture bottles (Sarstedt AG & Co., Nümbrecht, Germany). Once in a week the medium was renewed by shaking the bottles, removing the old medium with swimming acanthamoebae in it. Fresh medium was added to the remaining acanthamoebae.

3.2.2. *A. castellanii* on Soft Contact Lenses

In order to systematically investigate the effect of material properties on acanthamoeba adhesion and contamination, the following contact lens materials were investigated concerning the adhesion of *A. castellanii*:

Hydrogels: Vitafilcon A, Ocufilcon F, P[Alkyl-NVP-Copolymer]

Silicone Hydrogels: Narafilcon A, Filcon II 3, Aerofilcon A.

The lenses were washed once with sterile filtered buffered saline solution, in which the lenses are typically immersed when provided by the manufacturer. Subsequently, the lenses were cut twice from the sides with a sterile scalpel. The prepared contact lenses were put into a twelve-well plate (Techno Plastic Products AG, Trasadingen, Switzerland) containing PYG-Medium. *A. castellanii* were counted with a Neubauer counting chamber and 2×10^4 acanthamoebae in PYG (1 ml) were added to the wells containing the contact lenses and incubated at RT either for 1 h or for 24 h (Figure 3-1).

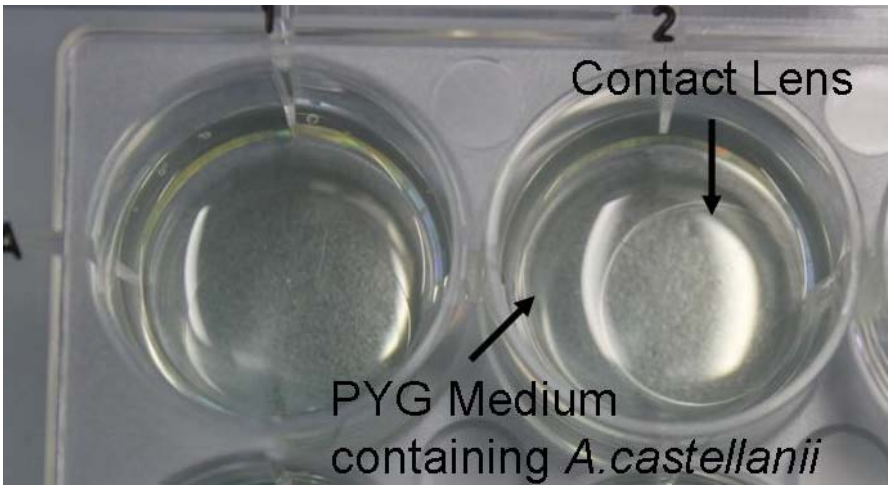

Figure 3-1 Contact lenses inside the wells of a twelve well plate containing PYG medium with *A. castellanii*.

After incubation, the lenses were taken out of the wells and placed on an objective glass and covered with a cover slip. Samples were imaged using the phase contrast microscope CKX41 of Olympus equipped with a CCD camera (C9300, Hamamatsu, Hamamatsu, Japan). 30 images per sample were taken at arbitrary positions and the number of adherent acanthamoebae was counted. All lenses were tested for *A. castellanii* adhesion three times in triplicate (n=9). The significance of the results was checked by applying a two-sample t-test (see appendix 3) [117].

As in the experiments PYG medium was used instead of the normally used saline storage solution, the influence of the PYG medium on the contact lenses was checked. Swelling of the lenses in the culture medium could lead to changes in their water content and their elastic properties. For that reason the contact lens diameter was

accurately measured using an Optimec Ltd. geometry measurement instrument. The swelling of the lenses was measured after 24 h incubation at RT either in saline solution or in PYG medium. Furthermore, lenses incubated for 24 h in PYG were measured after 3 h of regeneration in saline solution. Also this experiment was repeated three time in triplicate for each lens (n=9). These experiments were conducted in collaboration with WÖHLK-CONTACT-LINSEN GmbH.

3.2.3. Contact Lens Care and Disinfection

In order to investigate the influence of disinfection and contact lens care on the contamination of the lenses with acanthamoebae, the lenses were washed after 24 h of incubation in a contact lens multipurpose solution (WÖHLK CONTACT CARE, containing Actipro and Polyhexanide (0.0001 %)) and after a few minutes the lenses were disinfected by using a peroxide solution (stabilized 3% hydrogen peroxide, WÖHLK PEROXID). To the peroxide solution, a neutralizing tablet was added and the contaminated lenses were incubated in this solution overnight. Afterwards the lenses were imaged as described before and the number of adhering *A. castellanii* was counted. The experiment was repeated three times in triplicate for each lens (n=9).

For checking the influence of the single steps of contact lens cleaning and disinfection, independent experiments with multipurpose solution and peroxide solution were performed. 10^5 *A. castellanii* were seeded in petri dishes or cell culture bottles (both Sarstedt AG & Co., Nümbrecht, Germany) in PYG medium and incubated at RT for 15 min to let them adhere. Subsequently, the medium was removed and either 7 ml of the multipurpose solution or the peroxide solution with neutralizing tablet were added to the petri dishes and incubated over night at RT. After the incubation period images were taken as described before.

In order to investigate the influence of the solutions on the survival of the acanthamoebae, the experiments in the petri dishes were repeated in two independent experiments, once with 10^5 acanthamoebae and once with 10^6 acanthamoebae per petri dish (n=4). For each solution, the multipurpose solution and the peroxide solution, two petri dishes with adhering trophozoites were prepared. The solutions were added and incubated over night as described before. The acanthamoebae-containing solutions were centrifuged using a biofuge primo (Heraeus Holding GmbH, Hanau, Germany) at 800 g for 5 min. The supernatant was removed and 50 mM sodium chloride was added to wash the acanthamoebae once. *A. castellanii* were resuspended in the sodium chloride and again centrifuged. In the next step, sodium chloride was removed, followed by resuspension of acanthamoebae in PYG medium and transfer to a new tissue culture bottle. After two and five days of incubation the growth of the acanthamoebae was checked by imaging of the acanthamoebae with the phase contrast microscope and counting them.

3.3. Results

3.3.1. Adhesion of *A. castellanii* to Soft Contact Lenses

The adhesion of *A. castellanii* to three different hydrogel (Hy) and three silicone hydrogel (SiHy) contact lens materials was measured by counting the acanthamoebae adhering to a certain surface area of the contact lenses after one and 24 hours. The material properties of the investigated lenses are shown in Table 3-1. Vitafilcon A, Qcufilcon F and P[Alkyl-NVP-Copolymer] are hydrogels, while Narafilcon A, Filcon II 3, and Aerofilcon A are silicone hydrogels. The results of the adhesion experiments with incubation times of 1 h and 24 h are shown in Figure 3-2 A and B, respectively.

Table 3-1 Material properties of the investigated materials. The materials are divided in hydrogels and silicone hydrogels. Additionally, elastic modulus, water content, ionic properties, as well as contained wetting agents are listed.

Lens Material	Hydrogel (Hy) / Silicone Hydrogel (SiHy)	Elastic modulus / MPa	Water content / %	Ionic	Wetting Agent
Vitafilcon A	Hy	0.3	54	-	-
Ocufilcon F	Hy	0.3	55	+	-
P [Alkyl-NVP-Copolymer]	Hy	0.3	66	-	-
Narafilcon A	SiHy	0.66	46	-	+
Filcon II 3	SiHy	0.5	58	-	-
Aerofilcon A	SiHy	0.4	69	-	-

The experiments shared, that after 1 h and 24 h there were significantly more trophozoites adhering to two distinct contact lenses. One of these lenses, the P[Alkyl-NVP-Copolymer], is a hydrogel, the other one, the Aerofilcon A, is a silicone hydrogel. The significance of these results was proven by the t-test (see appendix 3), which showed that after one hour the difference between Vitafilcon A, Ocufilcon F, Narafilcon A and Filcon II 3 (low adhesion) compared to the P[Alkyl-NVP-Copolymer] lens with more adherent acanthamoebae was significant with $p < 0.01$ (**). A significant difference (* $p < 0.05$) in the adhesion quantity was also revealed for Aerofilcon A, with high adhesion in comparison to Ocufilcon F, Narafilcon A and Filcon II 3.

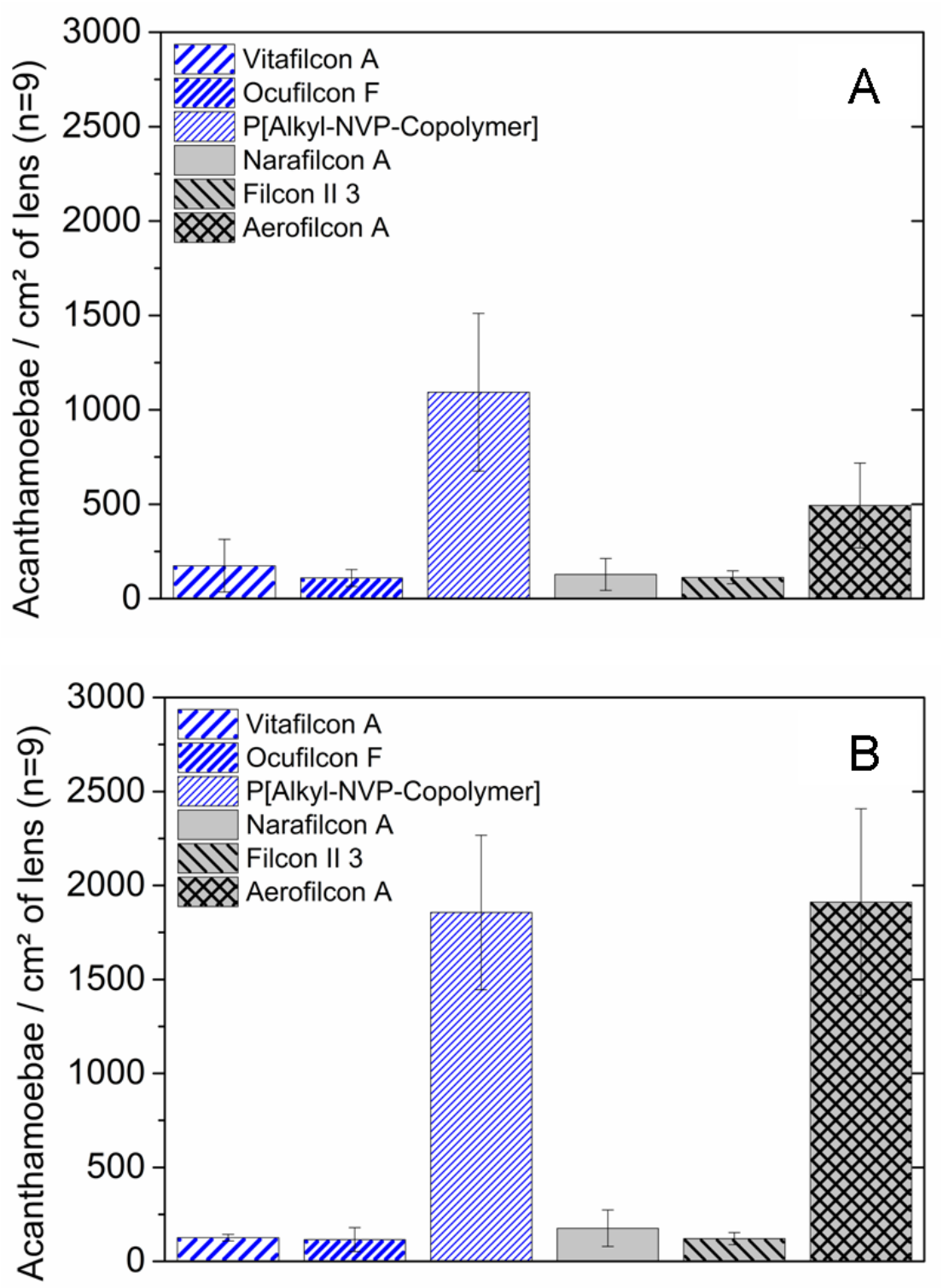

Figure 3-2 Average number of adhering *A. castellanii* trophozoites per cm² of lens after 1 h (A) and 24 h (B) of incubation. The first three lenses, named Vitafilcon A, Ocufilcon F and P[Alkyl-NVP-Copolymer] are Hy lenses (first three), Narafilcon A, Filcon II 3 and Aerofilcon A are SiHy (last three). Both Hy and SiHy are listed with increasing water content (n=9). The highest number of acanthamoebae was detected on the P[Alkyl-NVP-Copolymer] and on the Aerofilcon A lens. This effect was observed after 1h as well as after 24 h.

The results for the two sample t-test are shown in Table 3-2. The 24 h adhesion results showed the consistent trend: the adhesion to the P[Alkyl-NVP-Copolymer] was significantly higher than to Vitafilcon A, Ocufilcon F, Narafilcon A and Filcon II 3 at a significance level of $p < 0.001$ (***). Also to Aerofilcon A significantly more acanthamoebae (*** $p < 0.001$) were adhering than to those four low adhesion lenses.

Table 3-2 Results of the T-Test of Aerofilcon A and P[Alkyl-NVP-Copolymer] compared to the other tested materials. T-Test results are given for 1 h and 24 h incubation time. * describes a statistical significant result with a significance level of p < 0.05, ** depict a significant result with p < 0.01, and * depict a significant result with significance level p < 0.001.**

1 h	Aerofilcon A	P[Alkyl-NVP-Copolymer]	24 h	Aerofilcon A	P[Alkyl-NVP-Copolymer]
Vitafilcon A	Not significant	**		***	***
Ocufilcon F	*	**		***	***
P [Alkyl-NVP-Copolymer]	Not significant	-		Not significant	-
Narafilcon A	*	**		***	***
Filcon II 3	*	**		***	***
Aerofilcon A	-	Not significant		-	Not significant

In order to ensure that the PYG medium does not change the lenses' material properties, the contact lens swelling in buffered saline solution, in PYG, and in PYG with additional subsequent regeneration in buffered saline solution were measured. The average measured diameters of the lenses are graphically shown in Figure 3-3.
From the graph it becomes obvious, that there are no significant differences in the diameter of the lenses incubated either in saline solution or in PYG. Also the recovery in saline solution did not change the diameter of the lenses.

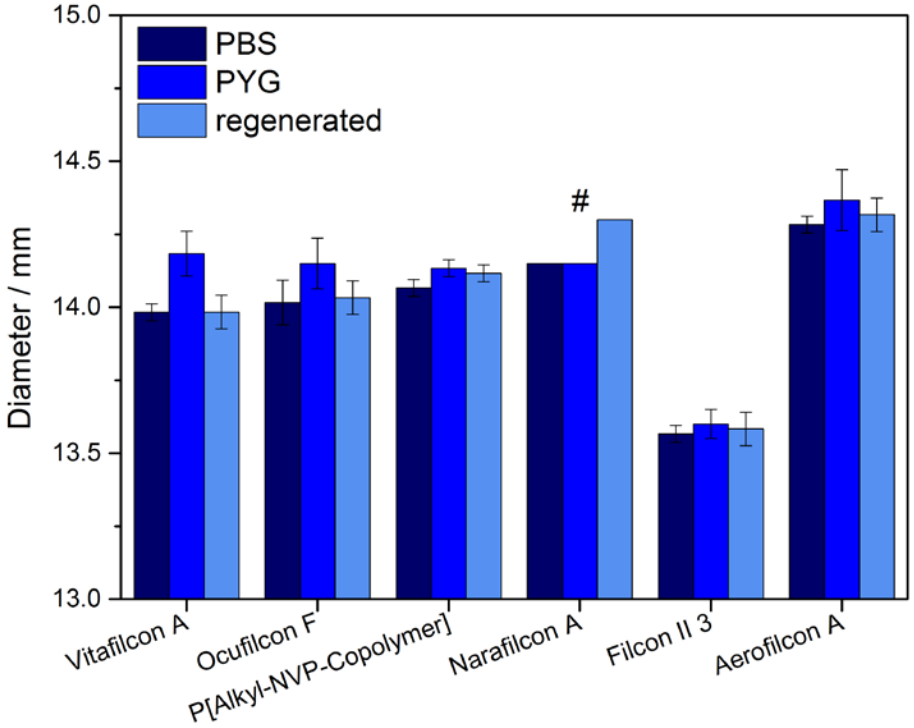

Figure 3-3 Diameters of the investigated lenses after 24 h incubation in PBS (dark blue), after 24 h incubation in PYG (blue) and after 24 h incubation in PYG and subsequent regeneration for 3 hours in PBS (light blue). In case of Narafilcon A (#) the values were the same in all measurements and therefore no error bars are presented here. The used medium does not have any influence on the contact lens diameter. Error bars mark the standard deviation.

3.3.2. Contact Lens Care and Disinfection

Contact lenses incubated with *A. castellanii* for 24 h were disinfected according to the manufacturer's recommendation. Figure 3-4 shows *A. castellanii* on an Aerofilcon A lens before rinsing and disinfection, while Figure 3-5 shows an Aerofilcon A lens after rinsing with multipurpose solution and disinfection with peroxide solution and neutralizing tablet. The images confirm that before the cleaning procedure many trophozoites are present on the surface of the contact lens. After the cleaning and disinfecting process, no acanthamoebae are adhering to the surface of the lens anymore. The same result could be shown for all investigated contact lens materials in all experiments. Moreover, no cysts and no non-adhering acanthamoebae were found in the investigated areas on all of the tested contact lenses.

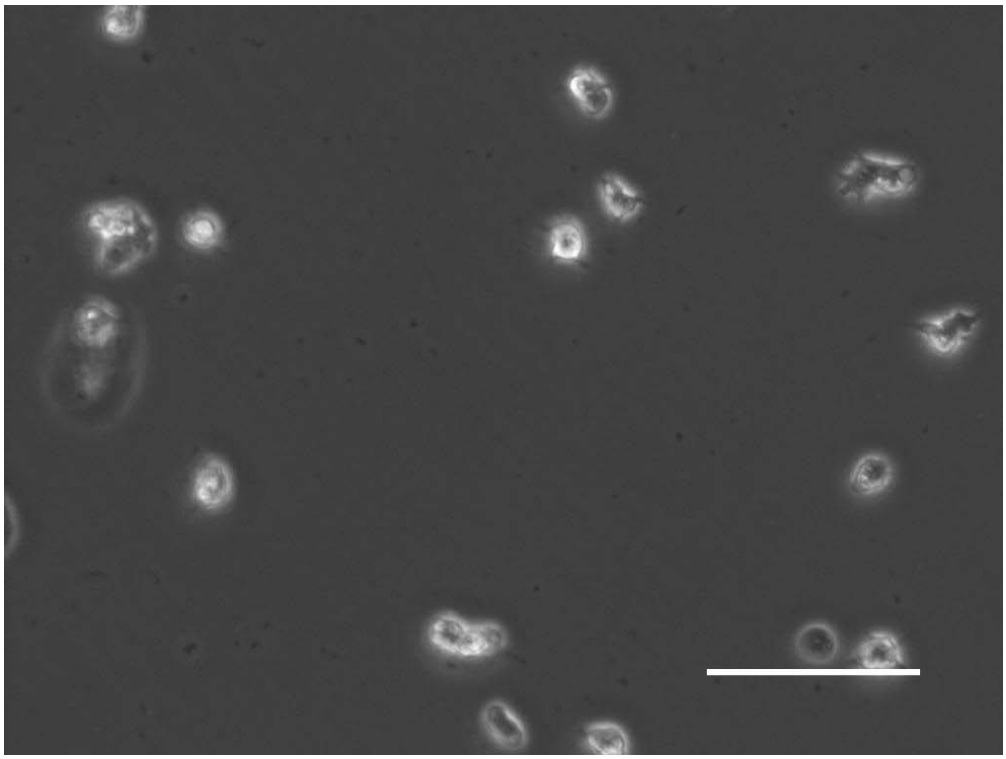

Figure 3-4 *A. castellanii* adhesion on Aerofilcon A (after 24 h incubation before cleaning). Many acanthamoebae are adhering on the surface. Without cleaning this lens material prior to application in the eye, acanthamoebae could potentially get into the eye and cause a sight-threatening keratitis. Scalebar = 100 µm.

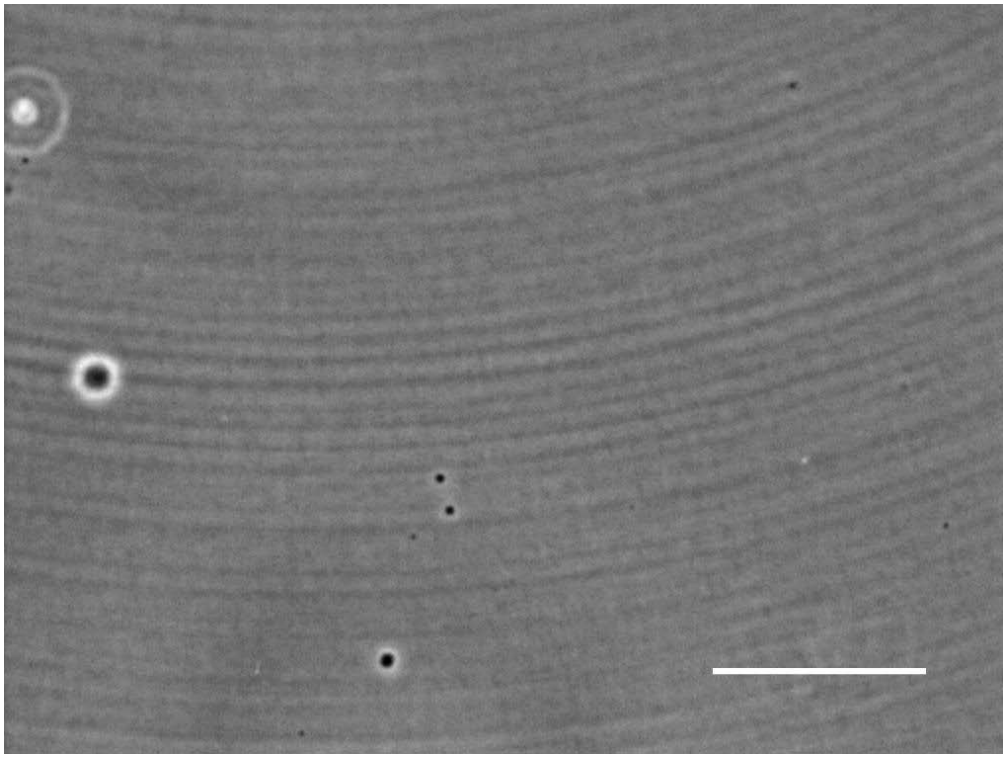

Figure 3-5 Aerofilcon A after incubation with *A. castellanii* and subsequent cleaning and disinfection. No living trophozoites or cysts could be identified on any sample. Therefore, the combination of both solutions is effectively removing acanthamoebae from the contact lens. Scalebar = 100 µm.

In order to investigate the effects of multipurpose solution and peroxide solution independently, *A. castellanii* were incubated in either of the solutions. After addition of the multipurpose solution, the trophozoites started to detach from the surface of the used petri dishes within a few minutes. The same effect was observed for the peroxide as well. After addition of the neutralizing tablet and incubation at RT overnight, all acanthamoebae appeared to be smaller, round up, and no intracellular movement could be observed. In case of the multipurpose solution incubated overnight, there were slight movements inside the acanthamoebae although they were smaller, and rounded up, and detached from the surface. In order to clarify and confirm the effects of the two solutions, two groups (10^5 and 10^6) of acanthamoebae were centrifuged separately, washed and resuspended in PYG. After two days of incubation in tissue culture bottles with PYG, there were clear differences between the acanthamoebae treated with multipurpose solution and peroxide solution. Only in case of the peroxide solution (Figure 3-6) in the experiment with initially 10^5 acanthamoebae, no adhering trophozoites were found on the surface. Only a few small rounded up acanthamoebae were observed in the bottles. In case of initially 10^6 acanthamoebae per petri dish, single living trophozoites were identified (~1 of 1000). Even after 5 days recovery, the number of trophozoites did only increase slightly.

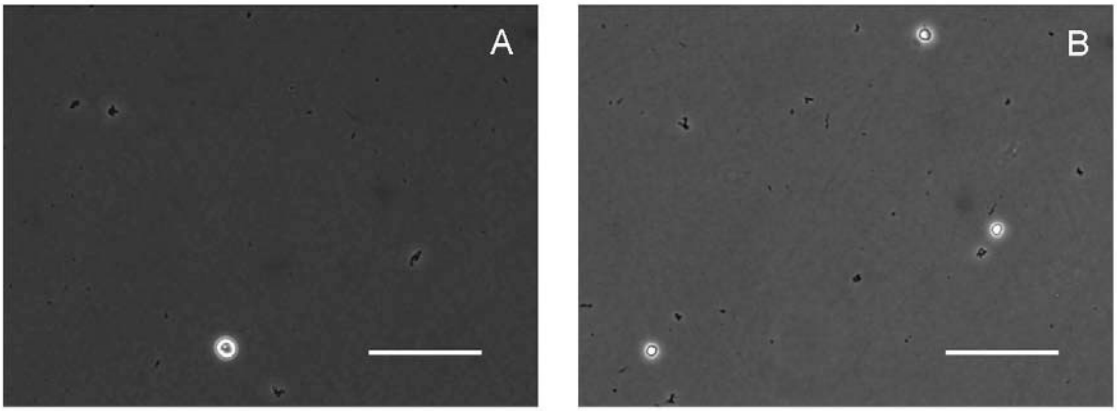

Figure 3-6 *A. castellanii* trophozoites (initially 10^6 acanthamoebae per petri dish) after incubation in peroxide solution with neutralizing tablet and recovery for 48 h (A) and after 5 days (B) in PYG medium. Nearly only rounded (i.e. weakly adhering) acanthamoebae can be observed on the surface. The cells are not in the cyst state and as the proliferation is nearly stopped it can be concluded that the cells are killed by the peroxide solution. Scalebar = 100 µm.

In the experiment, where acanthamoebae were incubated in the multipurpose solution, after two days significantly more *A. castellanii* trophozoites were found, which adhered to the surface (Figure 3-7).

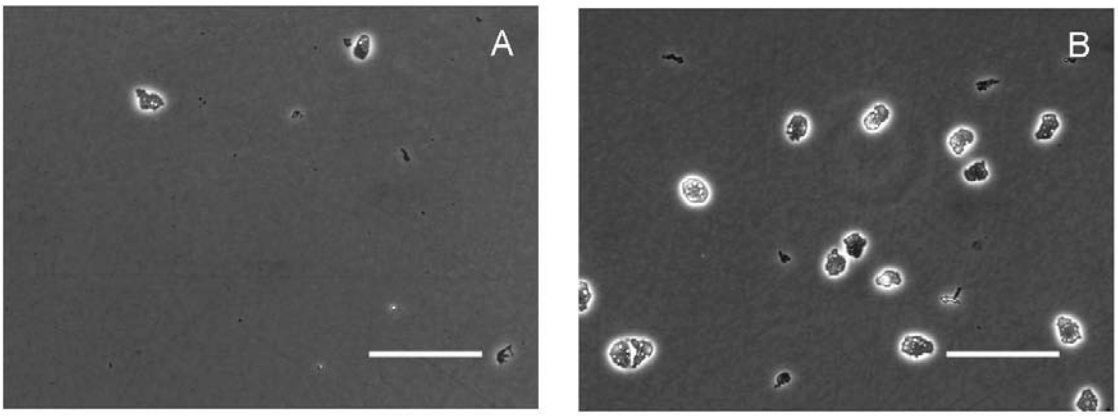

Figure 3-7 *A. castellanii* trophozoites (originally 10^6 acanthamoebae per petri dish) after incubation in multipurpose solution and recovery for 48 h (A) and after 5 days incubation in PYG medium (B). It becomes obvious that the trophozoites recovered from the multipurpose solution and proliferated again. After 2 days the trophozoites seem to be smaller but are already actively crawling on the surface. After 5 days the number of acanthamoebae as well as the size of the cells had increased. Scalebar = 100 µm.

After three more days the growth was checked again and there were many more trophozoites adhering to the surface of the tissue culture bottle, indicating a good proliferation.

3.4. Discussion

The adhesion of pathogenic acanthamoebae to soft contact lenses is known to be influenced by different factors such as water content, ionic nature, silicone content and surface coating. As it was shown for tissue cells, it is possible that cells can sense differences in the mechanical properties of materials. They react of different stiff substrate materials (~1 kPa up to 100 kPa) by changes in the cell spreading, adhesion structures (e.g. focal contacts), cell contraction, and in the constitution of the cytoskeleton [110]. Hints for the so called mechanosensing were also discovered in *Dictyostelium discoideum*. A signaling protein involved in mechanosensing has been observed to co-localize with molecular motors and filaments also involved in this process [112]. For that reason it is possible, that acanthamoebae can also sense differences in the elastic modulus of the substrate material. If this is true, differences in the adhesion quantity could be related to the elastic modulus of the materials used in this study.

The elastic modulus of the different tested lenses ranges from 0.3 to 0.66 MPa, which is much larger compared to the regimes, in which mammalian tissue cells respond to changes in substrate stiffness (several kPa). Aerofilcon A, which showed a high contamination probability has an elastic modulus of 0.4 MPa, P[Alkyl-NVP-Copolymer] has an elastic modulus of 0.3 MPa. Nevertheless, lenses with lower adhesion probabilities have similar elastic moduli. Two of the lenses with low amoebic adhesion, Narafilcon A and Filcon II 3 have slightly higher values for the

elastic modulus. Thus no interrelation could be identified between the adhesion quantity and the elastic modulus.

To further investigate why acanthamoebae adhered predominantly to two certain kinds of lenses, also the ionic properties, the influence of surface coatings and water content were compared. Only one of the tested contact lenses, the Ocufilcon F is an ionic lens, while all others are non-ionic. The Ocufilcon F lens shows a relatively low contamination with acanthamoebae compared to Aerofilcon A and P[Alkyl-NVP-Copolymer]. As the ionic lens does not show a higher contamination with *A. castellanii*, no correlation could be identified between the contamination level and the ionic properties.

The silicone content, which was found to influence the amoebic adhesion in case of first generation silicone hydrogels [107] but not in case of second generation silicone hydrogels [108], could also be excluded as influencing factor for the amoebic adhesion to the investigated materials. Aerofilcon A is a silicone hydrogel, whereas the P[Alkyl-NVP-Copolymer] is a hydrogel material, which shows that there is no preferred adhesion to one distinct material class. As all investigated silicone hydrogel materials are second generation silicone hydrogels, which contain more water and lack a surface coating compared to first generation silicone hydrogels, the result agrees with the earlier study [108].

The Narafilcon A lens used in this study has a surface coating, which should make the lens more hydrophilic. As the Narafilcon A lens shows a low amoebic contamination also the surface coating could be excluded as an influencing factor for amoebic adhesion. The water content in comparison seems to play a role in adhesion. This was referred in previous studies [105, 114]. Aerofilcon A (69 %) and P[Alkyl-NVP-Copolymer] (66 %) have the highest water content of all investigated materials (Vitafilcon A 54 %, Ocufilcon F 55 %, Narafilcon A 46 %, Filcon II 3 58 %) and show the highest contamination with acanthamoebae. The water content and the number of adhering acanthamoebae is not linearly related (Figure 3-2 A and B, Table 3-1).

In order to avoid contaminations with acanthamoebae a proper contact lens care and disinfection is necessary. For the contact lens materials used in this chapter, a cleaning protocol recommended by the manufacturer was conducted. First the lenses were washed with a multipurpose solution and subsequently disinfected in a peroxide solution combined with a neutralizing tablet. The results showed that by following this protocol the contamination with acanthamoebae could be avoided.

The multipurpose solution as well as the peroxide solution were tested independently for their effects on the acanthamoebae. In growth experiments it could be shown that the multipurpose solution leads to decreased adhesion of the acanthamoebae but does not kill them. In comparison to that the peroxide solution in combination with a neutralizing tablet effectively kills the acanthamoebae. For that reason the multipurpose solution should always be used in conjunction with regular disinfection

with peroxide solution and neutralizing tablet in order to avoid contamination with acanthamoebae.

The fact that no adhering acanthamoebae were found after the cleaning and disinfection of the lenses together with the results of the independent growth experiments, where the trophozoites detached from the surface immediately, leads to the conclusion, that adhesion is essential for the contamination with acanthamoebae. Non-adherent acanthamoebae can be washed away if the cleaning and disinfection protocols are followed. Nevertheless also if the adhesion was significantly reduced by using the multipurpose solution the user should not resign disinfection of the lenses in order to reduce the risk of a contamination to minimum.

4. Controlling Acanthamoeba Adhesion by Functionalized Surfaces

On their way to the target-cells in the corneal stroma and the optic nerves in the eye, acanthamoebae are able to move through the epithelial tissue. In order to pursue this movement they have to adhere to elements of the ECM, such as fibronectin or collagen. On this account experiments with different protein and carbohydrate coatings were carried out in order to evaluate their influence on adhesion of acanthamoebae.

The adhesion of pathogenic acanthamoebae to target-cells is the essential first step in the amoebic target-cell killing process. As the adhesion to target-cells has been suggested to be mediated by mannose [5-8], adhesion studies on acanthamoebae to mannose functionalized and non-functionalized surfaces were performed. In order to evaluate, whether the adhesion of pathogenic and non-pathogenic acanthamoebae is based on a similar mechanism but without target-cell killing in case of the non-pathogenic species, experiments were carried out with pathogenic *A. castellanii* compared to non-pathogenic *A. comandoni*.

In order to investigate, whether mannose alone is sufficient or if other surface molecules are required for stable adhesion, mannose-functionalized gold nanostructures were utilized. Furthermore, the influence of the density of mannose ligands on the adhesion properties was determined. For this purpose glass surfaces were covered with quasi-hexagonal patterns of gold nanodots with distances between single dots of 49 nm and 127 nm. The gold nanodots were specifically functionalized with mannose and the space between the dots was passivated against adhesion. In this way, different densities of mannose on the target-cell coat are mimicked and the influence on the adhesion of acanthamoebae was evaluated. Finally, atomic force microscopy (AFM) based force spectroscopy was employed to investigate the binding strength of *A. castellanii* to mannose using carbohydrate functionalized AFM cantilevers.

4.1. Adhesion of *A. castellanii* to Fibronectin and Matrigel Functionalized Surfaces

As pathogenic acanthamoebae can move through the tissue on their way to target-cells, different surface protein coatings were tested for amoebic adhesion. Typical approaches to mimic a protein composition, which is similar to that of the ECM, are the use of the protein fibronectin or protein mixtures such as Matrigel™ [118]. Fibronectin is a glycoprotein in the extracellular matrix, which plays an important role in tissue regeneration, cell adhesion and cell migration [35]. Matrigel™ is secreted by Engelbreth-Holm-Swarm mouse sarcoma cells. It mainly consists of laminin, entactin and collagen, which can also be found in the ECM [36]. Therefore, both fibronectin and Matrigel™ were used for surface functionalization of glass slides in order to investigate their influence on the number of adhering *A. castellanii* trophozoites.
Fibronectin, laminin, collagen and Matrigel™ have already been subject in different studies about the number of adhered pathogenic and non-pathogenic acanthamoebae other than *A. castellanii* [118-120]. It has been observed that pathogenic *A. polyphaga* preferentially bind to collagen I and laminin followed by fibronectin [118]. Pathogenic *A. culbertsoni* show increased binding to laminin and collagen followed by fibronectin. For this species a laminin binding protein was detected but not in the non-pathogenic *A. astronyxis* [120].

4.1.1. Materials and Methods

Matrigel-Functionalized Surfaces

For the functionalization of glass substrates with Matrigel™ (BD Biosciences, Heidelberg, Germany), round cover slips (∅ 24 mm) were cleaned with ethanol (70 %) (Walter CMP GmbH, Kiel, Germany), placed in the wells of a six well plate, and subsequently washed with sterile home-made phosphate buffered saline (1×PBS) (PBS composition see appendix 4). Matrigel™ (10 µL) was mixed with DMEM (990 µL) (Biochrom, now Merck KGaA, Darmstadt, Germany); and the cleaned glass slides were covered completely with this solution for 60 min at room temperature (RT). Afterwards, the solution was removed from the surface and the coated cover slips were cleaned once more with PBS in order to obtain thin film of Matrigel™ on the substrate.
A. castellanii were cultured as described in section 3.2.1. A defined number of trophozoites (10^5 acanthamoebae in 1.5 ml PYG) was seeded on each functionalized glass slide and incubated at RT to let the acanthamoebae adhere to the surface. After 20 min the medium was removed, the cover slips were rinsed with sterile medium and placed in a new well with clean medium. 30 images per sample were recorded by using a phase contrast microscope (CKX41, Olympus GmbH, Hamburg, Germany) with a CCD camera (Hamamatsu C9300, Hamamatsu, Japan), the number of adhering

A. castellanii was evaluated. The experiment was conducted twice and each in triplicate (n=6).

Fibronectin-Functionalized Surfaces

Prior to functionalization with fibronectin (Sigma-Aldrich Chemie GmbH, Munich, Germany), round cover slips (∅ 24 mm) were cleaned as described before (s. Matrigel). A fibronectin solution was prepared in PBS (50 µg/ml). The glass slides were covered completely with the fibronectin solution and incubated for 30 min at RT. Afterwards, the glass slides were placed in a six well plate and 10^5 *A. castellanii* were seeded on the samples and incubated for 20 min to let them adhere to the surface. Subsequently, the samples were rinsed with sterile medium and placed into new wells. The samples with the adherent *A. castellanii* were imaged with the phase contrast microscope and the images were evaluated as described for Matrigel™. Again, the experiment was repeated twice and each in triplicate (n=6).
Uncoated cleaned glass cover slips (∅ 24 mm, round) were used as reference. The same number of *A. castellanii* were seeded on the cleaned glass slides, incubated at RT for 20 min to let the acanthamoebae adhere, rinsed with sterile medium and placed into new wells. Images were taken with the same microscope and camera as used for Matrigel™ (30 images per sample).

4.1.2. Results

The number of pathogenic *A. castellanii* adhering to protein coated surfaces was compared and uncoated glass slides were used as reference. The results of these experiments are summarized in Figure 4-1.
The adhesion studies on substrates coated by fibronectin and matrigel compared to an uncoated glass sample as a reference showed that the number of adhering *A. castellanii* trophozoites increased from glass to fibronectin to matrigel. The amount of adhering acanthamoebae is given in % normalized to the glass reference. The significance of the results was proven by a two sample t-test, which showed, that the difference in the number of adhering acanthamoebae between the glass reference and the fibronectin-coated sample is relevant at a significance level of *** $p < 0.001$. Furthermore, the difference between fibronectin and Matrigel™ was determined to be significant a level of ***$p < 0.001$.

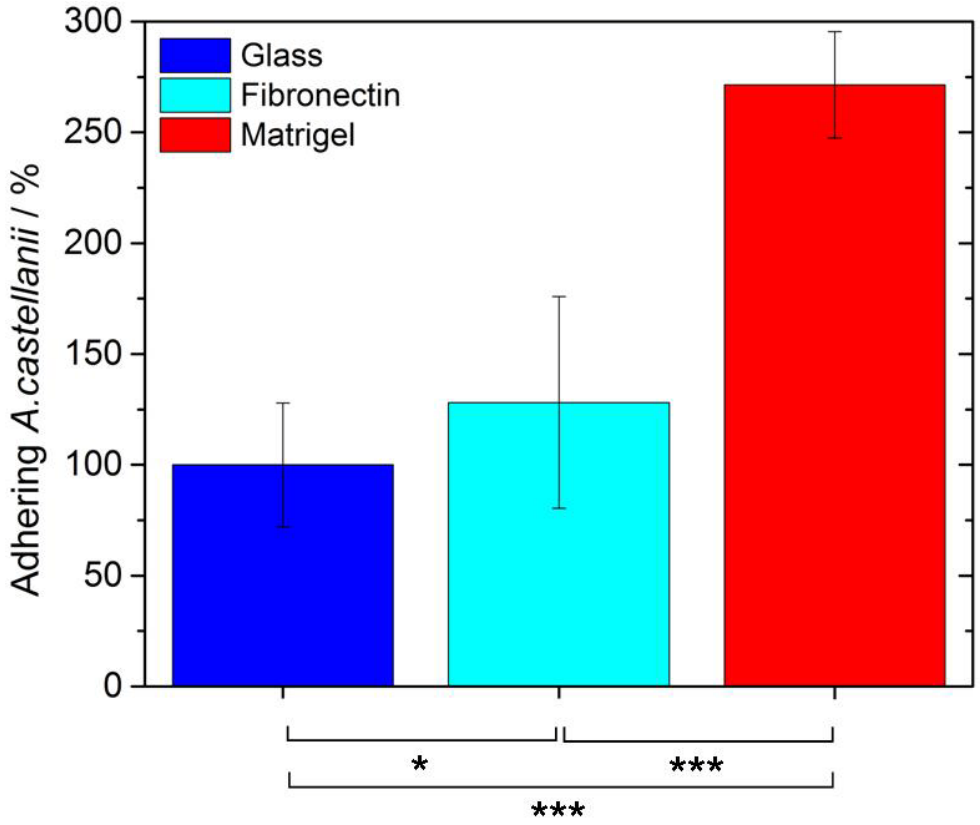

Figure 4-1 Number of adhering *A. castellanii* on protein-functionalized glass surfaces. The bars show the results for uncoated glass reference (blue), fibronectin coated glass (cyan), and matrigel coated glass (red). The amount of adhering acanthamoeba is given in % and is normalized to the glass reference. To the fibronectin coated samples (* $p < 0.05$) as well as to the matrigel coated surfaces significantly more (* $p < 0.001$) acanthamoeba were adhering than to the glass reference. When comparing the matrigel coated substrates to the fibronectin coated ones, significantly more (*** $p < 0.001$) acanthamoeba are adhering to the matrigel coated sample. The experiment was conducted twice and each in triplicate (n=6). Error bars depict the standard deviation.**

4.1.3. Discussion

The experiments revealed significant differences in the number of adhering *A. castellanii* on the different substrates. The highest amount of adhering *A. castellanii* was found on the matrigel coated surface followed by fibronectin and the glass control. Matrigel™ is a protein mixture containing mainly collagen, laminin and entactin. In a previous study fibronectin, collagen IV and laminin were found to promote the adhesion of pathogenic *A. polyphaga* [118]. This study had reported the highest adhesion to surfaces coated with laminin, followed by collagen IV, and fibronectin. In another study a significant difference in the number of adhering acanthamoebae on collagen I, laminin and fibronectin compared to a glass reference was also shown for *A. culbertsoni* and the non-pathogenic *A. astronyxis*. The pathogenic *A. culbertsoni* showed significantly higher adhesion to the laminin and collagen I coated surfaces than *A. astronyxis*, the adhesion to fibronectin was comparable for both strains [120]. Furthermore, a laminin binding protein was

identified in *A. culbertsoni*, which was not found in *A. astronyxis* [120]. Consequently, a reason for the increased number of adhering acanthamoebae to the matrigel coated surface might also be attributed to the presence of a laminin binding protein. Beside the laminin binding protein, also the MBP present in *A. castellanii* [5, 7-8] could cause an increase in the number of adhering acanthamoebae. In case of laminin it is known that it contains mannose structures [121], which also lead to mannose-specific binding of acanthamoebae. Matrigel is a protein mixture, which amongst other proteins contains laminin. Therefore, binding proteins in pathogenic acanthamoebae bind to laminin and potentially to mannose on the matrigel-functionalized surface, leading to an increased adhesion and consequentially to a higher number of adhering acanthamoebae.

Possibly also the glycoprotein fibronectin contains mannose. In hamster-plasma fibronectin mannose molecules could be detected [122]. Mannose contents of fibronectin would explain the observed increased amount of adhering *A. castellanii* on fibronectin coated substrates. Gordon et al. showed that the adhesion of *A. polyphaga* to the extracellular matrix proteins collagen, laminin and fibronectin could be inhibited by adding α-mannopyranoside, which is a conformation of mannose [118]. This had also been observed for the adhesion of *A. culbertsoni* to fibronectin and collagen I [119]. These examples show that the MBP is involved in the amoebic adhesion to these proteins. The binding sites for the mannose molecules are saturated by adding mannose to the culture medium. Therefore, they are not available anymore for binding to the mannose molecules on the protein-functionalized surfaces. This leads to the conclusion that the increased adhesion to matrigel and fibronectin is an effect related to the pathogenic potential of acanthamoebae due to the expression of the MBP and the laminin binding protein.

4.2. Acanthamoeba Binding to Mannose-Functionalized Beads

As described in section 1.2.3 an essential prerequisite for the pathogenicity of acanthamoebae is the presence of a mannose binding protein (MBP) in the lipid membrane of the acanthamoebae, which itself contains mannose [5, 7-8, 123]. The MBP helps acanthamoebae to specifically bind to mannose present on the cell coat of the host cells [5]. The mannose-mediated binding is the essential first step in this cell killing machinery and for that reason this type of adhesion process has to be understood in more detail.

In order to mimic the target-cell coat, in this section mannose coated agarose beads and non-coated sepharose beads were used to compare the adhesion behavior of pathogenic *A. castellanii* to that of non-pathogenic *A. comandoni*. As pathogenic acanthamoebae express the MBP, while non-pathogenic species do not, differences in the number of adhering acanthamoebae are expected. The aim of the experiment is to test this hypothesis and to evaluate, whether this hypothesis is correct.

4.2.1. Experimental Procedure

Mannose/Agarose and Sepharose Coated Beads

Before the experiment *A. castellanii* as well as *A. comandoni* were cultured in tissue culture bottles (75 ml, Sarstedt AG & Co., Nümbrecht, Germany) containing PYG medium as described in 3.2.1.

For the experiment either D-Mannose Agarose beads or Sepharose CL-4B beads (both in suspension with destilled water) with sizes between 40 and 165 µm (both from Sigma-Aldrich Chemie GmbH, Munich, Germany) were used, respectively. Agarose is a polysaccharide consisting of D-Galactose. Sepharose is built up by cross-linked sepharose molecules containing a small amount of agarose molecules. For preparation of the experiment both bead solutions were diluted (1:10) in PBS and centrifuged at 1000 rpm for 5 min. The PBS was replaced and the washing procedure was repeated twice ending up with a 1:10 diluted solution of the beads in PBS. In order to achieve comparable results, the bead solutions were given into a tissue culture bottle (25 ml, Sarstedt AG & Co., Nümbrecht, Germany) and 30 images of each solution were recorded by using a CKX41 phase contrast microscope (Olympus GmbH, Hamburg, Germany). For statistical evaluation, the number of beads was counted, and the average size of the beads was calculated. In order to compare the carbohydrate-mediated adhesion behavior of pathogenic and non-pathogenic acanthamoebae, 3×10^5 acanthamoebae in 5 ml of PYG Medium of either *A. castellanii* or *A. comandoni* were seeded in tissue culture bottles (25 ml, Sarstedt AG & Co., Nümbrecht, Germany). To each bottle, 0.5 ml of one of the bead solutions were added..

By using an inverted phase contrast microscope (Olympus CKX41) equipped with a camera (C9300, Hamamatsu, Hamamastu, Japan), 50 images of each bottle were

taken at arbitrary positions right after addition, after 2 h and after 4 h of incubation at RT. For the evaluation, the number of acanthamoebae adhering to the beads ($N_{adhAmoebae}$), as well as the total numbers of beads ($N_{totalBeads}$) and the total number of acanthamoebae ($N_{totalAmoebae}$) in the analyzed areas of the bottles were counted. The number of adhering acanthamoebae per bead ($N_{adhAmoebae}$ / $N_{totalBeads}$) as well as the amount of adhering acanthamoebae of the total number of acanthamoebae ($N_{adhAmoebae}$ / $N_{totalAmoebae}$) was calculated.

4.2.2. Results

The average size of the two different kinds of beads was measured to ensure the comparability of the results. The results are shown in Figure 4-2.

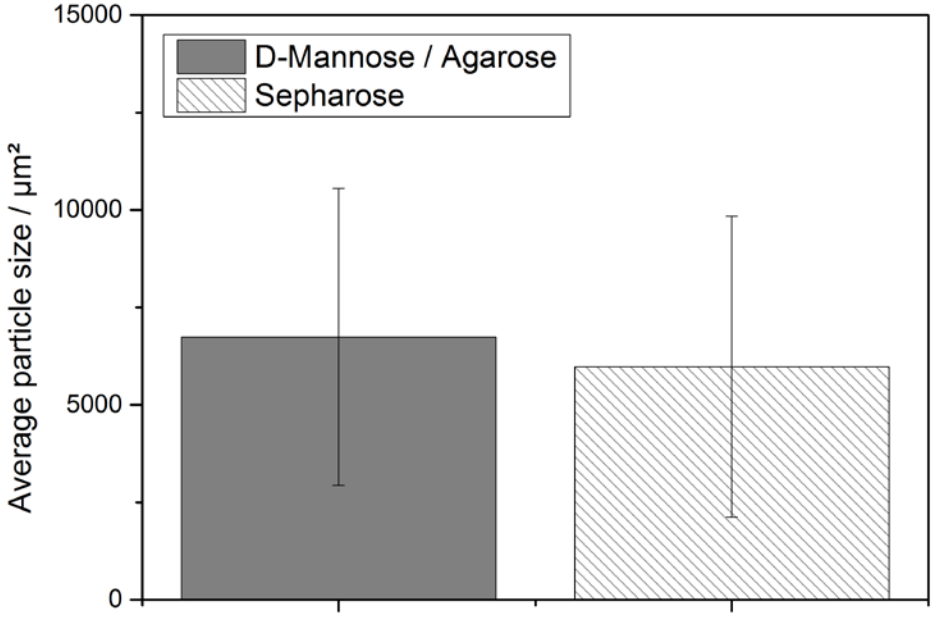

Figure 4-2 Size evaluation of Agarose (grey) and Sepharose (white with stripes) beads. The average size of both kinds of beads is nearly the same. Therefore, the results of the adhesion studies of *A. castellanii* and *A. comandoni* on these beads should be comparable. Error bars depict the standard deviation.

Figure 4-2 shows that the average particle sizes are nearly the same for both kinds of beads. In order to verify this, a two sample T-test was applied, which showed that there are no significant differences in the average particle size ($p = 0.24$). The beads were subsequently used for differentiating the adhesion properties of pathogenic and non-pathogenic acanthamoebae. In Figure 4-3 A and B the differences in the adhesion of pathogenic *A. castellanii* to mannose/agarose beads and sepharose beads are clearly visible.

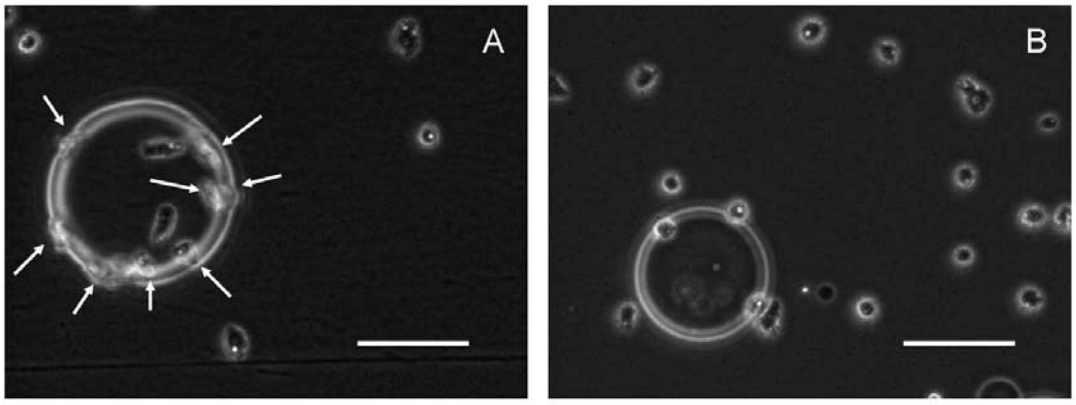

Figure 4-3 A *A. castellanii* adhering to a mannose-functionalized agarose bead. The trophozoites are attached to all sides of the bead. As the image was recorded by a simple phase contrast microscope, the acanthamoebae adhering to parts, which are not in focus, appear as a shadow and are not sharp (white arrows). Around the bead only few trophozoites are adhering to the surface of the six well plate. This indicates that most acanthamoebae adhere to the beads. B *A. castellanii* adhering to a sepharose bead and the surface of the six well plate. The acanthamoebae do not adhere specifically to the sepharose bead and seem to stick only slightly. Around the sepharose bead many acanthamoeba are ahdering to the surface of the six well plate. Scalebar = 100 µm

In Figure 4-3 A, a mannose-coated agarose bead is shown. To this bead many *A. castellanii* are adhering. As the image is taken in a non-confocal phase contrast microscope, parts, which are out of focus, appear diffuse. The shadows of the surface are acanthamoebae adhering to the surface of the bead (white arrows). During the experiment it could also be observed that the mannose-specific binding is very strong and that trophozoites can exert large forces after specific adhesion. Floating beads in the medium could be kept in a fixed position by a single acanthamoeba adhering to the bead and the surface of the petri dish. In comparison, Figure 4-3 B shows a sepharose bead incubated together with *A. castellanii*. It is obvious, that almost no acanthamoebae are adhering to the bead. Significantly more acanthamoebae are adhering to the petri dish instead of the sepharose bead. So this situation is clearly different from the result for mannose-agarose beads. The quantitative results of these experiments are given in Figure 4-4 A and B. The diagram (A) shows that the number of adhering *A. castellanii* (red) per mannose-coated bead increases with increasing time. In contrast, to the sepharose beads, the pathogenic *A. castellanii* only shows little adhesion, which is even independent of incubation time. In comparison to these results, the non-pathogenic *A. comandoni* (blue) shows only low adhesion numbers of adhering acanthamoebae to both kinds of beads, functionalized and non-functionalized ones (A). There is no significant increase in the number of adhering *A. comandoni* for the different bead types with time. The same tendencies could also be observed for the amount of adhering acanthamoebae with respect to the total number of acanthamoeba (B).

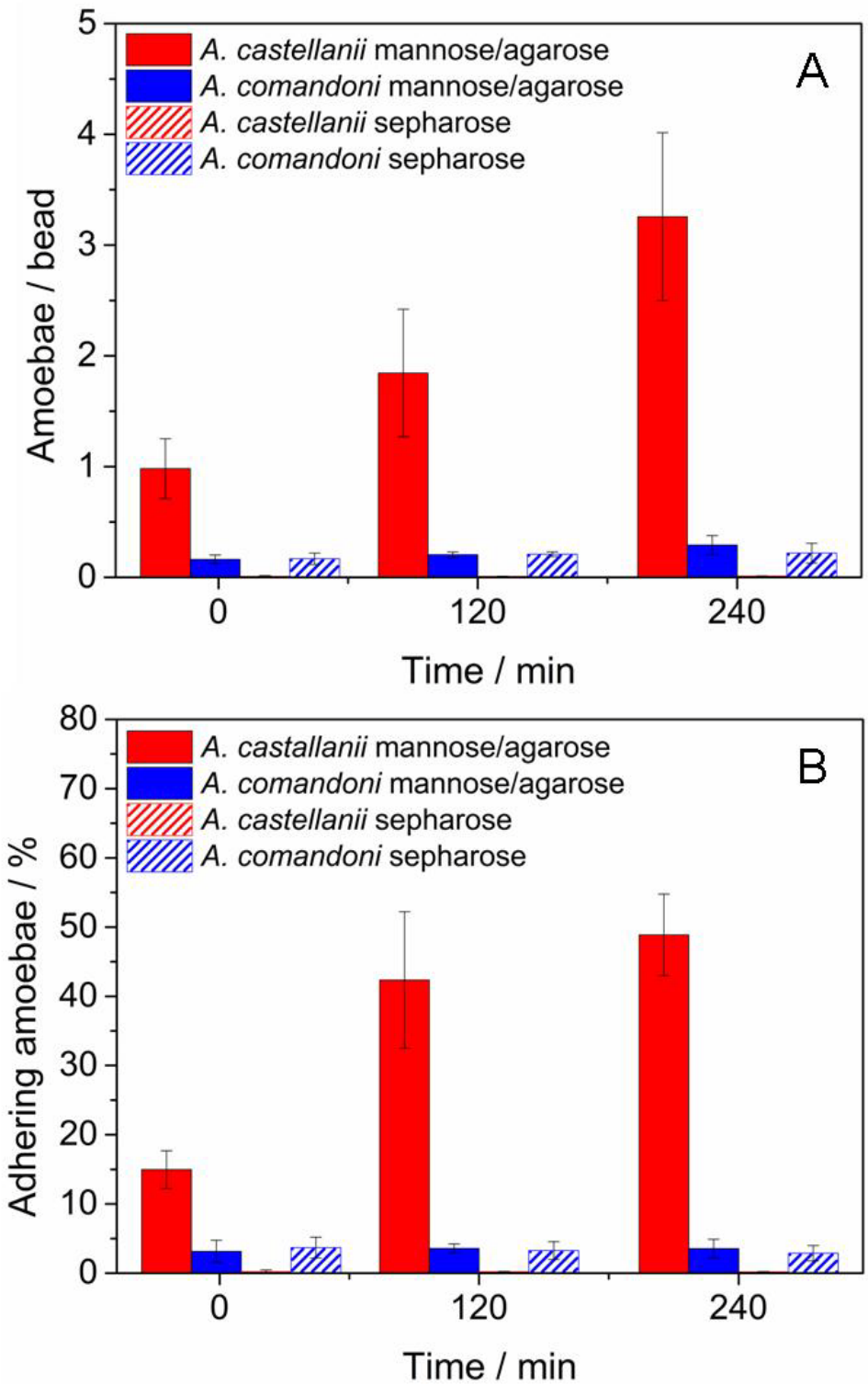

Figure 4-4 Adhesion of *A. castellanii* and *A. comandoni* trophozoites to beads made of mannose-functionalized agarose and non-functionalized sepharose. Number of adhering acanthamoebae per bead (A) and amount of adhering acanthamoebae of total number of acanthamoeba (B). With increasing time the number of adhering pathogenic *A. castellanii* to the mannose/agarose (A) as well as the amount of adhering *A. castellanii* increases (B). To sepharose beads, there is no specific adhesion and no increase of number of adhering *A. castellanii*. with time. Non-pathogenic *A. comandoni* does not show any specific adhesion to either of the beads, but the number of adhering *A. comandoni* to both kinds of beads as well as the amount of adhering *A. comandoni* is larger than that of *A. castellanii* to sepharose beads. Error bars depict the standard deviation.

4.2.3. Discussion

The number of pathogenic and non-pathogenic species of acanthamoebae adhering to two different kinds of beads was compared in the previously described experiments. As the diameter of the beads varies between 40 and 165 µm, a statistical size evaluation of the beads was carried out. It showed that there are no significant differences in the average sizes. Therefore, it is assumed that a similar distribution of bead sizes is present and that experiments with both types of beads are comparable. The results from the adhesion study clearly show that the adhesion of pathogenic *A. castellanii* to mannose-functionalized beads increases with increasing time. The number of non-pathogenic *A. comandoni* adhering to both types beads is much lower than for *A. castellanii* adhering to mannose-coated agarose beads, but is larger than for *A. castellanii* on sepharose beads. During the experiments with *A. comandoni* it could be observed that overall the adhesion also to the substrate was not as high as that of *A. castellanii*. In cell culture bottles of *A. comandoni* more swimming acanthamoebae were observed than in case of *A. castellanii*. This indicates that the overall, unspecific adhesion to substrates is also related to the pathogenic potential of these two acanthamoeba species. The findings of this study agree with previous studies on the mannose-specific adhesion of acanthamoebae, which showed that the pathogenicity of acanthamoebae is related to the expression of a MBP and therefore to adhesion to mannose [5, 7-8]. Pathogenic acanthamoebae express higher amounts of this protein and consequently the adhesion to the mannose containing target-cell coat increases. The results of the experiments reveal that *A. castellanii* express significantly higher amounts of the MBP than *A. comandoni*. Hence, it was here confirmed that the pathogenic potential of *A. castellanii* is also much higher. As described in the results, *A. castellanii* was able to stably fix the mannose-functionalized beads to one position. This is a considerable effect as the beads in this experiment are up to six times larger than the acanthamoebae. The experiments on *A. comandoni* and *A. castellanii* revealed significant variations in the mannose-specific adhesion between the two species. Due to these severe differences in the results, in the further mannose binding experiments *A. castellanii* was used, exclusively. In conclusion, the use of mannose coated beads and non-coated beads to evaluate the pathogenic potential of acanthamoebae is an easy model to simulate the contact formation between trophozoites and target-cells.

4.3. Mannose-Functionalized Gold Nanostructures

As shown by the experiments in the previous section 4.2, there are large differences in the adhesion of pathogenic and non-pathogenic acanthamoebae to carbohydrate-functionalized surfaces. Especially mannose has turned out to have a significant influence on the adhesion properties of pathogenic acanthamoebae [5, 8, 50]. These experiments quantitatively showed a significant difference in the mannose-specific binding between the distinct species of acanthamoebae. Pathogenic *A. castellanii* can specifically sense mannose in the cell coat of target-cells. It triggers the formation of a close contact to the target-cell that initiates the extracellular killing mechanism [5-6].
In order to elucidate the molecular mechanisms behind the specific mannose-mediated adhesion of *A. castellanii*, the mannose contents of the target-cell coat should be mimicked in a more precise way. Towards this end, the technique of diblock copolymer micelle nanolithography is used to create a quasi-hexagonal pattern of gold nanodots, where the gold dots are specifically functionalized with mannose. By controlling the spacing between the quasi-hexagonally arranged gold nanodots, the density of the mannose molecules on the surface can be precisely arranged. This imitates the distribution of individual mannose sugars as presented by the surface coat of a target-cell. The aim is to investigate, whether the acanthamoebae trophozoites need a certain density of mannose molecules in order to form a contact to the target-cell. In a first experiment, two different densities of gold nanostructures are created and functionalized, and the spreading of the acanthamoebae is evaluated. A schematic view of the functionalized nanostructure interacting with the transmembrane MBP of the acanthamoebae is shown in Figure 4-5.

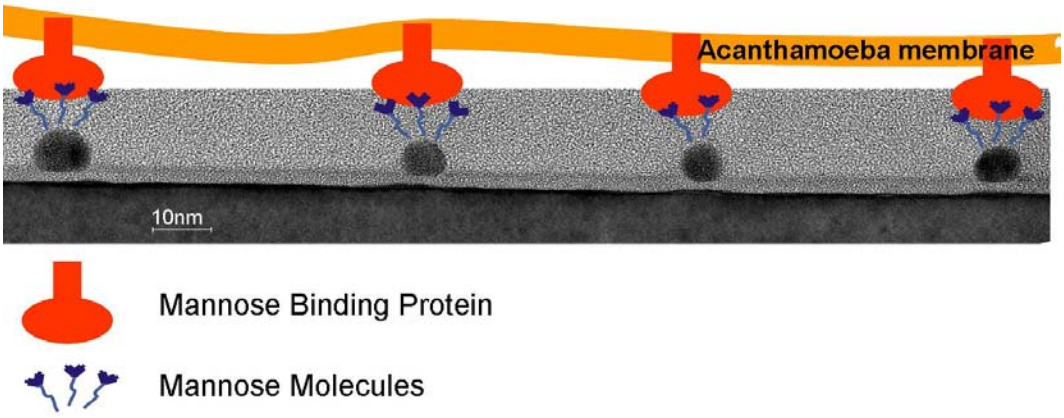

Figure 4-5 TEM image of gold nanodots on a silicon substrate (dark grey). On the surface a thin oxide layer is present (grey beneath gold dots). The mannose molecules on the dots are visualized by blue structures. The membrane of the acanthamoeba is schematically shown (yellow) containing mannose binding proteins (orange). Modified from [73].

In this kind of experiment the acanthamoebae do not exclusively adhere to the functionalized gold dots but also non-specifically to the glass surface in between the dots. For that reason in the further experiments the free space between the gold dots is passivated, i.e. with an adhesion inhibiting polymer, before further functionalization with mannose. PLL-g-PEG is a polymer, which is known for its passivating property against mammlian cell adhesion [96] and can also be applied for acanthamoeba. But preliminary tests revealed that is not suitable for the passivation of gold nanostructures, since it is electrostatically bound to the surface and the binding is lost during the gold dot functionalization procedure. In order to achieve a stable passivation instead a methoxy PEG Silane is used for covalent binding of the PEG to the glass substrate. Gold nanostructures with different spacings are passivated and subsequently functionalized with mannose (Figure 4-6). Spreading of the trophozoites is evaluated and compared to simple glass slides and nanostructures, which were passivated.

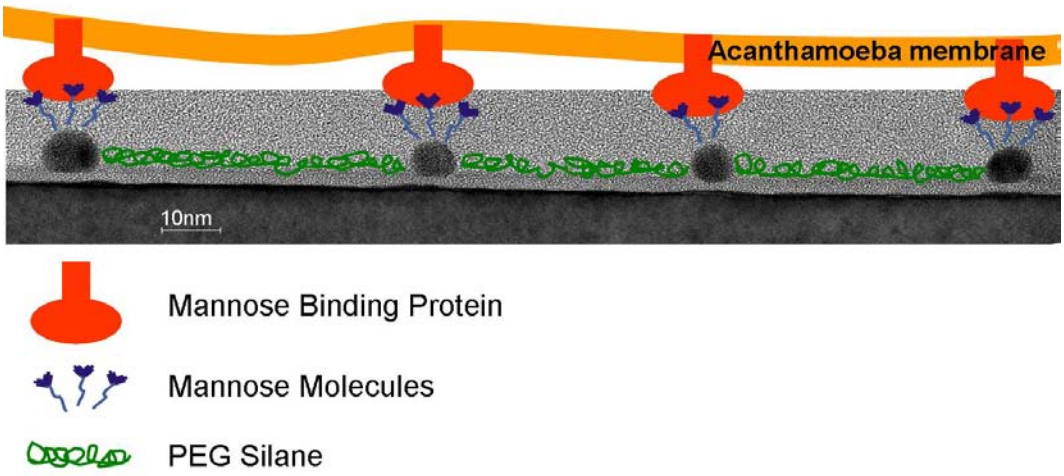

Figure 4-6 TEM image of gold nanodots on a silicon substrate (dark grey). On the surface a thin oxide layer is present (grey beneath gold dots). The mannose molecules on the dots are visualized by blue structures. The membrane of acanthamoeba is schematically shown (yellow) containing mannose binding proteins (orange). The inter-particle space is passivated by using a PEG Silane (green).

In order to prove that the observed effects can be attributed to a specific binding to mannose, additional experiments are carried out with glucose-functionalized gold nanostructures. Glass slides as well as non-functionalized nanostructures are used as control samples to ensure a healthy state of the acanthamoebae and serve as comparison to the functionalized nanostructures.

4.3.1. Experimental Procedures

Fabrication of Gold Nanostructured Surfaces

The preparation of the micellar solutions, which were needed for diblock copolymer micelle nanolithography, was carried out in the clean room. The PS(110000)-P2VP(52000) copolymer (Polymer Source Inc., Quebec, Canada) consisting of polystyrene (PS) (110000 g / mol) and poly-2-vinylpyridine (P2VP) (52000 g / mol) was weighted on a microbalance. The chemical structures are given in Figure 4-7.

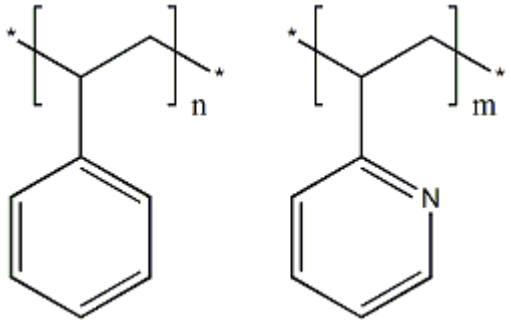

Figure 4-7 Chemical formulas of the components of the block copolymer. The copolymer consists of polystyrene (PS) (left) and poly-2-vinylpyridine (P2VP) (right). The PS is hydrophobic, while the P2VP is hydrophilic. Above the critical micelle solution in a solvent (toluene), micelles of the block copolymer form, where the PS block is in contact with the solvent, while the P2VP is oriented towards the center of the micelle.

The concentration of the copolymer in toluene was adjusted in toluene (Merck KGaA, Darmstadt, Germany) to a value above the critical micelle concentration (here 4 mg/ml). The solutions were stirred overnight in a closed flask in order to ensure a homogenous solution. After 24 h stirring, gold(III) chloride trihydrate ($HAuCl_4$ $3H_2O$) (Sigma-Aldrich Chemie GmbH, Munich, Germany) was added to the solutions at a concentration calculated according to

$$Mass\,of\ gold\,[mg] = \frac{Mass\,of\ polymer\,[mg]}{MW\ of\ polymer\,[g \setminus mol]} * 494.3 * 0.5 * MW\ of\ \mathrm{HAuCl_4}\,[g \setminus mol] \qquad (3)$$

MW: molecular weight.

After the addition of the gold(III) chloride trihydrate, the solutions were again stirred for 24 h on a magnet stirrer.

For the production of the gold nanostructures, glass cover slips of different sizes (∅20 mm, 22 mm, 24 mm round, 24 mm squared) were cleaned in piranha solution (H_2O_2 and H_2SO_4, 1 : 1). The piranha solution is an oxidizing agent, which removes organic residues and makes the glass slides more hydrophilic. The deposition of the copolymer solutions onto the glass cover slips was carried out by using a spin coater (WS-650-23NPP, Laurell Technologies Corporation, North Wales, USA) an appropriate vacuum pump. The spinning speed influences the inter-particle distanced

(IPD) of the gold nanodots, higher speed causes larger distances. For that reason different speeds were applied. For the spin coating, the glass slide was placed on the spin coater and the vacuum pump was switched on in order to keep the sample in a fixed position. The spinning was started and 50 µl of the polymer solution was dropped on the sample by a microliter pipette (Brand GmbH & Co. KG, Wertheim, Germany) as soon as the spinning speed was reached. The speed was kept for 1 min to let the micelles assemble on the surface in a quasi hexagonal pattern. After stopping the spin coater the samples were placed on a sample holder and dried for a few minutes. Subsequently, the samples were plasma treated in an H_2 / Ar plasma (0.4 mbar) with the plasma machine Sentech SI100 (Sentech Instruments GmbH, Berlin, Germany)to reduce the gold salt to elementary gold. Samples were produced with spinning speeds of 1000 rpm, 7000 rpm and 12000 rpm.

Characterization of inter-particle Distances

For characterization of the particle densities SEM images were taken by using the Carl Zeiss Ultra Plus SEM (Carl Zeiss AG, Oberkochen, Germany). This was carried out with the friendly help of Laith Kadem.
Images were recorded by using an in-lens secondary electron detector at different magnifications.
From the SEM images the IPDs could be calculated. For this purpose a hexagonal pattern of gold nanodots was assumed and the number of gold dots per area was determined. The distance d_{dots} between the single gold dots was calculated according to the formula

$$d_{dots} = \sqrt{\frac{2}{\sqrt{3}n}} \qquad (4)$$

with n = number of dots / area.

The IPDs were determined manually and with a MATLAB program written by Julia Purtov by the described procedure.

Passivation of inter-particle Space

Glass cover slips with gold nanostructures as well as piranha cleaned glass cover slips without nanostructures were passivated using a PEG silanization reaction. For this reaction the glass slides of different sizes with nanostructures were placed into a Schlenk flask, which was connected to a Schlenkline. The Schlenkline was connected to a nitrogen bottle and set under nitrogen atmosphere including the flask with the samples.
In the next step, a vacuum was generated in the flask using a vacuum pump of the type Vacuubrand 2C (Vacuubrand GmbH & Co. KG, Wertheim, Germany). The flask was heated using a hot air gun and subsequently the bottle with the samples was again set to nitrogen atmosphere. This process is repeated three times in order to achieve a

dry atmosphere for the silanization reaction. In the following step abs. toluene (Sigma-Aldrich GmbH, Munich, Germany) was filled into the flask under reverse flow of nitrogen by injecting it with a syringe through the silicone rubber septum, which was used for sealing the flask. Right afterwards, the methoxy PEG silane, mPEG-Si (2000 g / mol) (Figure 4-8) (Nanocs Inc., New York, USA), was added to the flask again under reverse flow of nitrogen. Samples were incubated at RT for three to four days.

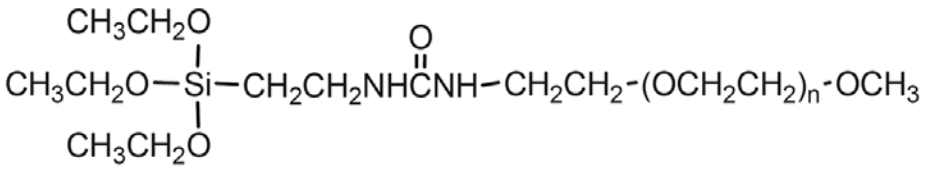

Figure 4-8 Structure of methoxy PEG Silane. In case of the used PEG silane the purity was 95%. When binding to the surface, ethoxy groups (left) are separated from the PEG-silane and the PEG binds covalently to the glass surface.

Functionalization of Gold Nanostructures

After passivation of the gold nanostructures, the samples were functionalized using mannose or glucose disulfide (Figure 4-9). The disulfide was produced by Vijayand Chandrasekaran, Organic Chemistry, CAU Kiel.

A 1 mM solution of the compound in methanol was prepared. The passivated gold nanostructures were placed in glass petri dishes and either covered with mannose disulfide solution or with methanol. The control in methanol was carried out, in order to confirm that the PEG-passivation stays intact during functionalization. The petri dishes were closed and sealed with Parafilm® and samples were then incubated in their solutions at RT for at least 1 h. Afterwards the samples were washed with methanol and dried in air.

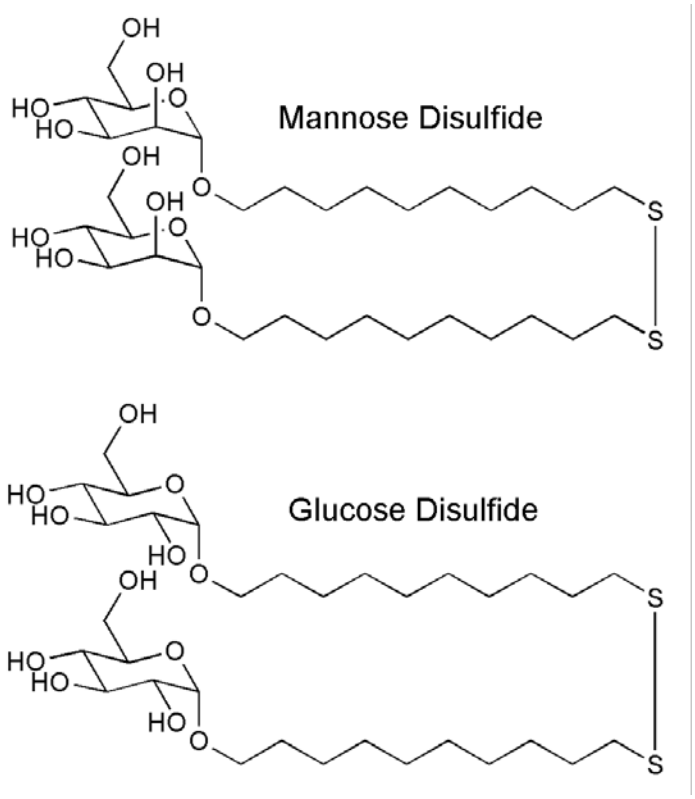

Figure 4-9 Chemical formulas of Mannose Disulfide and Glucose Disulfide, which were used in these experiments. Two carbohydrate molecules are coupled by a disulfide bond. When reacting with gold the disulfide bond breaks and the sulfur atoms bind to the gold.

Beside the passivated gold nanostructures, also nanostructures without passivation were functionalized with mannose. In this case, samples with IPD of either 52 nm or 91 nm were chosen. If the samples had been produced more than 2 days before funtionalization, the gold nanostructured glass slides were treated with oxygen plasma in the plasma machine Sentech SI 100 (Sentech Instruments GmbH, Berlin, Germany) at a power of 50 W and a pressure of about 0.4 mbar for 25 minutes. Subsequently, gold nanostructures were functionalized according to the protocol, but with incubation times of the mannose-disulfide of up to 48 h at RT. Afterwards, the samples were washed as described above.

As control specimens, piranha cleaned glass slides, methanol-cleaned glass slides, as well as nanostructures without functionalization or passivation were used.

For all types of samples *A. castellanii* were counted and 4×10^4 acanthamoebae in 2 ml PYG medium were added to each sample placed in one well of a six-well plate. After 15 min incubation time, 30 images per sample were recorded by phase contrast microscopy with a CKX41 microscope (Olympus GmbH, Hamburg, Germany) equipped with a Hamamatsu C9300 camera (Hamamatsu, Hamamatsu, Japan). For analysis the cell spreading area of the cells was measured by manually marking the border of the acanthamoebae with Image J.

4.3.2. Results

Spreading of *A. castellanii* on Mannose-Functionalized Gold Nanostructures without Passivation Layer

On conventional glass slides the acanthamoebae adhere well, but as shown in section 4.1, the adhesion can be improved by surface functionalization. For this reason, it was expected that acanthamoebae adhesion would be further stimulated by mannose. Therefore, in order to investigate the mannose-specific adhesion of *A. castellanii* in more detail, initially experiments on gold nanostructures without PEG coating were carried out.

Nanostructures with different densities of gold dots were functionalized with mannose and the spreading of *A. castellanii* was investigated. The results of three independent experiments, each in triplicate, are summarized in Figure 4-10.

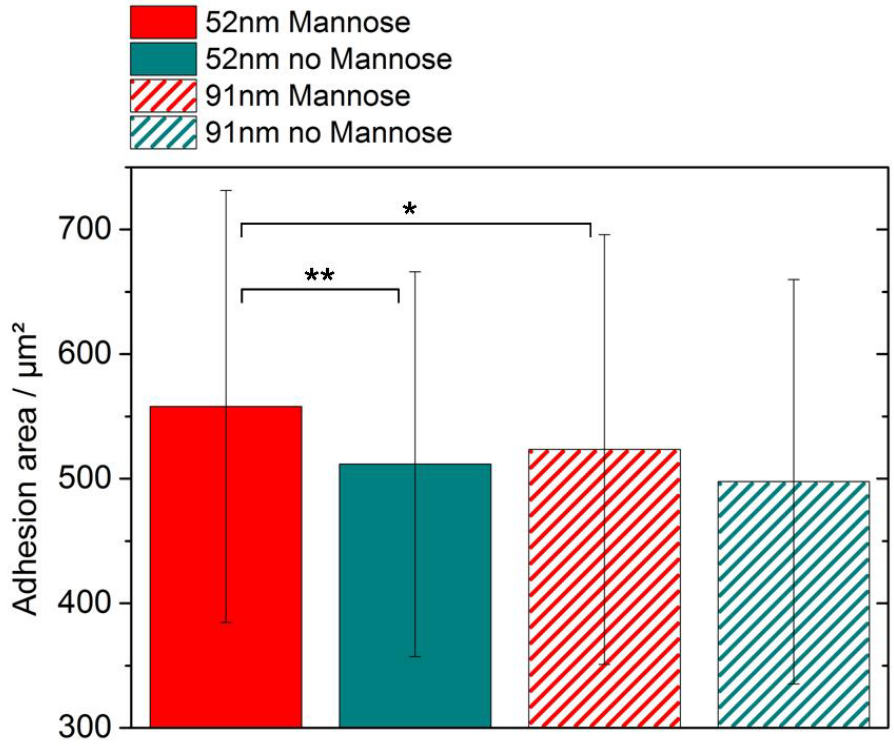

Figure 4-10 Spreading area of *A. castellanii* on mannose-functionalized (red) and non-functionalized (cyan) gold nanostructures. It becomes obvious that acanthamoebae spread wider on mannose-functionalized nanostructures than on non-functionalized ones (significance level ** $p < 0.01$). Also a slight difference can be observed for nanostructures with different IPDs. Cell areas are significantly (* $p < 0.05$) larger on 52 nm IPD samples (filled) than on 91 nm IPD ones (patterned). Error bars mark the standard deviation.

The spreading on samples with an IPD of 52 nm was compared to that on samples with an IPD of 91 nm. Figure 4-10 indicates that the average cell area of acanthamoebae spread on functionalized nanostructures with 52 nm IPD

(558 ± 173 µm²) was significantly larger (* $p < 0.05$) than on non-functionalized nanostructures with the same IPD (512 ± 154µm²) (both filled). For the samples with 91 nm IPD, the differences in the spreading area of acanthamoebae between the mannose-functionalized (523 ± 172µm²) and the non-functionalized nanostructures (498 ± 162 µm²) were not significant (both patterned). On the functionalized samples with 52 nm IPD the cell spreading area was significantly larger (** $p < 0.01$) than on the samples with 91 nm IPD.

Adhesion of *A. castellanii* on Mannose-Functionalized Gold Nanostructures with Passivation Layer

Whereas in the previous section adhesion was superimposed by the non-specific adhesion of *A. castellanii* to the bare glass, here experiments on purely mannose-mediated adhesion are shown. Figure 4-11 summarizes the results of the number of adhering acanthamoebae on the mannose-functionalized samples and the control samples (i.e. piranha cleaned glass (dark grey), ethanol cleaned Glass (grey), Nanostructure without further treatment (light grey)). For the evaluation, the number of adhering and floating acanthamoebae on each sample was counted, the results are given in % of the overall number of acanthamoebae per sample in order to exclude errors during the seeding procedure. Each experiment was conducted three times and in triplicate.

These experiments were carried out partly in cooperation with Gunnar Zoch, and partly by Gunnar Zoch under my supervision as part of his master thesis

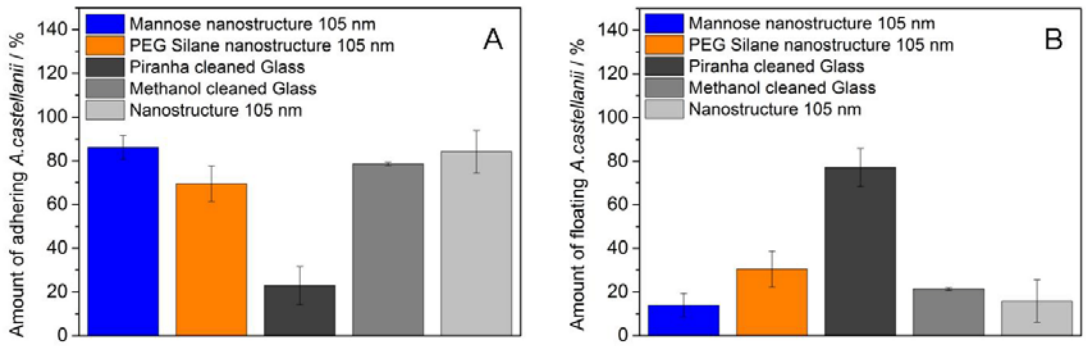

Figure 4-11 Relative numbers of adhering (A) and floating (B) *A. castellanii*. The results are given in % of the total number of counted acanthamoebae per sample (adherent + floating), in order to exclude errors during the seeding of the cells. On the mannose-functionalized nanostructures (blue) nearly the same amount of adhering acanthamoebae as on the nanostructure, which was not functionalized and not passivated (light grey) was found. On the methanol-cleaned glass slides (grey) slightly less acanthamoebae adhered, followed by the PEG-passivated nanostructures (orange) and the piranha cleaned glass slides (dark grey). The amount of the floating acanthamoebae is vice versa. Error bars mark the standard deviation.

The nanostructures used in this experiment were produced with a spinning speed of 7000 rpm and had an IPD of 105 ± 5 nm. In the graph the average number of adhering (Figure 4-11 A) and floating acanthamoebae (Figure 4-11 B) on each sample is shown. On the mannose-functionalized and passivated gold nanostructure 86 ± 5 % of the counted *A. castellanii* were adhering to the sample surface. A comparable number of adhering acanthamoebae was determined for the nanostructured surface (84 ± 10 %) without further functionalization or passivation. On the PEG-passivated gold nanostructures without functionalization fewer of the counted acanthamoebae were adhering (70 ± 8 %) compared to the two samples described before. On the methanol-cleaned glass slide more acanthamoebae were adhering (79 ± 1 %) than on the PEG-passivated nanostructure, while the lowest number was found for the piranha treated glass slide (23 ± 9 %). For the number of floating acanthamoebae, the distribution was vice versa (Figure 4-11 B). In a further analysis step, the spreading area of the adhering and floating acanthamoebae was compared. The results are shown in Figure 4-12 A and B.

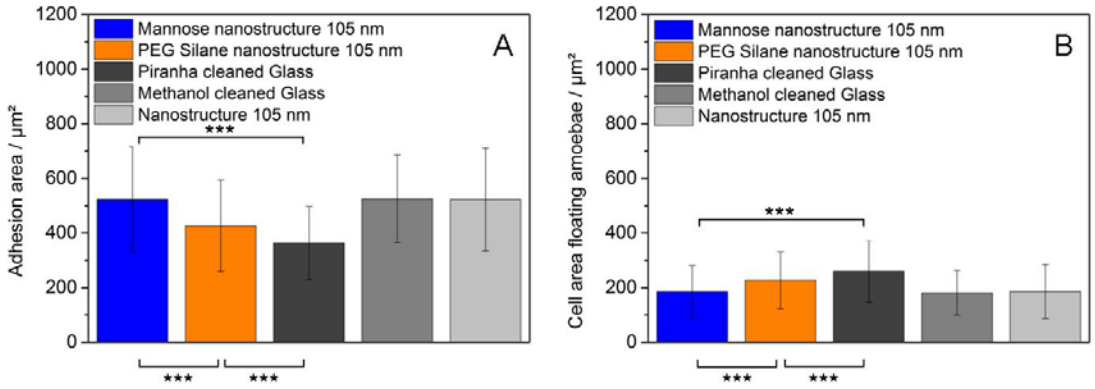

Figure 4-12 Cell area of *A. castellanii* trophozoites, which adhere (A) to different samples or swim in solution (B). On mannose-functionalized and passivated gold nanostructures (blue) with IPD of 105 nm the acanthamoebae spread nearly as wide as on methanol-cleaned glass (grey) and on nanostructures without functionalization or passivation (light grey). On clean glass (dark grey) and PEG-passivated samples (orange), the acanthamoebae spread significantly less. This was proven by a two sample t-test (* $p < 0.001$ for both samples).The size distribution of the floating acanthamoebae is vice versa. Error bars mark the standard deviation.**

A. castellanii trophozoites grown on passivated and mannose-functionalized nanostructures showed an average adhesion area of 523 ± 192 µm². A similar cell spreading area was found for the acanthamoebae adhering to the non-treated glass slides (525 ± 160 µm²) and to the nanostructures without any other surface treatment (523 ± 188 µm²). When comparing the spreading on these two sample types no significant difference was found. In comparison to that the adhering acanthamoebae on PEG-passivated nanostructures had a significant smaller average adhesion area of 427 ± 167 µm². On the cleaned glass slides, the cell size was even smaller with 363 ± 134 µm². The significance of the differences between the mannose sample, the

PEG-passivated sample and the cleaned glass slides was proven by a two sample t-test (*** $p < 0.001$).

The area of the floating acanthamoebae (Figure 4-12 B) was much smaller than that of the adherent ones, as the acanthamoebae rounded up when swimming in the liquid. The smallest average cell size was determined for the acanthamoebae on the mannose-functionalized surfaces, the non-treated glass slides and the non-functionalized nanostructures with about $185 \pm 96\ \mu m^2$, $181 \pm 82\ \mu m^2$ and $186 \pm 99\ \mu m^2$, respectively. The area of the acanthamoebae floating in the liquid of the PEG and the cleaned glass slide were found to be significantly larger (*** $p < 0.001$) with cell sizes of $227 \pm 104\ \mu m^2$ and $260 \pm 113\ \mu m^2$, respectively. Also here a two sample t-test was applied to verify the significance of the results.

Cell Size on Mannose-Functionalized Gold Nanostructures with Varying inter-particle Distances

In order to evaluate the influence of the IPD on the cell spreading area of *A. castellanii* trophozoites on mannose-functionalized and passivated nanostructures, the experiments were repeated with samples having different IPDs. Figure 4-13 shows the results of the measured cell spreading area of trophozoites adhering to mannose-functionalized and passivated nanostructures with IPDs of 49 nm, 127 nm, and 105 nm compared to PEG-passivated surfaces.

It is obvious from Figure 4-12 that the spreading area on the mannose-functionalized and passivated samples with 49 nm IPD ($545 \pm 207\ \mu m^2$) was significantly larger (* $p < 0.05$) than on the samples with 105 nm ($523 \pm 192\ \mu m^2$) and 127 nm IPD ($523 \pm 219\ \mu m^2$). Between the samples with 105 nm and 127 nm IPD no significant difference in size of the acanthamoebae was observed. On all three kinds of mannose-functionalized surfaces the acanthamoebae spread wider (*** $p < 0.001$) than on the PEG-passivated samples ($450 \pm 188\ \mu m^2$).

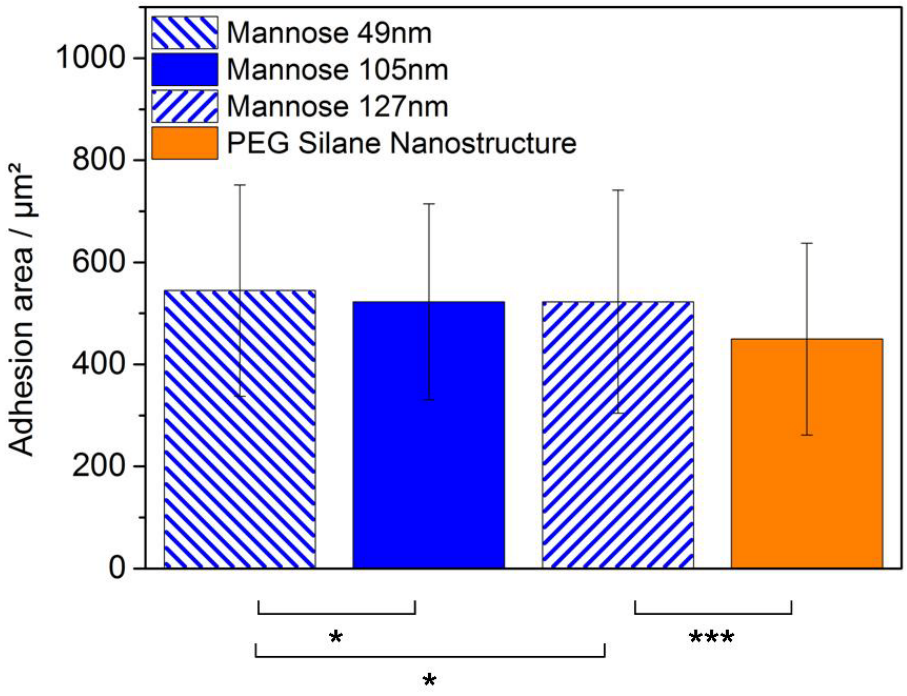

Figure 4-13 Cell area of adherent *A. castellanii* on different mannose-functionalized and passivated nanostructures. The PEG silane coated gold nanostructure (orange) served as control sample. Acanthamoebae adhering to mannose-functionalized and passivated gold nanostructures (blue) show the larger spreading areas than on PEG. The change of the IPD lead to deviations in the spreading area. On the mannose-functionalized gold and passivated nanostructures with 49 nm IPD (n=3) (blue left), the spreading area of *A. castellanii* was significanly larger (* $p < 0.05$) than on the nanostructures with 105 nm (blue middle) and 127 nm IPD (blue right) (both n=9). Acanthamoebae adhering to PEG-passivated gold nanostructures are significant smaller in size than on the functionalized nanostructures (* $p < 0.001$). Error bars mark the standard deviation.**

Comparison of Mannose-Functionalized with Passivated and Functionalized Nanostructures

For comparison, in Figure 4-14 the results of the mannose-functionalized samples without (red) and with PEG passivation (blue) are depicted.

The *A. castellanii* showed the largest adhesion area on mannose-functionalized nanostructures without PEG coating with an IPD of 52 nm (red, filled). There was a significant difference in the spreading area of acanthamoebae on this sample type compared to the nanostructures without PEG with 91 nm IPD (* $p < 0.05$). The spreading area on nanostructures with an IPD of 52 nm without PEG was compared to the nanostructures with PEG and larger IPD (105 nm or 127 nm). The sizes of the acanthamoebae were significantly larger on samples without PEG (** $p < 0.01$). On 91 nm IPD samples without PEG and on samples with PEG and IPDs of 105 nm and 127 nm the average spreading area of the acanthamoebae was nearly the same. The difference in the average cell size between 52 nm IPD (mannose-functionalized) and 49 nm IPD (mannose-functionalized and PEG) was not significant ($p = 0.37$).

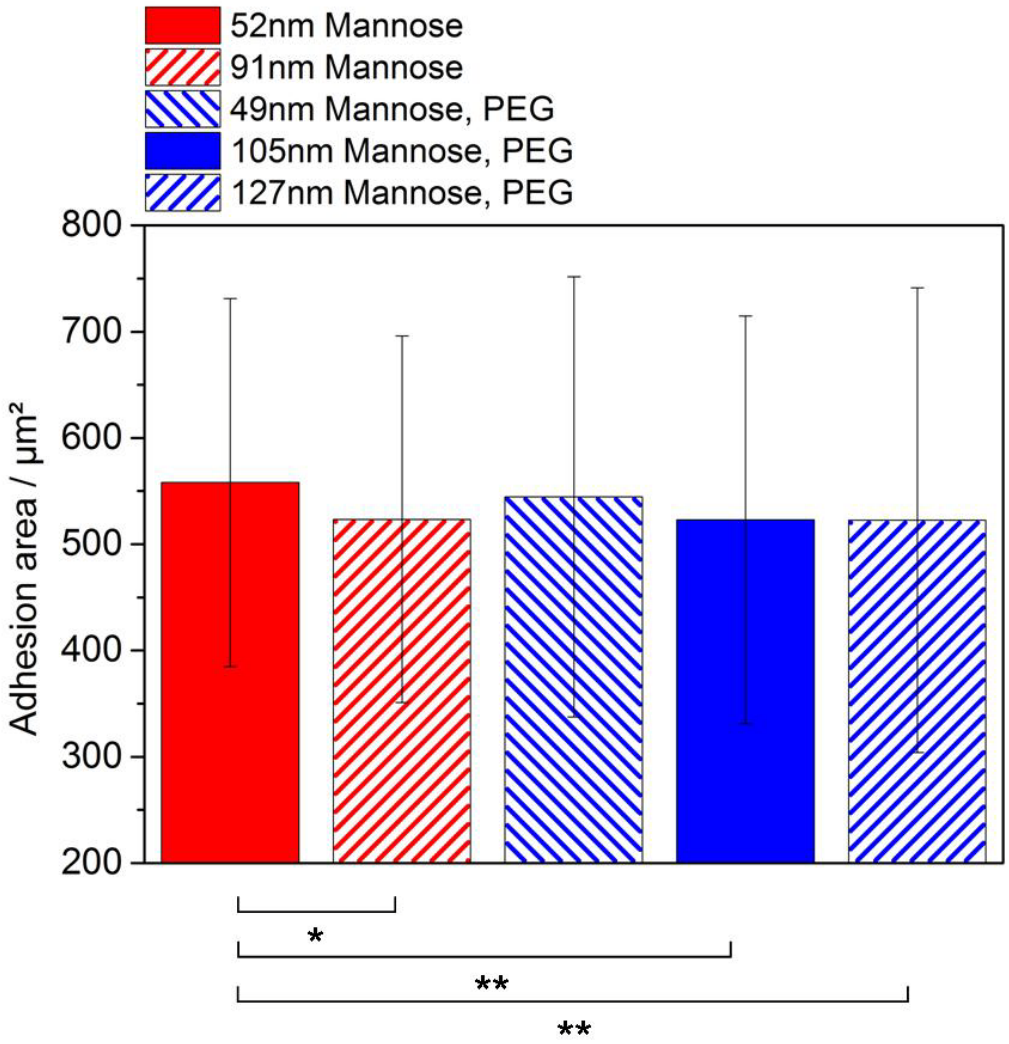

Figure 4-14 Spreading area of *A. castellanii* on mannose-functionalized gold nanostructures with different IPDs without (red) and with PEG passivation (blue). On mannose-functionalized gold nanostructures with 52 nm IPD the acanthamoebae exhibit the largest spreading area compared to all other samples. Significant differences could be observed when comparing mannose-functionalized nanostructures without PEG to the same sample type with 91 nm (* $p < 0.05$) and compared to functionalized and passivated nanostructures with 105 nm and 127 nm IPD (both ** $p < 0.01$). On the passivated and functionalized nanostructures the acanthamoebae spread wider on nanostructures with 49 nm IPD than on the other two types. Error bars mark the standard deviation.

Adhesion of *A. castellanii* on Glucose-Functionalized Gold Nanostructures with Passivation

In the adhesion of pathogenic acanthamoebae to target-cells besides mannose also other carbohydrates such as glucose might be involved. In previous studies glucose derivatives were tested as inhibitor for target-cell adhesion [7, 124] but only little is known about adhesion on glucose-functionalized substrates. For that reason in addition to the experiments on nanostructures with mannose-functionalization, similar experiments were conducted using glucose-functionalization with PEG-passivation.

The results of the comparison of acanthamoebae adhesion on mannose, glucose and PEG are summarized in Figure 4-15.

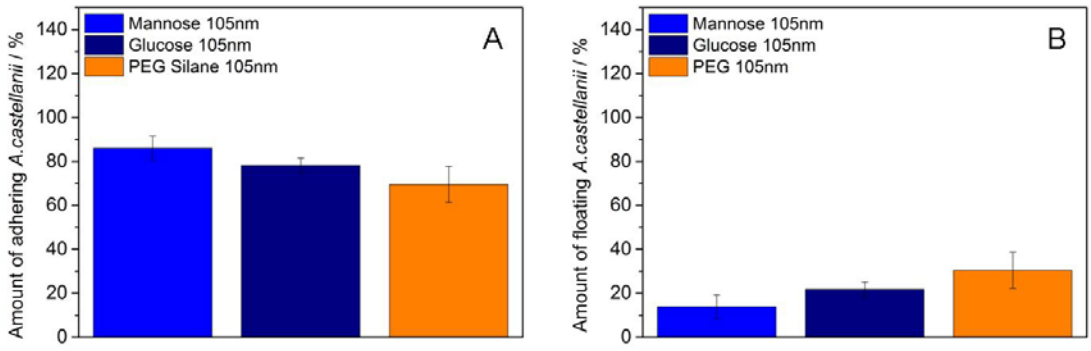

Figure 4-15 Relative numbers of adhering (A) and floating (B) *A. castellanii*. The amount of adhering and floating acanthamoebae in the imaged areas is given in % normalized to the total number of acanthamoebae per sample (floating + adhering). On the mannose-functionalized nanostructures, the largest amount of acanthamoebae is adhering followed by the glucose-functionalized samples and the PEG-passivated surfaces. Error bars mark the standard deviation.

The graph shows that most acanthamoebae adhered to the passivated and mannose-functionalized nanostructures (86 ± 5 %). The numbers of adhering acanthamoebae on the passivated and glucose-functionalized substrates (78 ± 3 %) as well as on the PEG-passivated surfaces (70 ± 8 %) were considerably lower. A similar effect was observed for the cell spreading area on these three kinds of substrates (Figure 4-16)

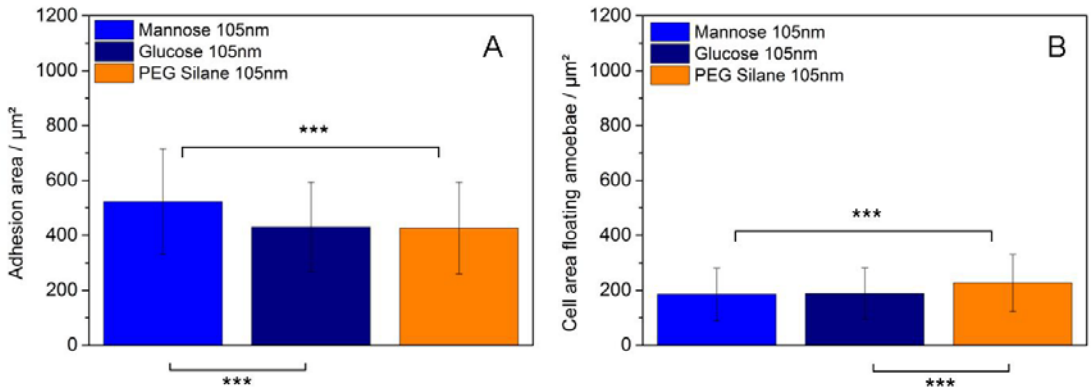

Figure 4-16 Cell area of *A. castellanii* adhering to different substrates (A) or floating in liquid (B). The cell size is largest for acanthamoebae adhering to mannose-functionalized and passivated gold nanostructures. On samples, which were functionalized with glucose disulfide, the acanthamoebae spread significantly less (* $p < 0.001$). The size of the floating acanthamoebae is much smaller because they are rounded up. Error bars mark the standard deviation.**

In Figure 4-16 A, the adhesion area of acanthamoeba trophozoites on the mannose- and, the glucose-functionalized nanostructures as well as on the PEG-passivated surfaces is shown. These data show that the spreading area on the mannose-functionalized substrates (523 ± 192 µm²) was significantly larger (*** $p < 0.001$) than on the glucose-functionalized (431 ± 163 µm²) and the PEG-passivated surfaces (427 ± 167 µm²).
For floating acanthamoebae also differences in the cell area could be observed. However, their size was almost identical for the glucose- and the mannose-functionalized nanostructures (185 ± 96 µm² for mannose, 188 ± 93 µm² for glucose), while it was significantly larger (*** $p < 0.001$) for the PEG-passivated surfaces (227 ± 104 µm²).

4.3.3. Discussion

In this section, the mannose-specific binding of *A. castellanii* was evaluated in detail. For this purpose glass substrates were coated with quasi-hexagonally arranged patterns of gold nanodots by using diblock copolymer micelle nanolithography. These gold patterns could be easily functionalized by mannose disulfide or glucose disulfide, which reacts with the gold. In this way, precisely arranged anchoring sites for the mannose binding protein of acanthamoebae and hence for thorough investigation of acanthamoebae adhesion were produced. The distances between the single dots were varied in order to mimic certain densities of the mannose ligands on the surface of a target-cell.
In a first experiment, the adhesion of *A. castellanii* to mannose-functionalized gold nanostructures was evaluated. As here a passivating layer in between the gold dots was missing, the acanthamoebae did not exclusively adhere to the functionalized gold dots, but also to the glass substrate in between the dots. Nevertheless, there was a significant effect of the mannose on the spreading behavior of the acanthamoebae trophozoites. The mannose-functionalization lead to an increase in the cell spreading area compared to non-functionalized surfaces. On mannose-functionalized nanostructures with an IPD of 52 nm, the spreading area of the acanthamoebae was largest, followed by functionalized gold dots with an IPD of 91 nm and non-functionalized nanostructures (Figure 4-10). With decreasing IPD the density of the gold dots and consequently the density of the anchoring sites are increasing. The reason for the larger spreading area with increasing number of particles and thus increasing mannose density is presumably the binding of the MBP in the membrane of the pathogenic acanthamoebae trophozoites to mannose ligands on the surface. Possibly, the increased mannose ligand density activates more receptors at the membrane of acanthamoebae for stronger binding. The contact formation of pathogenic acanthamoebae to target-cells is triggered by the MBP [5, 7-8, 123], which was also observed during the experiments on adhesion of pathogenic *A. castellanii* and non-pathogenic *A. comandoni* to mannose-functionalized and non-functionalized

beads. The logical consequence would be that the acanthamoeba tends to build a maximum adhesion area to the corresponding surface and the spreading area increases. The effect depends on the density of the mannose molecules, as is evident by the increase in adhesion area from 91 nm to 52 nm IPD.

In order to improve the understanding of the details of the contact formation, the gold nanostructures were functionalized with mannose and the area in between the dots was passivated with PEG. In this way, the binding of the acanthamoebae to the inter-particle space should be inhibited in order to ensure the exclusive adhesion of *A. castellanii* to the mannose on the functionalized dots. In these experiments significant differences in the number of adhering acanthamoebae as well as in the cell spreading area between the mannose-functionalized nanostructures with PEG passivation and the control samples were observed (Figure 4-11, Figure 4-12). The highest number of adhering *A. castellanii* was observed for the mannose functionalized and passivated nanostructures and the nanostructured surface without any further treatment followed by the methanol-cleaned glass sample. To the PEG-passivated gold nanostructures less acanthamoebae than to all other samples adhered. The only exception was the piranha cleaned glass. The decreased number of acanthamoebae adhering to the PEG-passivated nanostructures, compared to the non-functionalized, and the mannose-functionalized nanostructure without PEG, shows that the PEG passivation was successful and that it is also suitable for the acanthamoebae. A reason for the adhesion of some acanthamoebae to the PEG-passivated nanostructures is that PEG covers the glass surface in between the gold dots but not the gold dots themselves. For that reason, the acanthamoebae can adhere non-specifically to the free gold dots.

An explanation for the low number of adhering acanthamoebae on the piranha-cleaned glass slide might be that the surface charges are changed due to cleaning. After treatment with piranha solution the glass slides became more hydrophilic, most organic substances were removed, and the substrate became negatively charged [125]. As most cell membranes are negatively charged, the negative charges of the glass surface and of the acanthamoeba membrane repel each other, which could cause the radically decreased adhesion.

The size distribution of the adhering cells was comparable to the number of adhering acanthamoebae on the different substrates. Adhering trophozoites on the PEG sample were significantly smaller than on all other samples apart from the piranha cleaned glass, for which the smallest size was observed. The area of the acanthamoebae adhering to the mannose-functionalized nanostructures was nearly the same and even slightly larger than on methanol-cleaned glass slides and nanostructures without functionalization and passivation. Considering the large IPD of 105 nm, this is a striking result as on the mannose-functionalized and passivated nanostructures comparably few binding spots with mannose lead to a similar adhesion area of acanthamoebae as on the glass samples, where they can adhere all over the surface. This result indicates that mannose indeed plays an enormous role for the adhesion

process. It is also a hint that many MBPs are present on the acanthamoeba surface, leading to a strong binding to target-cells.

In order to investigate, whether there is a critical density of mannose molecules, which is needed for stable adhesion of acanthamoebae, samples with different IPDs were produced. With the smallest IPD (49 nm, highest density of binding sites) a larger spreading area of the trophozoites compared to samples with larger IPD could be observed. This, together with the results from the experiments on nanostructures that were only mannose-functionalized, lead to the conclusion that a higher density of mannose molecules on the substrate leads to an increased cell size.

The overall density, which is needed for stable adhesion is relatively low, as for 127 nm IPD still the sizes of the acanthamoebae were nearly the same as for those on 105 nm IPD. In comparison, for the receptor-ligand system of c(RGDfK) and the integrin $\alpha_v\beta_3$, the IPD between the single ligands should not be lower than 73 nm in order to achieve stable adhesion [95]. When comparing the mannose-functionalized nanostructures without PEG with the samples with PEG, it can be concluded that the spreading tends to be larger without passivation.

In order to prove that the increase in spreading area of the acanthamoebae on mannose-functionalized nanostructures is due to a specific binding to mannose, additional experiments were conducted on glucose-functionalized gold nanostructures. The fact that the adhesion area of the acanthamoebae growing on glucose-functionalized surfaces with PEG compared to those on the PEG-passivated surfaces is nearly the same, shows that glucose does not enhance the acanthamoebae adhesion. This result agrees with a previous study, where it had been observed that acanthamoebae do not bind to surfaces coated with glucose derivatives [7]. These results confirm that MBP is essential for the specific adhesion of pathogenic acanthamoebae to target-cells and therefore also for the pathogenic potential of the acanthamoebae.

4.4. Quantifying Acanthamoeba Adhesion by AFM Force Spectroscopy

An interesting observation in the experiments was that trophozoites can exert large forces to their target-cells.

With the aim to demonstrate the pathogenic nature of *A. castellanii*, acanthamoebae were cocultured with human nerve cells of the type SHSY5Y (experimental procedure, see appendix 5). The acanthamoebae reacted on the mannose in the surface coat of the target-cells. In some cases it was observed, that the acanthamoebae exert large forces on the host cells. Consequently, the nerve cells detached from the surface and the *A. castellanii* pulled them in their direction of movement. This behavior is also shown in Figure 4-17 on the next page.

In section 4.2 it was described, that the acanthamoebae are able to keep floating beads with sizes up to six times larger than the acanthamoebae in a fixed position by adhering to the surface and to the bead. In both cases, the coculture with nerve cells and with mannose-coated beads, the mannose-specific binding presumably played an essential role in the adhesion process and lead to a very strong binding.

For that reason the strength of the mannose binding to acanthamoeba is investigated by AFM force spectroscopy, where a mannose-functionalized cantilever is approached to an adhering acanthamoeba. In order to prove the specificity of the mannose binding, blocking experiments are performed. Such a blocking can be achieved either by inactivation of receptors in the membrane of the acanthamoebae, or by passivation of the cantilever against specific binding [126]. For saturating the mannose binding proteins in the acanthamoeba membrane, mannose is added to the medium. The molecules in the medium bind to the MBP and lead to a saturation of the MBP with mannose in the membrane. Therefore, the MBP cannot bind to other mannose molecules on the approached cantilever anymore.

For comparison, experiments with two other carbohydrates are carried out: glucose and 1-Amino-1-deoxy-D-mannitol. Glucose so far is not known to promote the adhesion of pathogenic acanthamoebae, but in several studies it was shown that glucose in comparison to mannose does not inhibit the mannose-specific binding of acanthamoebae to target-cells [7, 99, 124]. Mannitol has been shown to be involved in the adhesion of pathogenic strains of acanthamoebae, while adhesion of non-pathogenic acanthamoebae was inhibited [127].

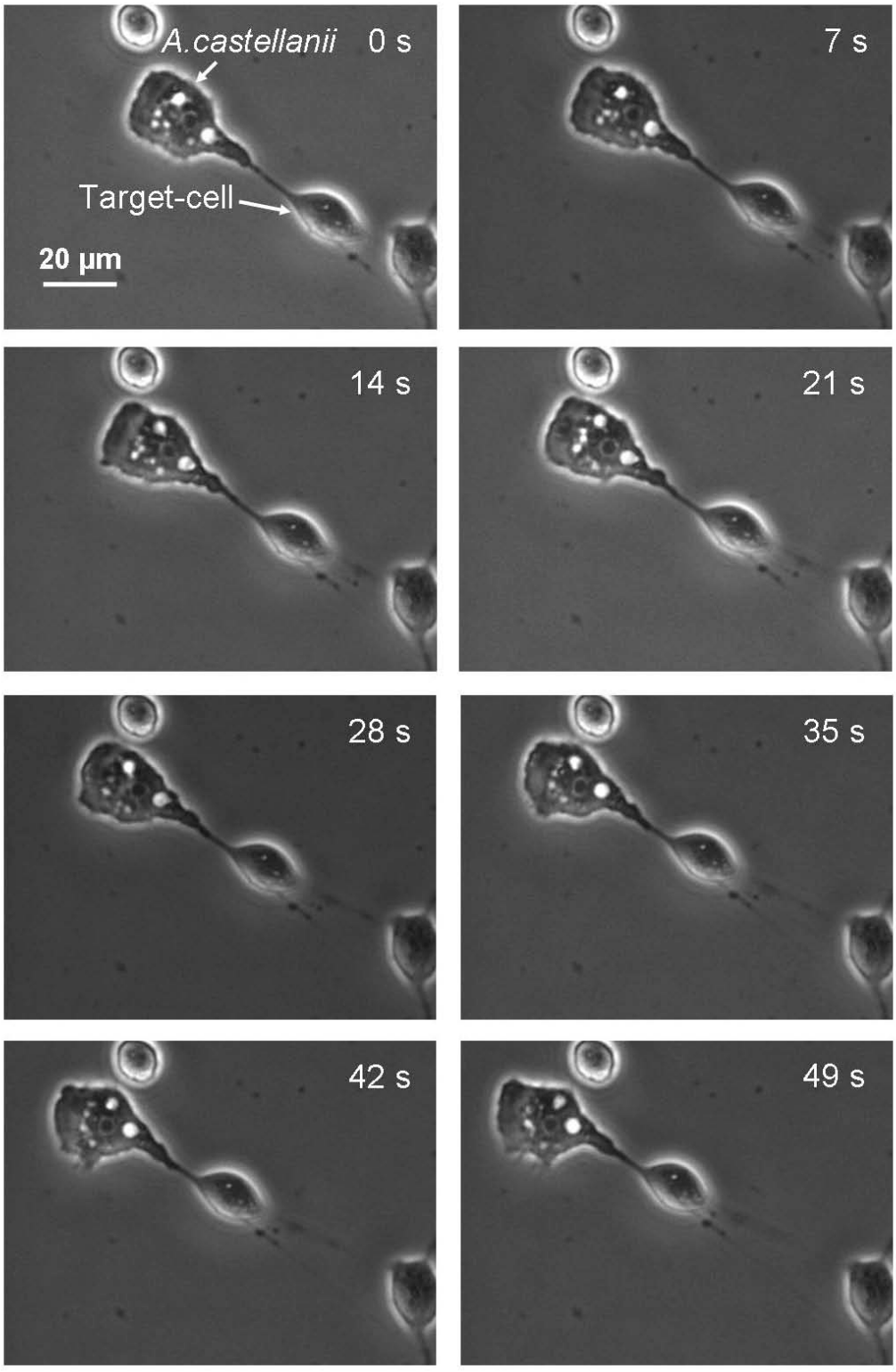

Figure 4-17 ***A. castellanii*** **pulling on a nerve cell of the type SHSY5Y. It becomes obvious, that the acanthamoebae are able to exert large forces on their target-cells. The images were recorded every 7 s. The acanthamoeba is moving towards the left top corner and is detaching the nerve cell from the surface.**

4.4.1. Materials and Methods

Cantilever Calibration

For the force spectroscopy measurements on *A. castellanii* two types of tipless cantilevers were utilized, namely MLCT-O10 and NP-O10 (both Bruker AFM Probes, Camarillo, USA). The cantilevers behave like Hookean springs with a linear elastic behavior. The cantilevers types were chosen since on each chip there are several cantilevers with different stiffness so that a cantilever suitable for the experiments can be chosen. In case of *A. castellanii* cantilevers with spring constants ranging from 0.03 N / m up to 0.35 N / m were used. Different stiff cantilevers were used in order to exclude cantilever-specific effects during the measurements. As the real spring constant can strongly deviate from the manufacturer's information, every cantilever had to be calibrated before the measurement. Besides this also the cantilever sensitivity is calibrated, which is calculated in V / nm and together with the spring constant (in N/m) is needed for the conversion of the photodiode signal (in V) into force.

Prior to calibration, cantilevers were washed in acetone (Sigma-Aldrich Chemie GmbH, Munich, Germany), dried in air and washed again in distilled water. Afterwards, the cantilevers were calibrated using the CellHesion head of the JPK AFM setup. Calibration was carried out employing the well-established thermal noise method in liquid (sodium chloride), which is implemented into the software of the JPK AFM instrumentation. For the calibation in liquid, a correction factor has to be taken into account [128]. To determine the spring constants of the cantilevers, each cantilever was measured for at least three (independent) times. For each measurement the cantilever was retracted from the surface for more than 1000 µm and approached again in order to obtain a reliable average value for the spring constant.

Cantilever Functionalization

As described in section 2.2, it is not possible to stably fix the *A. castellanii* to the cantilever applying standard procedures. For that reason a functionalized cantilever is used in these experiments by approaching it to acanthamoeba trophozoites. In this way, the specific binding of acanthamoeba to carbohydrates can be investigated. For the experiments, different types of cantilevers (MLCT-O10, NP-O10, Bruker AFM Probes, Camarillo, USA) were functionalized by a BSA biotin - streptavidin - α-D-mannose-sp-biotin sandwich. For control experiments, cantilevers were functionalized with a BSA biotin - streptavidin - α-D-glucose-sp-biotin sandwich, or BSA biotin - streptavidin - 1-Amino-1-deoxy-D-mannitol-sp-biotin, respectively. The functionalizations were carried out similar to the protocol described in [129].

For the functionalization, Parafilm® was put into the wells of a six well plate and a 50 µl drop of BSA biotin (0.5 mg / ml) (Sigma-Aldrich Chemie GmbH, Munich, Germany) was placed on top. The cantilevers on the chips were immersed in the drop

and incubated at RT over night for at least 16 hours. Afterwards, the chips were rinsed with 1×PBS and subsequently put into a 50 µl drop of streptavidin (0.5 mg / ml) (Sigma-Aldrich Chemie GmbH, Munich, Germany). After incubation at RT for 30 minutes to 1 hour, the chips were rinsed again in 1×PBS buffer. In the third step, the cantilevers were immersed into 50 µl of either α-D-mannose-sp-biotin, α-D-glucose-sp-biotin, or 1-Amino-1-deoxy-D-mannitol-biotin (0.1 mg / ml, GlycoTech Corporation, Gaithersburg, Maryland, USA) for one to two hours and afterwards again rinsed in PBS buffer. The cantilevers either were directly used or stored up to five days immersed into a drop of the carbohydrate-biotin solution in a six well plate sealed with Parafilm® at 5°C.

AFM Force Spectroscopy

As described in section 2.2, for carrying out AFM experiments on living cells, special equipment is needed. For the force spectroscopic experiments, an AFM from JPK instruments equipped with a CellHesion Head and a colour CCD camera (The Imaging Source Europe GmbH, Bremen, Germany) was used, because the CellHesion has a piezo with 100 µm z-travel. In comparison, the Nanowizard head has 15 µm z-travel.

Before the experiment, the cantilever was mounted on a special glass block and was clamped in by a small spring. The cantilever position was aligned very precisely on the glass block and introduced to the AFM head.

For the measurements, 2×10^4 *A. castellanii* were seeded in a plastic petri dish (Techno Plastic Products AG (TPP), Trasadingen, Switzerland) in PYG medium. The petri dishes were chosen as they have a lower edge and can therefore be used in the JPK PetriDishHeater, a special equipment of the JPK AFM setup, in which the temperature can be controlled and experiments in liquid can be conducted. In the AFM experiments, instead of PYG medium sodium chloride was used, in order to exclude interactions of the acanthamoebae and contamination of the cantilever with the components of the PYG medium. Therefore, after the acanthamoebae had adhered to the surface, they were washed once with 50 mM sodium chloride and afterwards 1.5 ml of the same solution were added. For blocking the MBP, 50 mM α-D-mannose (Sigma-Aldrich Chemie GmbH, Munich, Germany) were added to the sodium chloride solution as in [7] and [118] similar concentrations were used. After its addition an incubation time of 30 min at RT was needed.

The petri dish was placed into the JPK PetriDishHeater (Figure 4-18, top left) and mounted to the inverted microscope stage (Olympus IX71) of the AFM setup (right). Subsequently, the AFM head with the cantilever was placed on top of the PetriDishHeater (down left). The complete setup is shown in Figure 4-18, right.

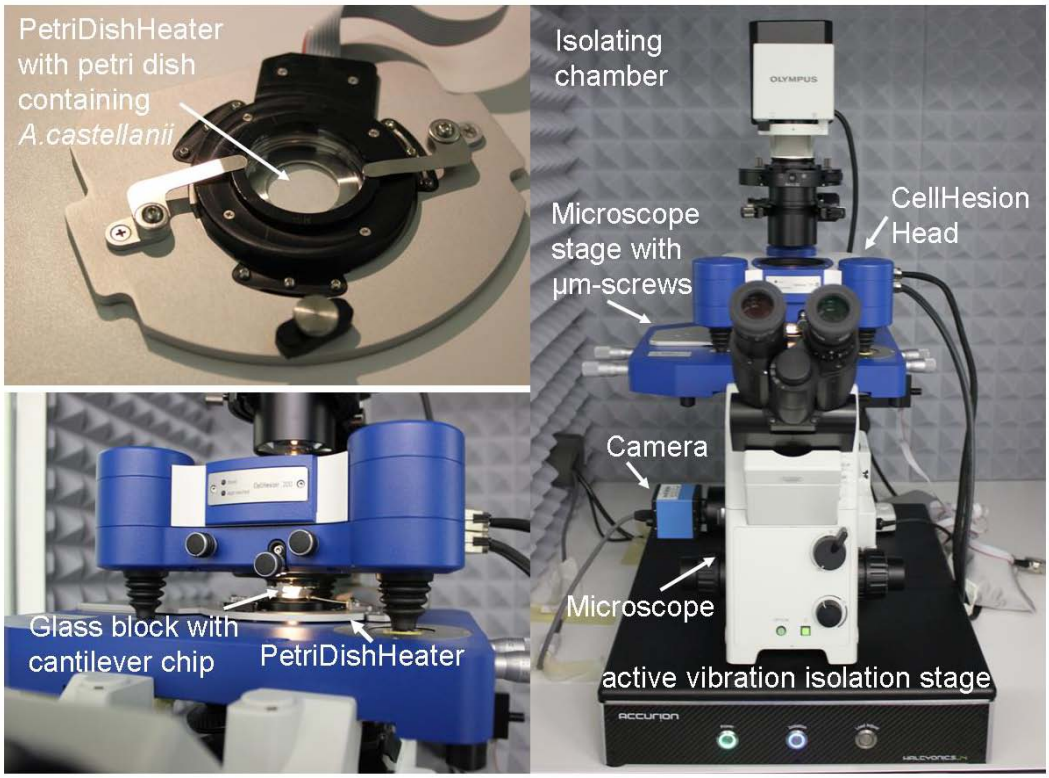

Figure 4-18 AFM Setup with CellHesion Head, where the glass block with the cantilever is mounted to (left bottom). A petri dish containing adhering *A. castellanii* is placed into the PetriDishHolder (left top) and mounted on the microscope stage with µm-screws. The complete setup is shown in the right image.

Via the JPK SPM Desktop software the AFM, the laser and the camera were controlled. First the coarse approach of the cantilever to the surface was done manually by using the stepper motors of the SPM Desktop software. As soon as the laser was in the liquid, the laser was positioned on the cantilever such that the maximum sum signal is achieved and that the lateral and vertical deflection were zero. When the cantilever was close to the surface, the fine approach was carried out automatically until a certain force is reached to avoid damaging of the cantilever. The piezo was retracted again and the sensitivity of the used cantilever was calibrated. Afterwards an adhering trophozoite was positioned beneath the cantilever. The cantilever was approached to the cell, kept in contact with the acanthamoeba for a defined time period and retracted again. Due to the viscoelastic response of cells on an external force, two modes of force application are distinguished: constant force and constant height mode. Constant height mode means that the cantilever was approached to the cell until a certain force was reached, kept at this height for a defined time and subsequently retracted. Experiments in constant force mode were conducted by approaching the cantilever to an acanthamoeba until the preset force was reached. Here, the cantilever height was constantly adjusted by the feedback loop

to account for viscoelastic responses and for movements of acanthamoebae in order to keep the acting force constant.
During the measurements, force-distance curve were recorded. This procedure was repeated 20 to 50 times for each cell. Overall three to seven cells were measured for each set of parameters. The parameters for the measurements are given in Table 4-1. All measurements were carried out at RT as acanthamoebae are also cultured at RT and show optimum growth at this temperature.

Table 4-1 Experimental parameters of the force spectroscopic measurements on *A. castellanii*. The force setpoint gives the contact force, which is applied by the cantilever, the pulling length is the distance the cantilever moves during the retract, and the speed of the retract and the approach is given by the extend speed. The contact time gives the time between approach, and retract and the sampling rate is the rate, by which data points are recorded.

Force Setpoint / nN	Pulling Length / µm	Extend Speed / µm/sec	Contact time / sec	Sampling Rate / Hz	Mode
8-16	50-90	5	0.1 sec	4096	Const. force
8-16	50-90	5	0.5 sec	4096	Const. height
8-16	50-90	5	5 sec	4096	Const. force / const height
8-16	50-90	5	10 sec	4096	Const. height

Data Processing

In order to visualize the data analysis in Figure 4-19 a force distance curve before and after data analysis is depicted. The recorded force distance curves were evaluated using the JPK DataProcessing software (version spm 2.4.58). Prior to determining force values, all curves were smoothed (grade 3), the x- and y-baseline is set to zero (red arrow) and tilt corrected, as due to drift of the cantilever the zero position of the curve can vary drastically. The smoothing is carried out in order to flatten oscillations in the curves. The factor should not be too high as due to the smoothing also information can be lost. In the depicted curves the smoothing as well as the tilt-correction only had a little effect as the curves did not show strong oscillations or tilt before.
Important data, which were calculated by the software during the analysis, are the maximum adhesion force and the adhesion energy (Figure 4-19). The maximum adhesion force is calculated from the deepest point of the force distance curve. The area below the baseline gives the adhesion energy. For the different parameters such as contact time and operation mode these values are determined and statistically evaluated.

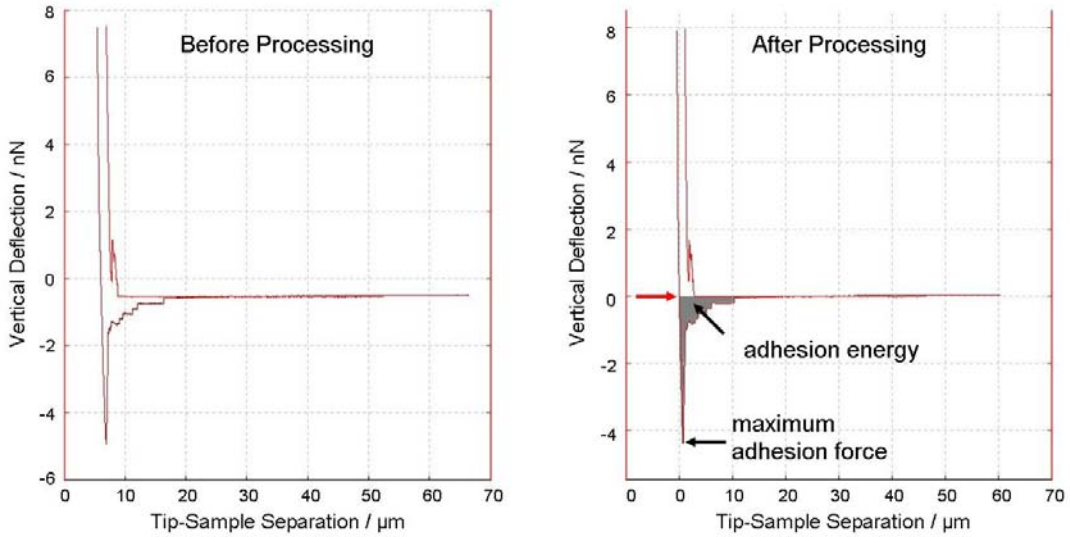

Figure 4-19 Force distance curve before (left) and after processing (right). In order to evaluate the curves, they first have to be processed such that the roughness of the curves is reduced, the x- and y-baselines have to be set to zero position (red arrow), and, in case that the curve is strongly tilted e.g. due to drift of the cantilever, the curves have to be tilt corrected. From the minimum of the curve the maximum adhesion force can be determined. The area between baseline and curve is the adhesion energy.

4.4.2. Results

For each set of parameters shown in this section, at least four cells were measured and the results from single cells were compared with each other in order to exclude outliers due to cell behavior. The results of the different experiments are summarized and shown as histograms depending on the operation mode in the following.

Experiments in Constant Height Mode

For the evaluation of the force spectroscopic experiments, the adhesion energy as well as the maximum adhesion force were calculated.

In Figure 4-20 the statistical results of the adhesion energy for experiments conducted with a mannose-functionalized cantilever at constant height mode are shown. In these experiments, contact times of 0.5 s, 5 s and 10 s were applied.

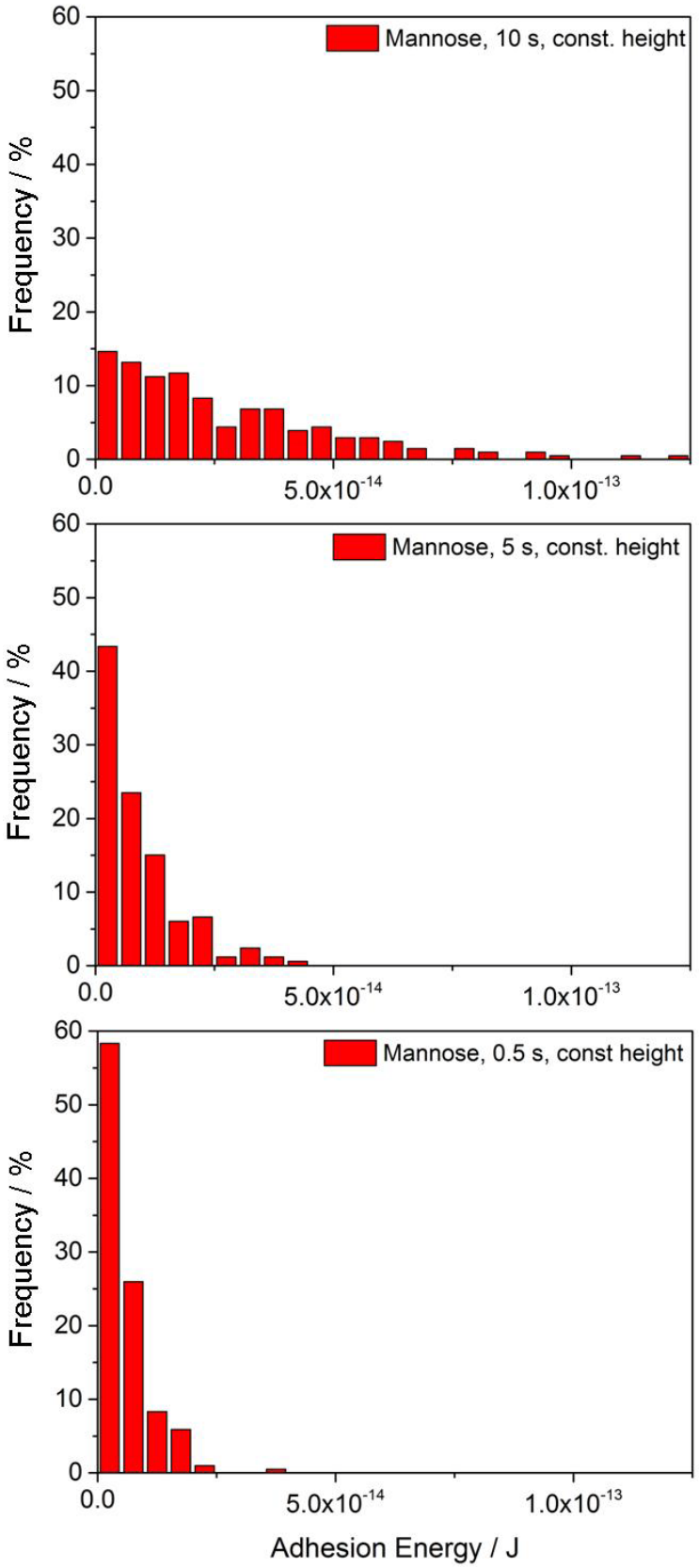

Figure 4-20 Adhesion energy of curves recorded in constant height mode with different contact times of 10 s (top), 5 s (middle) and 0.5 s (bottom). The distribution of the values is much broader in case of 10 s contact time than in the other two cases. The median for 10 s contact time is at 1.98×10^{-14} J, for 5 s it is at 0.668×10^{-14}, and for 0.5 s the median is 0.367×10^{-14}.

The histograms in Figure 4-20 (interval 0.5×10^{-14} J) show that the adhesion energy after 0.5 s (bottom) and 5 s contact time (middle) tends to be much smaller than after 10 s contact time (top). The median for 10 s contact time is 19.8×10^{-15} J, which means that 50 % of the measured adhesion energy values are above, and 50 % are below this value. With 5 s contact time the median is about two third lower (6.68×10^{-15} J) than for 10 s. The results of the experiments conducted with 0.5 s contact time give a median of 3.67×10^{-15} J. Furthermore, the distribution is much broader after 10 s than after 0.5 s and 5 s. After 10 s it ranges from 0.25×10^{-14} J up to 12.5×10^{-14} J, while with 0.5 s in contact the range is much smaller with values up to 4×10^{-14} J. For 5 s contact time the distribution is only slightly broader and ranges between 0.25×10^{-14} J and 4.5×10^{-14} J.

A similar development is observed for the maximum adhesion force (Figure 4-21) (interval 1 nN), where the adhesion forces stray strongest for 10 s contact time (top) compared to 5 s (middle) and 0.5 s (bottom). After 10 s, in constant height mode the values range between 0.5 nN and 31 nN with a median of 9.71 nN. After 5 s contact time, the maximum adhesion force is lower, but the distribution is much narrower, ranging from 0.5 to 12 nN with a median of 2.02 nN. After short contact of 0.5 s the force distribution is confined to a very small range between 0.5 nN and 7 nN (median 1.26 nN).

From the median it becomes obvious that the adhesion energy as well as the maximum adhesion force increase with increasing contact time, but the increase is not in direct proportion.

Besides this effect, it could be observed that during the measurements at constant height the acanthamoebae exert strong forces on the cantilever. They crawl beneath the cantilever and push it away from the surface, which can lead to increased forces acting on the cell, as shown in from the curve depicted in Figure 4-22.

In Figure 4-22, the force is plotted over time. After the approach of the cantilever, the force decreases within less than 0.5 seconds, due to viscoelastic relaxation of the amoeba. Subsequently, the force increases to values nearly twice as large as the adjusted force, as the acanthamoeba is pushing against the cantilever. This behavior was observed for most of the recorded curves.

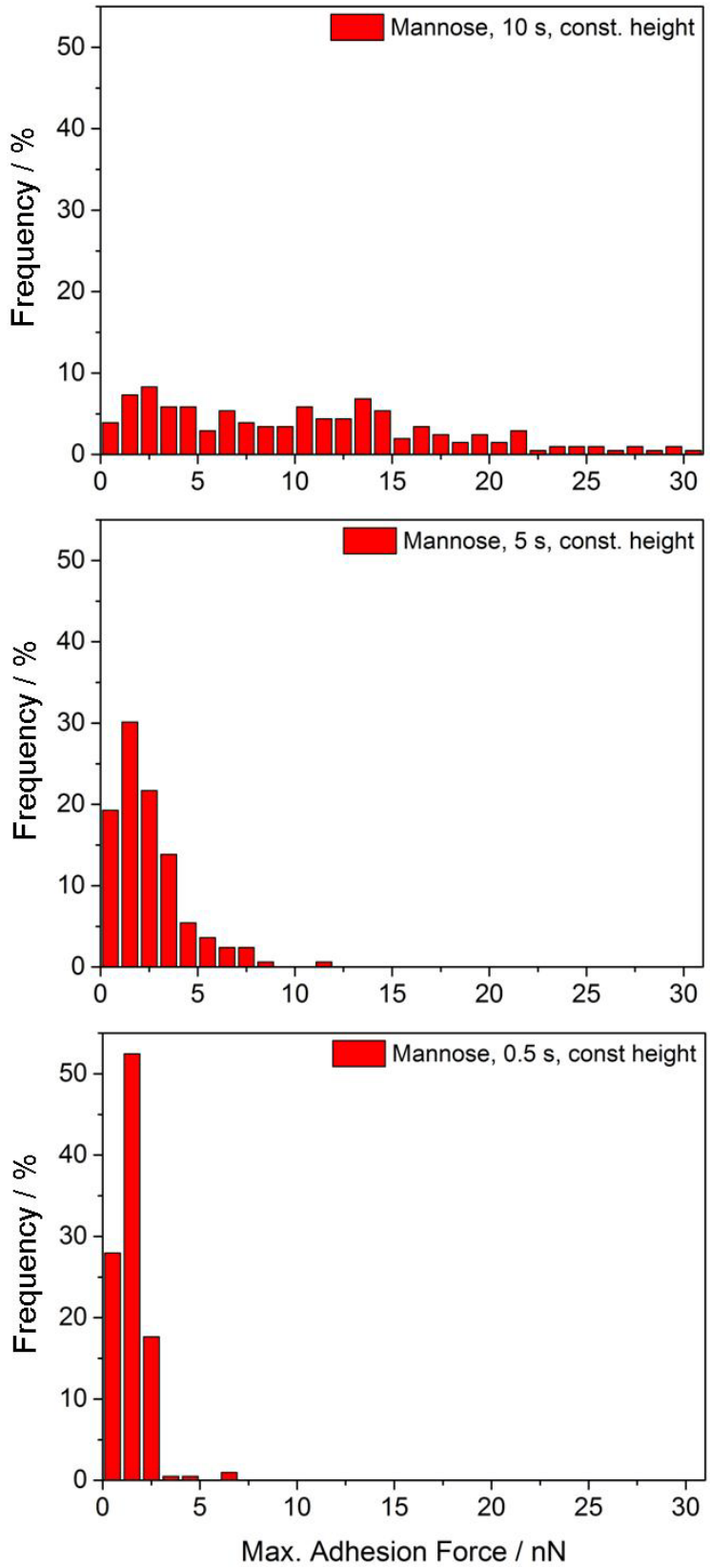

Figure 4-21 Maximum adhesion force for measurements carried out in constant height mode with contact times of 10 s (top left), 5 s (top right) and 0.5 s (down). The distribution of the values is much broader in case of 10 s contact time than for the two other contact times. The median for 10 s contact time was 9.71 nN. For 5 s it was much smaller with 2.02 nN, and for 0.5 s with 1.36 the median was the lowest.

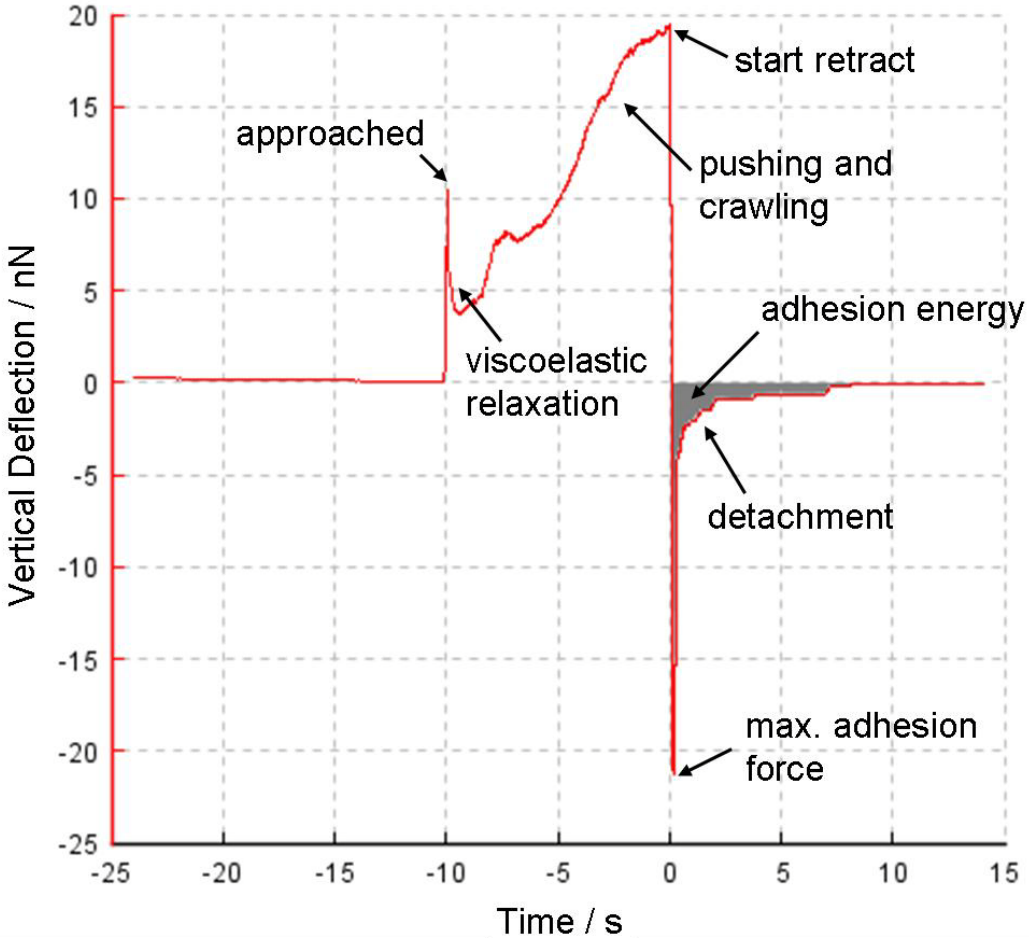

Figure 4-22 Force plotted over time during the measurement with 10 s contact time in constant height mode. The cantilever is approached to the cell at -10 s and the force increases to an adjusted force. Viscoelastic relaxation leads to a decreased force. Subsequently the force increases again to values much larger than the adjusted force as the acanthamoeba pushes against the cantilever.

Experiments in Constant Force Mode

As the acanthamoebae strongly interact with the cantilever in constant height mode, and in this way change the contact area with the cantilever, experiments were also performed in constant force mode. Here, the height of the cantilever was continuously adjusted to maintain the force at a setpoint. These experiments were conducted with acanthamoeba-cantilever contact times of 0.1 s and 5 s, as the previous measurements revealed a wide distribution of recorded data and as the feedback might sometimes not work steadily at extended contact times of 10 s. The results for the adhesion energy and the maximum adhesion force are displayed as histograms in Figure 4-23 and Figure 4-24.

Figure 4-23 (interval 1×10^{-15} J) shows that a longer contact time (5 s, top) leads to a slightly broader distribution of the values for the adhesion energy (interval 1×10^{-15} J). In this case, the values range between 0.5×10^{-15} J up to 20×10^{-15} J with a median of 1.64×10^{-15} J. After 0.1 s contact time (middle) the measures range between 0.5×10^{-15} J and 12.5×10^{-15} J, and the median is 0.305×10^{-15} J. After adding mannose to the medium (bottom) in order to saturate the mannose receptors in the membrane of the acanthamoebae, even with contact times of 5 s the median (0.485×10^{-15} J) is three times lower than for the same contact time without the block. It is still slightly higher than for 0.1 s contact time without mannose block. The values range between 0.5×10^{-15} J and 9×10^{-15} J. This shows that the binding in previous measurements was mannose-specific.

The effects of contact time and mannose addition are also observed for the maximum adhesion force (interval 0.2 nN) (Figure 4-24). With 5 s contact time (top) the median is 0.69 nN with a distribution of the values between 0.1 nN and 9.2 nN. For 0.1 s (top) the median is 0.423 nN and the measures range from 0.1 nN up to 2.4 nN. The addition of mannose to the used sodium chloride solution (bottom) results in a further decrease of the maximum adhesion force such that the median is 0.29 nN in this case with values distributed between 0.1 nN and 2 nN.

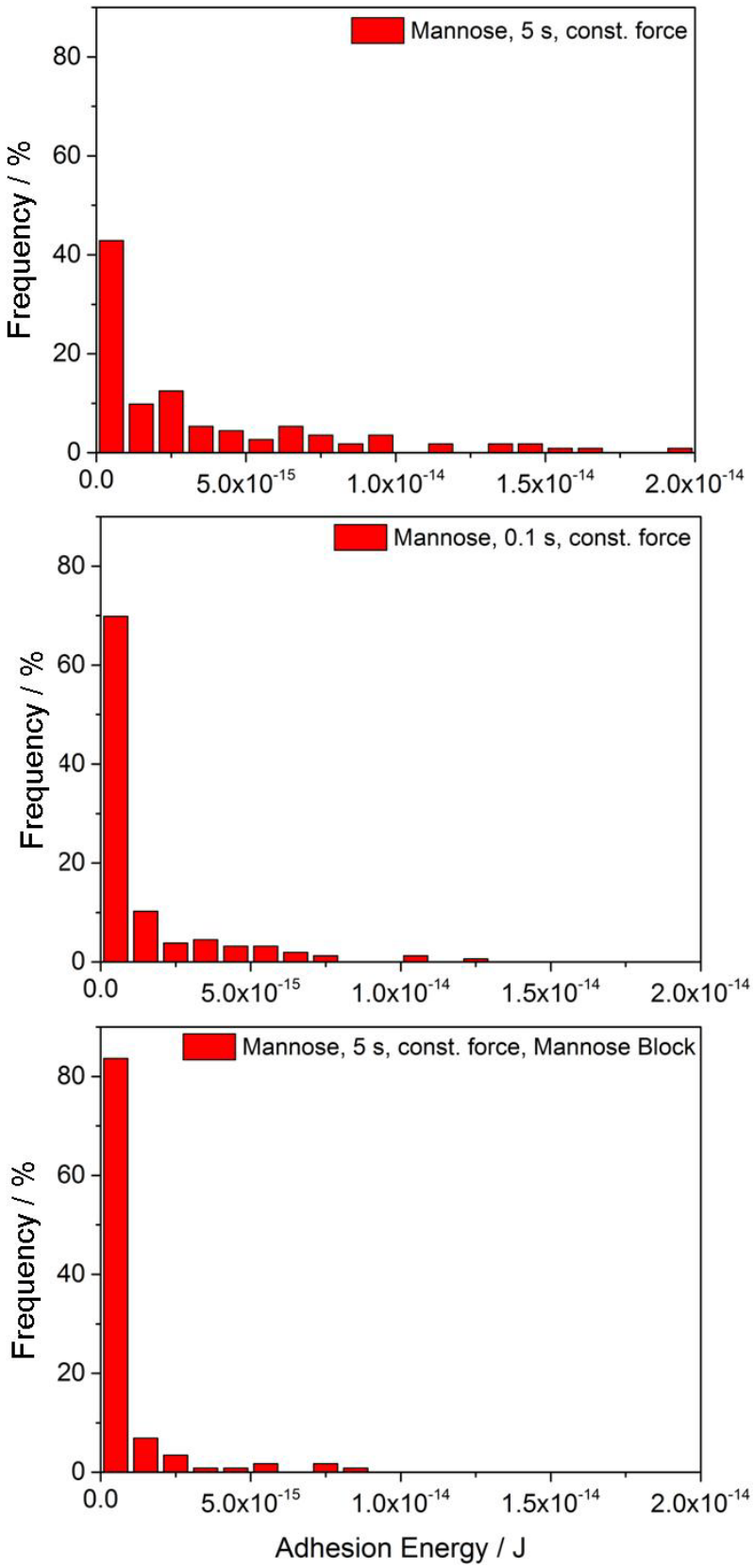

Figure 4-23 Adhesion energy of curves recorded in constant force mode with different contact times of 5 s (top), 0.1 s (middle) and 5 s with mannose added to the sodium chloride solution (bottom). The distribution of the values is broader in case of 5 s contact time than in the other two cases. The median of the adhesion energy after 5 s contact time is 1.64×10^{-15} J, with 0.1 s contact time it is 0.305×10^{-15} J. After the mannose block and 5 s contact time it is 0.485×10^{-15} J.

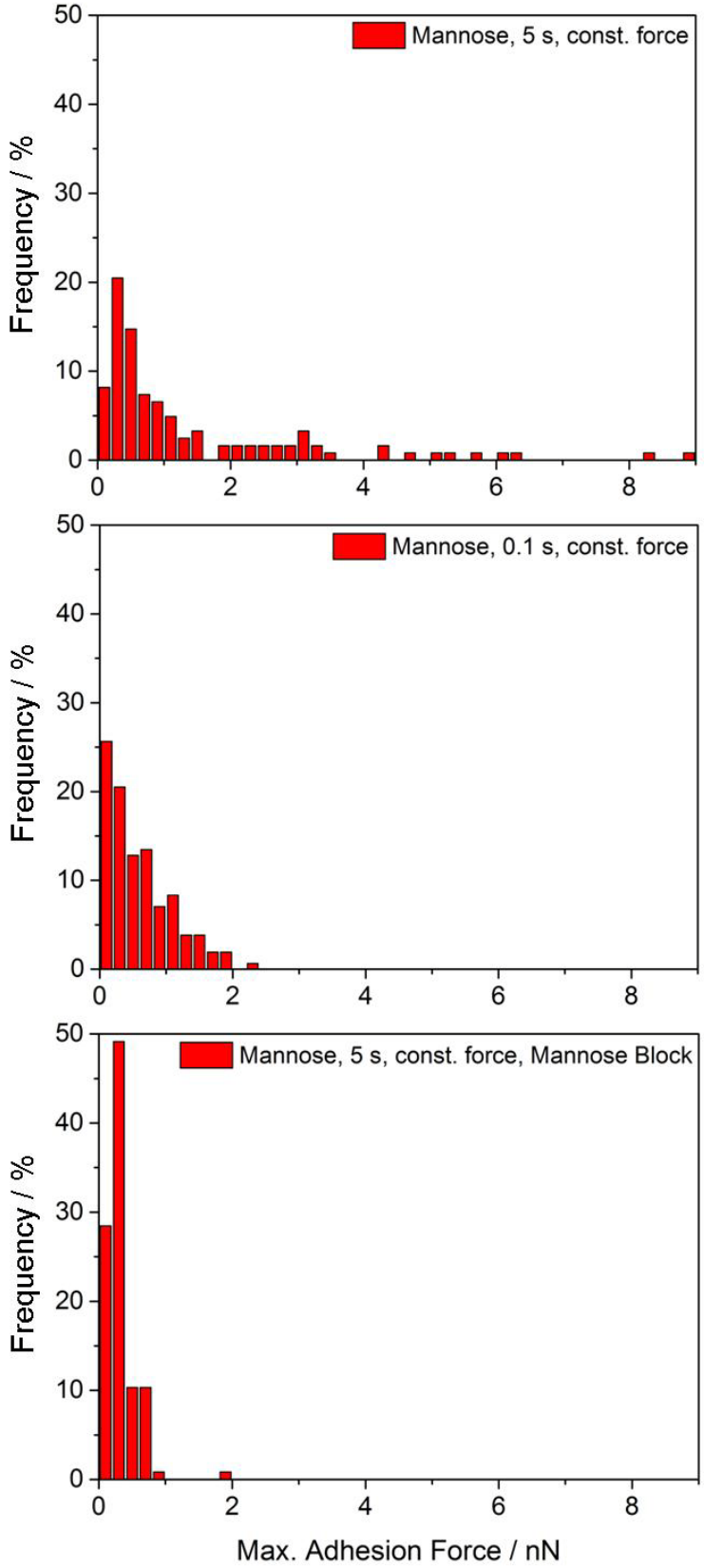

Figure 4-24 Maximum adhesion force for measurements performed in constant force mode with contact times of 5 s (top), 0.1 s (middle) and 5 s with mannose added to the sodium chloride solution (bottom). The distribution of the values is much broader in case of 5 s contact time than for the two other measurements. With 5 s contact time 50 % of the values are below, and 50 % are above 0.69 nN (median). With 0.1 s contact time the median is 0.423 nN. After addition of mannose the median decreases to 0.29 nN.

Comparison of Constant Height and Constant Force

In order to compare the different force modes, Figure 4-25 and Figure 4-26 display results from experiments in both modes.

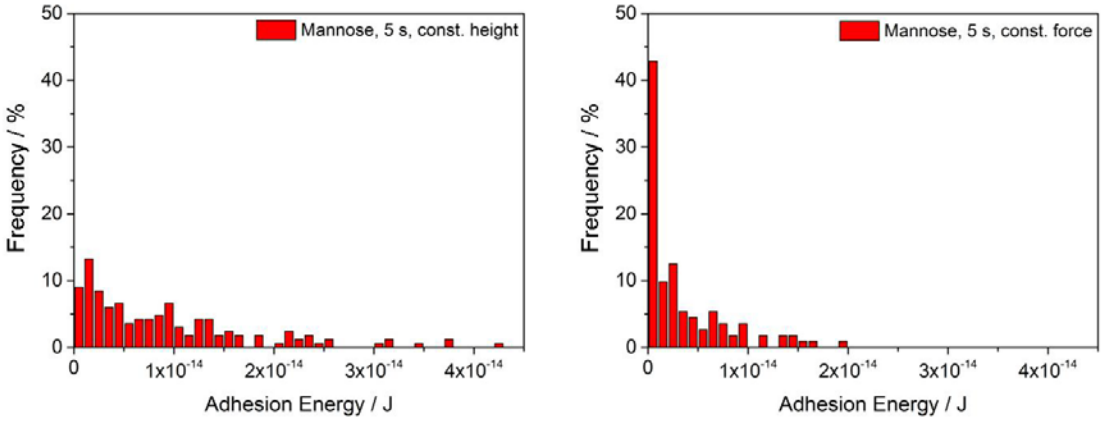

Figure 4-25 Adhesion energy of curves recorded in constant height (left) or constant force mode (right) with contact times of 5 s. The distribution of the values is broader in case of constant height mode than for constant force mode. 66 % of the values are lower than 1×10^{-15} J for constant height, while 90 % of the values are in this range for constant force mode.

The distribution of the values for the adhesion energy (Figure 4-25) is much broader for measurements conducted in constant height mode than for constant force mode (interval 1×10^{-15} J). For constant height mode (right) the values range between 2.5×10^{-15} J and 42.5×10^{-15} J. In case of constant force mode (left) the largest value in the distribution is close to 20×10^{-15} J. Also the median values differ strongly. With 6.68×10^{-15} J for constant height mode, the value is about four times higher than for constant force mode (1.64×10^{-15} J).

Also for the maximum adhesion force (Figure 4-26) the values tend to be lower in constant force mode than in constant height mode (interval 1 nN). In case of measurements in constant height mode (left) the median is 2.02 nN, while in constant force mode (right) it is 0.69 nN. The highest value recorded with constant height mode is nearly 12 nN, while it is lower than 9 nN for constant force mode.

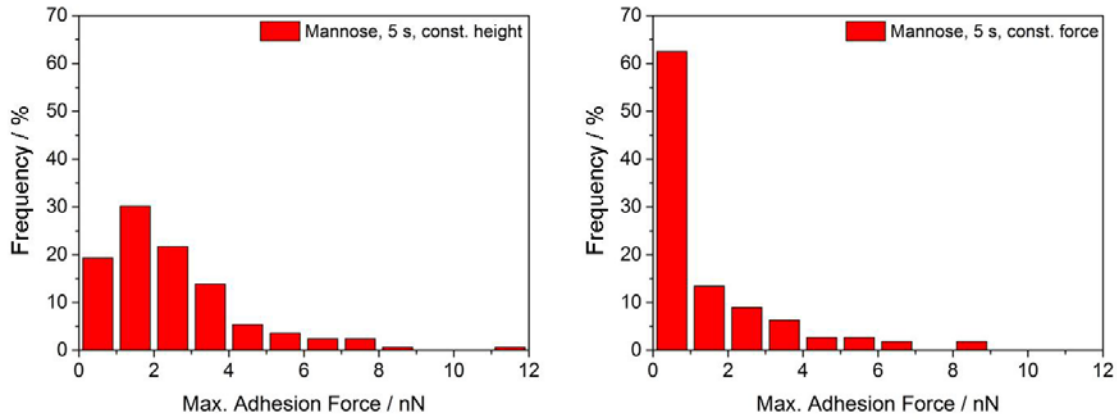

Figure 4-26 Maximum adhesion force of curves recorded in constant height (left) or constant force mode (right) with contact times of 5 s. The distribution of the values is broader in case of constant height mode than for constant force mode. In case of constant height mode the median is 2.02 nN, while it is 0.69 nN for constant force mode.

Mannitol Functionalization

In order to investigate other carbohydrates, which might be involved in the target-cell binding, mannitol-functionalized cantilevers were utilized in constant force mode. Furthermore, a block with mannose was conducted in order to evaluate, whether the binding is mannose-specific or not. The results for the adhesion energy and the maximum adhesion force of the experiments conducted with and without mannose in the sodium chloride are plotted in Figure 4-27 and Figure 4-28, respectively. The distribution of the values appears to be broader for the measurements conducted with mannose in the medium for both, the adhesion energy and the maximum adhesion force. In case of the adhesion energy (Figure 4-27), without mannose (left) the median is 1.48×10^{-15} J with values distributed between 1×10^{-15} J and 28×10^{-15} J (interval 2×10^{-15} J). For measurements with mannose added to the sodium chloride the values are distributed between 1×10^{-15} J and 36×10^{-15} J with a median of 5.59×10^{-15} J (right). The maximum adhesion force (Figure 4-28) shows similar tendencies (interval 1 nN). The median lies at 1.39 nN in case of constant force measurements without mannose in the medium (left), it is 2.46 nN when mannose was added to the sodium chloride solution before the measurements (right). In the distribution there are also differences. Without mannose, most of the values range between 0.5 nN and 6 nN, while single curves with higher adhesion energies were recorded (up to 10 nN). In case of mannose in the medium the values are distributed between 0.5 nN and 8 nN.

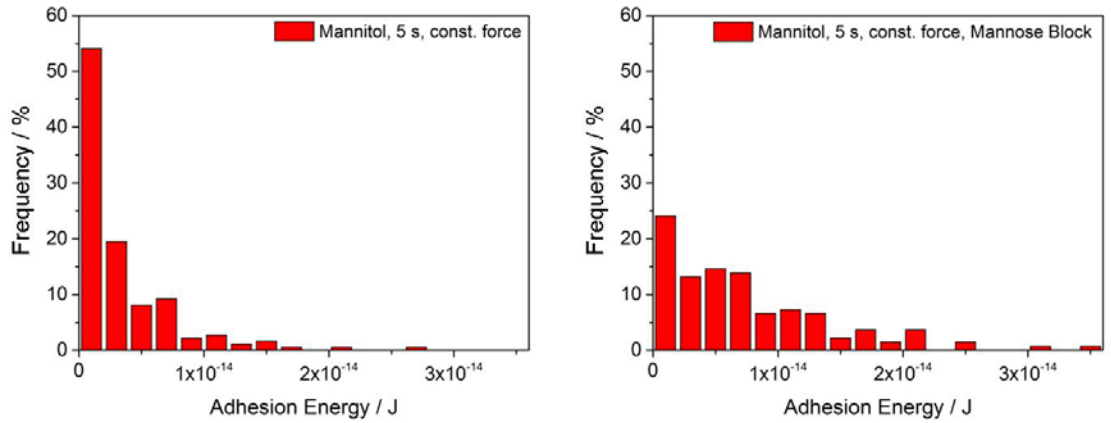

Figure 4-27 Adhesion energy of curves recorded in constant force mode with a mannitol-functionalized cantilever without (left) and with mannose added to the sodium chloride solution (right). Contact time was 5 s. The distribution of the values appears to be broader after addition of mannose to the sodium chloride solution than before. Before addition of mannose the median is 1.48×10^{-15} J, while after addition it is 5.59×10^{-15} J.

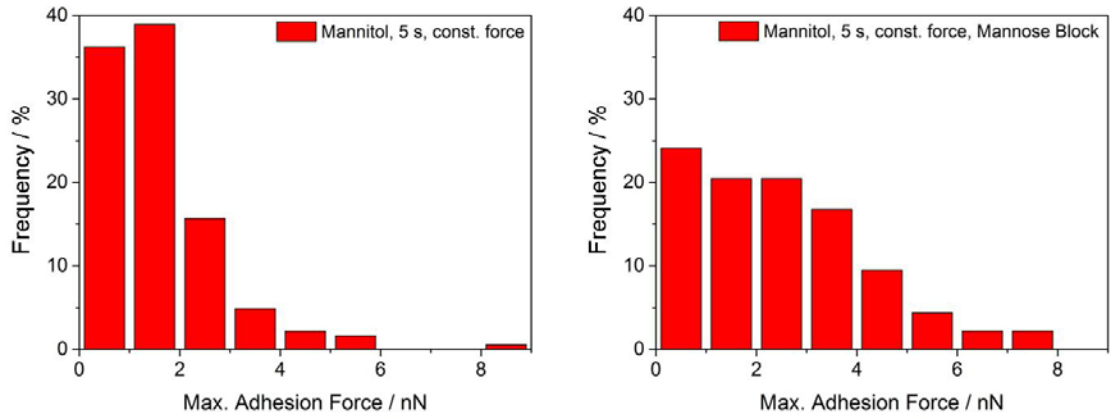

Figure 4-28 Maximum adhesion force of curves recorded in constant force mode with a mannitol-functionalized cantilever without (left) and with mannose added to the sodium chloride solution (right). Contact time was 5 s. As for the adhesion energy also the distribution of the values for the maximum adhesion force appears to be broader after addition of mannose to the sodium chloride solution than before. Before addition of mannose the median is 1.39 nN, while after addition it is higher with 2.46 nN.

Comparison of Mannose to Glucose

As glucose is known to not inhibit the binding between acanthamoebae and target-cells, it was used as a second control in the AFM experiments. Also here measurements were carried out in constant force mode. The results for the adhesion energy are presented in Figure 4-29.

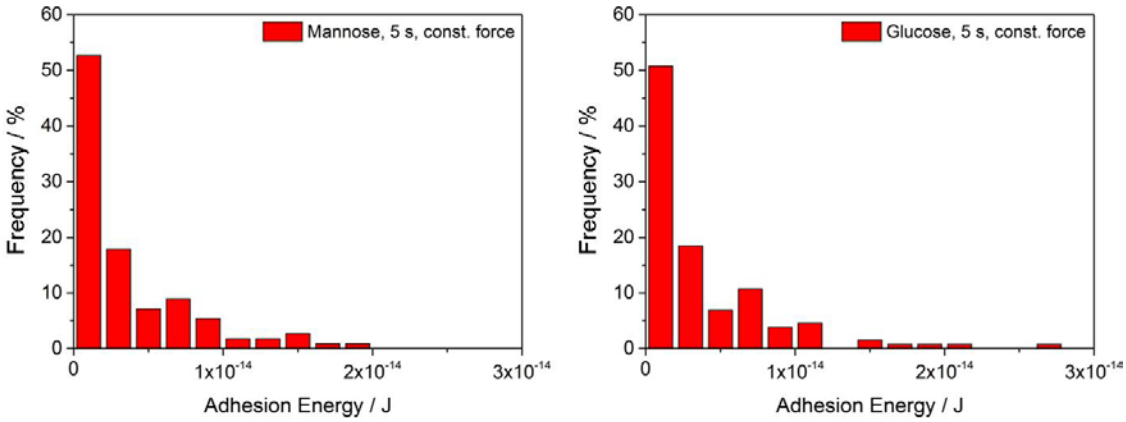

Figure 4-29 Histograms of adhesion energy of curves recorded in constant force mode with a contact time of 5 s using mannose-functionalized cantilevers (left) compared to measurements with glucose-functionalized cantilevers (right). The median value for the measurements with mannose-functionalized cantilever is 1.64×10^{-15} J, while it is 1.97×10^{-15} J in case of glucose-functionalized cantilevers.

In case of glucose-functionalized cantilevers (right), the median is 1.97×10^{-15} J, while it is 1.64×10^{-15} J for measurements conducted with 5 s contact time and mannose functionalization (left) (interval 2×10^{-15} J). Also the distribution is broader for measurements with glucose. In this case the values range from 1×10^{-15} J up to 28×10^{-15} J, while in case of mannose they range up to 20×10^{-15} J. However the distributions appear very similar.

The histograms for the maximum adhesion force (interval 1 nN) of cells tested with mannose or glucose-functionalized cantilevers are depicted in Figure 4-30.

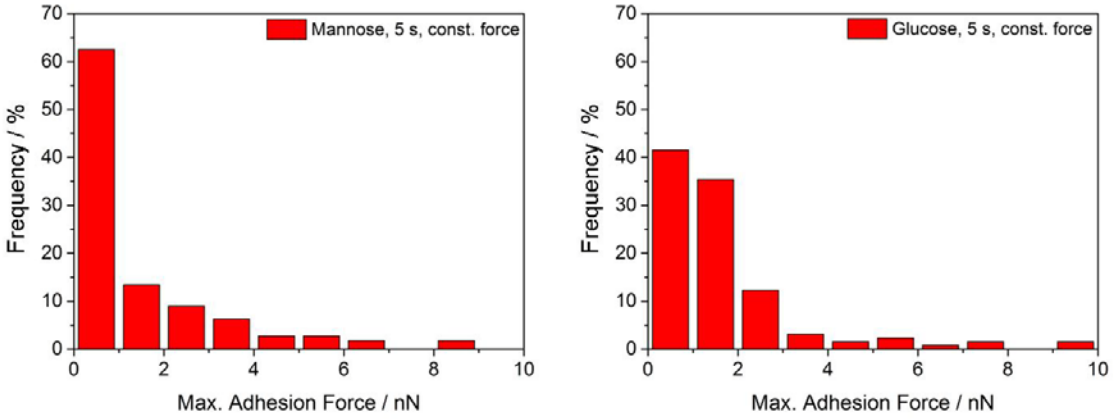

Figure 4-30 Histograms of maximum adhesion force of curves recorded in constant force mode with mannose-functionalized cantilever (left) compared to glucose-functionalized cantilever (right). Contact time was 5 s. The median for measurements performed with mannose-functionalized cantilevers is 0.69 nN, in case of glucose it is 1.25 nN.

In case of mannose the values range up to 9 nN, for glucose some curves with values of up to 10 nN were recorded. In case of mannose the median of 0.69 nN is lower than for glucose (1.25 nN).

4.4.3. Discussion

The aim of the presented AFM experiments was the analysis of mannose-specific binding of *A. castellanii* in order to obtain a more detailed insight into mannose mediated adhesion, related adhesion forces, and adhesion speed for pathogenic acanthamoebae. For fibroblasts, adhesion forces after 5 s contact time typically are below 1 nN [130]. Here, they were extremely large, but also the force setpoint was chosen much higher than for mammalian cells as at lower forces the acanthamoebae crawled away beneath the cantilever before an adhesion processes could occur.

When comparing the results achieved by using either constant height or constant force mode at 5 s contact time, it became obvious that there are significant differences in the distribution of the values of the maximum adhesion force and the adhesion energy. In case of constant height mode, the distribution of both, the adhesion energy and the maximum adhesion force, was broader than in constant force mode and also the median values were higher. A reason for this was that the force, which is applied to the acanthamoeba could not be controlled as precisely in constant height mode as in constant force mode. In constant height mode, as shown in Figure 4-22, the acanthamoeba was crawling beneath the cantilever and pushing and pulling on it during the movement, so the contact force changed drastically. Due to larger forces and increased interactions, this lead to an increased binding between acanthamoeba and cantilever. This effect could already be observed after 0.5 s contact time and was increasing with time, but not in a direct proportion. For this reason, the contact force deviated strongly from the setpoint and in many cases became larger. The larger force exerted by the cantilever lead to an increase in the maximum adhesion force and the adhesion energy, and consequently to differences in the results when comparing them to measurements conducted in constant force mode.

In constant force mode, the cantilever often started to oscillate in contact, when the acanthamoeba moved beneath the cantilever due to the force feedback. Moreover, acanthamoebae moved very fast. Hence the contact time was chosen not higher than 5 s in constant force mode. When comparing the results after 0.1 s, and 5 s contact time it became clear that binding of acanthamoeba to mannose is a relatively fast process. Already after 0.1 s contact time, binding between mannose molecules on the cantilever and the acanthamoeba surface could be observed. But there were differences in the maximum adhesion force and the adhesion energy for the two contact times, which showed that binding was increased with longer contact time. This was in agreement with the results of the experiments conducted in constant height mode, where contact times of 0.1 s, 5 s and 10 s were tested. After addition of mannose to the medium, the binding of the mannose-functionalized cantilever to the acanthamoeba surface was significantly decreased. The reason for this could be that

mannose binding receptors, MBP, in the membrane of acanthameobae were saturated by free mannose molecules in the medium. When the mannose-functionalized cantilever was approached to a trophozoite, there was no or only weak binding because possibly most MBPs were already occupied. This result confirms that the block was successful and that the observed binding of the acanthamoebae to the mannose-functionalized cantilever is mannose-specific.

As mannitol can be used to differentiate pathogenic from non-pathogenic strains of acanthamoebae [127], possibly the mannitol binding is also related to the MBP in the membrane of pathogenic acanthamoebae. In order to investigate this effect of mannitol, cantilevers functionalized with this carbohydrate molecule were used in further experiments. As shown in the results, trophozoites of *A. castellanii* bound to the cantilever independently of mannose content in the sodium chloride solution. However, with mannose in the sodium chloride solution, the distribution of maximum adhesion force and adhesion energy was even broader than without. The binding without mannose in the medium is not surprising, as mannitol can be used to differentiate pathogenic from non-pathogenic strains of acanthamoebae. It promotes the adhesion of pathogenic acanthamoebae like *A. castellanii*, while it inhibits the adhesion of non-pathogenic acanthamoebae [127]. The fact that the acanthamoebae still bound to the functionalized cantilever after addition of mannose showed a significant difference to the experiments conducted with mannose-functionalized cantilevers. In case of mannitol, the mannose binding sites on the membrane of the acanthamoebae were also saturated but this did not inhibit binding to mannitol, which leads to the conclusion that the binding of the acanthamoebae to the mannitol-functionalized cantilevers was not a specific reaction of the MBP with mannitol. Mannose even seems to have a cooperative effect in increasing the binding of trophozoites to mannitol that has not been reported in literature so far.

In order to evaluate the short term binding of acanthamoebae to glucose and to compare it to mannose, glucose was tested for binding capability to the acanthamoebae. Glucose-functionalized cantilevers were used for constant force experiments with 5 s contact time. Surprisingly, the *A. castellanii* trophozoites also bound to the glucose-functionalized cantilevers and the measurements even resulted in larger median values for the adhesion energy and the maximum adhesion force. These results were not expected and are not fully understood yet as there are no references about short-term glucose specific binding of *A. castellanii*. It is only known that glucose derivatives are not suitable for inhibiting the target-cell binding of acanthamoebae [7, 124] and that acanthamoebae do not bind to surfaces coated with glucose derivatives [7]. But glucose enhanced the uptake of particles in a concentration dependent way such that with increasing glucose content the phagocytosis is increased [98]. A possible interpretation of the unusual results might be that the usual culture medium, PYG, contains glucose, which the acanthamoebae need as a nutrient. Consequently, the acanthamoebae are also able to interact with glucose molecules but independent on the MBP.

Compared to mammalian cells, AFM measurements on acanthamoebae are significantly different. In single cell force spectroscopy experiments on mammalian cells, the cell is typically glued to the cantilever [85, 129]. This was not possible by the standard methods in case of acanthamoebae due to their great mobility. Another difference is that in case of mammalian cells often short term measurements with contact times in the range of few seconds, but also measurements with longer contact times ranging from 1 up to 2 h are conducted [131]. In case of *A. castellanii* the acanthamoebae moved beneath the cantilever leading to maximum contact times of 10 s. This movement beneath the cantilever and pressing against the cantilever in constant-height mode furthermore lead to drastically increased contact forces between cantilever and acanthamoebae. In case of mammalian cells an opposite effect had been observed, when measuring in constant height mode. For mammalian cells the preset force is normally not constant but decreases to lower value [87]. These facts show that the standard methods have to be changed in order to account for the extreme mobility of the acanthamoebae.

Overall, it can be concluded that *A. castellanii* bound to different carbohydrates. In case of mannose-functionalized cantilevers the addition of mannose to the medium lead to a significant narrower distribution of the adhesion energy and the maximum adhesion force, which showed that the binding is mannose-specific. For the measurements with mannose-functionalized cantilevers it can be concluded that the contact time as well as the operation mode influenced the binding of the cell to the mannose-functionalized cantilever. In summary, the AFM single cell force spectroscopy measurement procedure on *A. castellanii* is restricted due to the extreme mobility of the trophozoites. According to current knowledge, such AFM measurements on acanthamoebae adhesion to mannose were performed for the first time and may serve as basics for future studies.

5. Intracellular Dynamics

The cytosolic space of acanthamoebae is extremely crowded compared to the intracellular space of other cell types such as *Schizosaccharomyces pombe* or fibroblasts. It comprises different vacuoles like digestive and contractile vacuoles, and smaller vesicles and granules. The motion inside the cell plays an essential role in the extracellular target-cell killing, which was described in more detail in 1.2.2. Furthermore, actin has been reported to play a role in the contraction of the contractile vacuole, which regulates the osmotic pressure in the cell. It is also known that myosin IC is located around the vacuole prior to contraction [24, 132-134]. Myosin I is mainly present near the rear edge of the acanthamoebae and in the filopodia [23-24]. Myosin II can be found within the whole cytoplasm and is concentrated in the cell cortex [132]. Baumann and Murphy showed that mitochondria co-localize with the microtubules in *Acanthamoeba castellanii* and that the movement of mitochondria and small particles could be inhibited by colchicine, a microtubule depolymerizing substance [135]. This indicates that kinesins and dyneins are involved in the movement of these particles. Apart from such actively driven motion, Brownian motion and subdiffusive motion have been reported to play an important role in different cellular systems [136-138].

In acanthamoebae intracellular transport processes are essential for the target-cell killing process, as pore-forming proteins and other cytolytic factors have to be transported to the contact site between the acanthamoeba and the target-cell. Prior to understanding the complex impact of a target-cell, here the pure intracellular motion in acanthamoebae and the impact of different cytoskeletal filaments and molecular motors is studied.

In order to investigate the influence of molecular motors and other actively driven processes on intracellular dynamics in acanthamoebae, different substances were applied, that either influence the polymerization of microtubules or actin filaments, or inhibit molecular motors.

5.1. Materials and Methods

All experiments were conducted at least three times and at 10 to 100 particle tracks in different *A. castellanii* cells were evaluated. For clarity all results are shown and discussed at the example of a single representative cell.

5.1.1. High Speed Live Cell Imaging

For the microscopic observation of acanthamoebae, the medium in the tissue culture bottles were renewed, the acanthamoebae were counted, and about 10^5 acanthamoebae per milliliter were seeded on a flat surface (tissue culture bottle, six-well plate, Sarstedt AG & Co., Nümbrecht, Germany). The acanthamoebae attached and actively crawled on the surface. Motion of the whole cell as well as motion of

particles, such as lipid granula and vacuoles inside the acanthamoebae, were observed through an inverted phase contrast microscope (Olympus CKX41, Olympus Deutschland GmbH, Hamburg, Germany). Sequences of 30 s to 50 s were recorded with a high speed camera (Hamamatsu C9300, Hamamatsu, Japan) at fixed frame rates of either 80 or 97 frames per second (fps).

5.1.2. Inhibition of Myosin II with Blebbistatin

For inhibiting myosin II motors (-)-Blebbistatin is used. It penetrates through the membrane and binds to the ATPase, which is a catalyzer for ATP hydrolysis. It blocks the myosin heads in an actin unbound state as it slows down ATP hydrolysis, especially the release of phosphate [139].
(-)-Blebbistatin (Sigma-Aldrich Chemie GmbH, Munich, Germany) was dissolved in DMSO at a 1 mM concentration. Acanthamoebae were counted and 7×10^4 amoebae were seeded in each well of a 6-well plate (Sarstedt AG & Co., Nümbrecht, Germany). The acanthamoebae were incubated in 1.5 ml PYG Medium over night at RT. (-)-Blebbistatin was added to the medium with different concentrations of 50 µM, 60 µM, and 70 µM respectively. A few minutes after addition, sequences of the acanthamoebae were recorded in the same way as described before with frame rates of either 80 fps (full image size) or 97 fps (region of interest, reduced image size). 15 to 40 min after initial treatment, again sequences were recorded with the same parameters.

5.1.3. Depolymerization of Actin Filaments by Latrunculin A

Latrunculin A inhibits the polymerization of actin filaments as it binds to the subunits of the actin filaments and avoids a further reaction of the subunits to longer filaments [17].
Latrunculin A (Sigma-Aldrich Chemie GmbH, Munich, Germany) was dissolved in DMSO (Carl Roth GmbH & Co. KG, Karlsruhe, Germany) at a 1 mM concentration as a stock solution. Acanthamoebae (8×10^4) were grown in a six well plate and incubated over night at RT for surface adhesion. The medium was renewed and latrunculin A was added to the wells at concentrations of 2 µM, 5 µM, 7.5 µM and 10 µM, respectively. High speed sequences with 97 fps were recorded a few minutes after addition and after 1 to 2 h incubation at RT.

5.1.4. Depolymerzation of Microtubules by Nocodazole

For microtubule depolymerization nocodazole is used. Nocodazole binds to the subunits of the microtubuli and thus prevents polymerization [17]. Stock solutions of nocodazole (Sigma-Aldrich Chemie GmbH, Munich, Germany) in DMSO (Carl Roth GmbH & Co. KG, Karlsruhe, Germany) were prepared at 1 mM and 10 µM concentrations. The acanthamoebae were cultured as described in 5.1.3 and nocodazole was added at concentrations of 10 µM, 20 µM and 40 µM. Sequences were

recorded as described before at 97 fps a few minutes after addition of nocodazole and after 1 to 2 hours.

5.1.5. Analysis of Sequences

The motion of lipid granula and vacuoles inside the *Acanthamoeba* was evaluated from all recorded sequences using the MATLAB program Polyparticletracker [137, 140]. The program graphically isolates dark or bright particles even against a complicated background by using a Polynomial fit Gaussian Weight method, and tracks the motion of isolated particles by evaluating the x- and y-position as a function of time [137].

The tracks of the particles are further investigated by determining the time averaged mean square displacement (TA MSD)

$$\overline{\delta^2(\Delta,T)} = \frac{1}{T-\Delta}\int_0^{T-\Delta} dt\left[x(t+\Delta)-x(t)\right]^2 \tag{5}$$

where T is the duration of the sequence, Δ is the lag time and x is the time sequence of the position of a particle [141].

From the slope of the mean square displacement the diffusive exponent α can be determined, which gives important information about the type of motion of the particle. If the diffusive exponent is $\alpha < 1$ the motion is subdiffusive (suppressed), if $\alpha = 1$, the particle is moving in a Brownian motion (normal diffusive) and if $\alpha > 1$ the motion is superdiffusive (active) [141].

For acanthamoebae, which were not treated with any substance (in the following referred to as intact), besides the mean square displacement, the center of mass of the acanthamoebae was determined by a home-written MATLAB program available in the lab. The calculation of the center of mass was partly done by Ali Raza. In order to analyze, which impact the movement of the whole cell has on the intracellular dynamics the center of mass was subtracted from the particle track.

5.2. Results

5.2.1. Intracellular Motion in Intact *A. castellanii*

From high speed sequences of *A. castellanii* recorded with phase contrast microscopy, tracks of small granula and large vacuoles were determined. A sequence of images starting from 0 s, recorded every 5 s is shown in Figure 5-1.

In intact acanthamoebae strong movements of small granula (red arrows) and large vacuoles (yellow arrows) inside the cell were observed. In addition, the *A. castellanii* trophozoites showed a directed crawling motion on the surface of the petri dish, which also becomes obvious when comparing the images of the sequence in Figure 5-1.

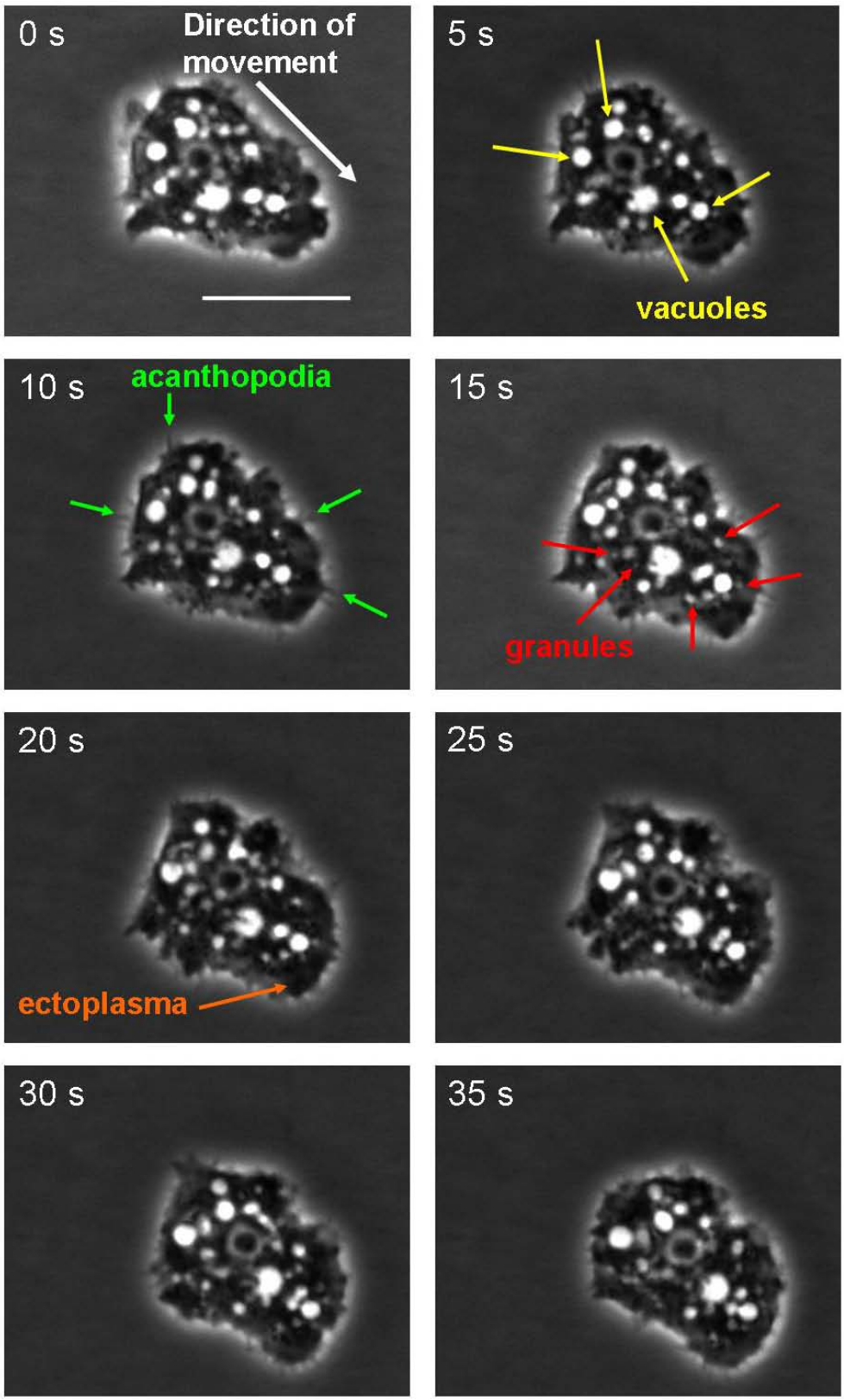

Figure 5-1 ***A. castellanii*** **trophozoite crawling on a surface towards the bottom right corner. The Acanthamoeba build acanthopodia (green arrows) by which the amoeba is pulled forward. These acanthopodia stay at one place during the movement of the acanthamoeba. The leading edge of the acanthamoeba consists of ectoplasma (orange arrow) without organelles.Vacuoles (yellow arrows) and granules (red arrows) perform strong movements with the fluid flow and also independently. Scalebar 20 µm.**

Also, the formation of small acanthopodia becomes visible in these images (some are marked with green arrows). These attached to the surface and stayed at one place while the cell was moving. The acanthamoebae pushed the ectoplasma (orange arrow), which does not contain any organelles, in the direction of movement and the cell body followed this direction.

In Figure 5-2, the tracks of individual particles as derived from the sequence are shown.

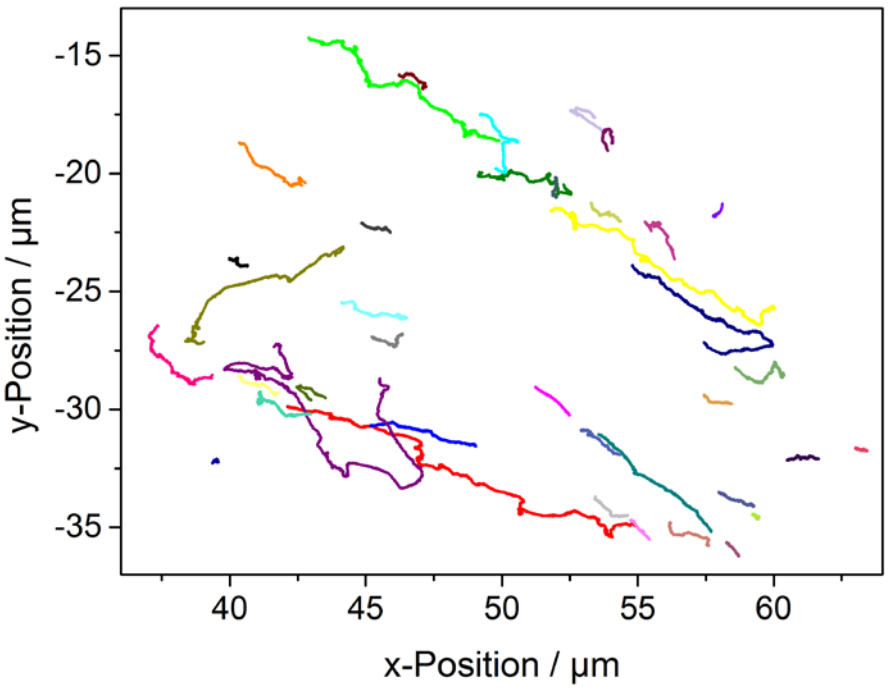

Figure 5-2 Trajectories of particles tracked inside the acanthamoeba shown in Figure 5-1. The acanthamoeba was crawling towards the right bottom of the image. This direction can also be observed from the particle trajectories.

In the case shown here, the acanthamoeba was moving towards the right bottom corner of the image. This movement also superimposes the motion of intracellular particles: nearly all tracks have the same directionality like the movement of the whole cell. The directionality of the movement of the acanthamoeba is clearly shown in

Figure 5-3, which depicts the center of mass of the moving acanthamoeba. During recording of the sequence the acanthamoeba moved about 5 µm in y-direction, and about 8 µm in x-direction. The oscillations in the track are reasoned by deviation in the area calculation of the MATLAB program.

In order to determine the influence of the center of mass on the particle motions, the x- and y-positions of the center of mass were substracted from the x- and y-positions of the particle trajectories. The trajectories of the particles after subtraction of the center of mass are depicted in Figure 5-4.

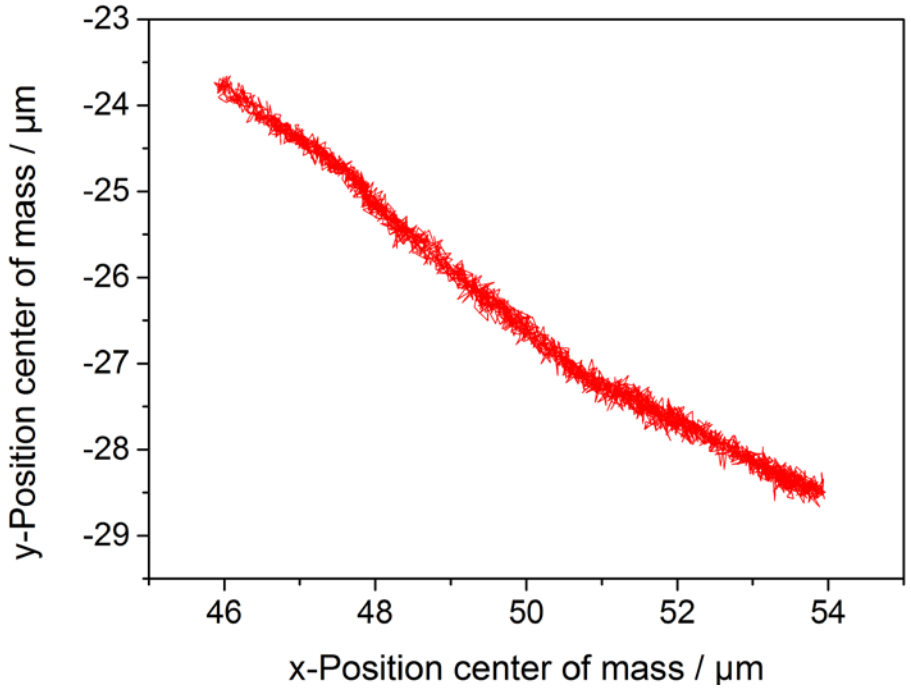

Figure 5-3 Center of mass of a moving *A.castellanii*. The direction of movement towards the right bottom corner becomes clear.

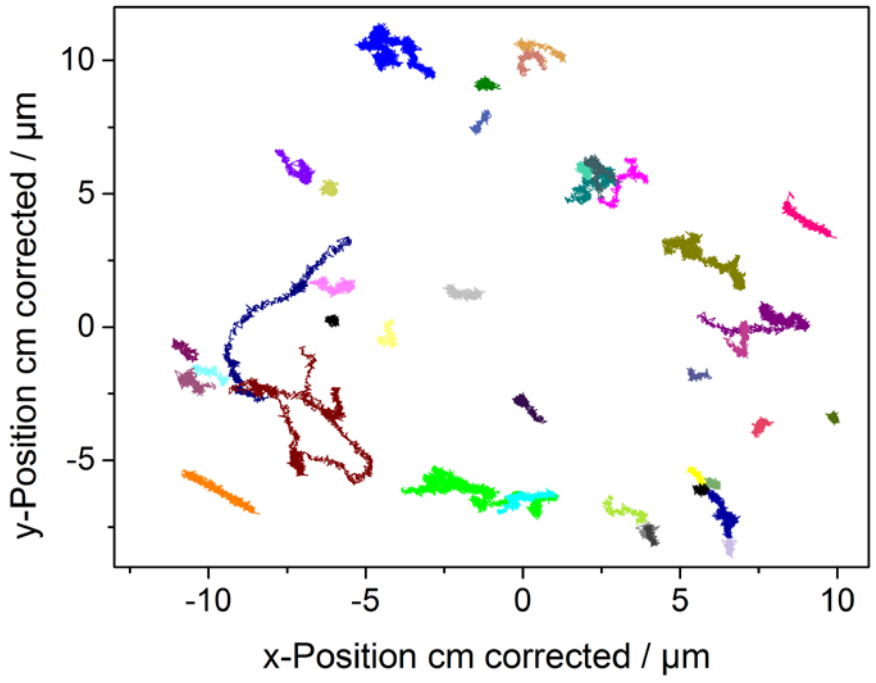

Figure 5-4 Particle trajectories of intracellular granules and vacuoles after subtraction of the center of mass. The positions of the single tracks are changed due to the subtraction. The trajectories do not show a strong directionality anymore.

The particle positions were changed drastically due to the subtraction of the center of mass. Due to the subtraction, the direction of the trajectories was also changed and

overall a distinct directionality cannot be observed from the graph anymore. Particles, which followed the direction of movement of the whole cell, showed much narrower trajectories after subtraction of the center of mass than before.

In Figure 5-5, the time-averaged mean square displacement of the tracks of vacuoles and granules inside an acanthamoeba, which was not treated with any chemicals, is plotted over time.

From the slope of the MSD curves, the diffusive exponent α was calculated. For most of the tracks, the diffusive exponent was between 1.6 and 1.9. Some single granules showed normal diffusive behavior. In total, more than 100 tracks from three cells were evaluated.

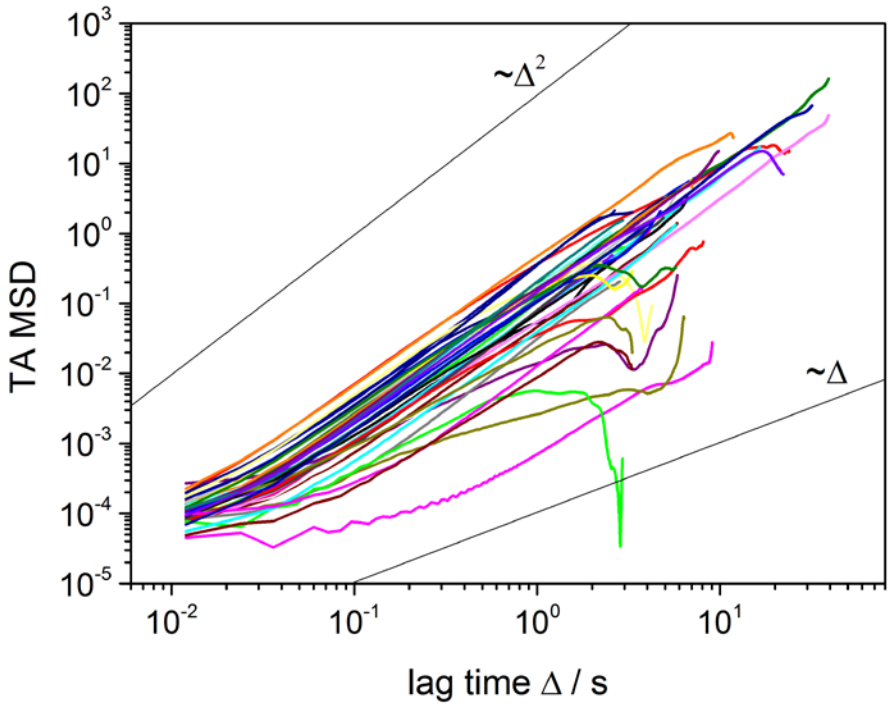

Figure 5-5 Time averaged MSD of intracellular particles and vacuoles. Most of the particles show superdiffusive motion with diffusive exponent close to α ~ 2. The coloured lines belong to the tracks marked by the same colour in Figure 5-2.

Also from the center of mass corrected data, the mean square displacement was determined (Figure 5-6). For short lag times ($\Delta \leq 0.2$ s) the center of mass corrected trajectories gave diffusive exponents of significantly less than $\alpha < 1$. This shows that the motion was strongly subdiffusive. For longer lag times ($\Delta \geq 0.2$ s) nearly all particles showed diffusive exponents of close to $\alpha = 2$ and therefore actively driven motion.

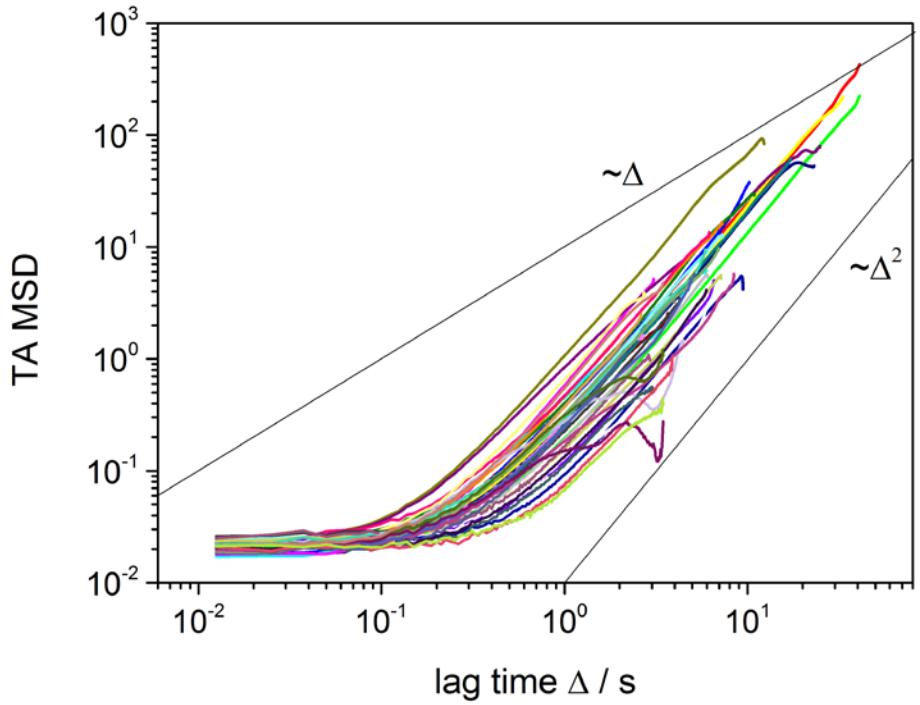

Figure 5-6 Mean square displacement of center of mass corrected particle trajectories. For short lag times ($\Delta \leq 0.2$ s) all particle show diffusive exponents of $\alpha < 1$. For longer lag times the diffusive exponent approaches nearly $\alpha = 2$. This shows that the subtraction of the center of mass does not influence the actively driven nature of the system significantly. Therefore, also other active transport mechanisms such as transport on molecular motors must be involved.

5.2.2. Inhibition of Myosin II by (-)-Blebbistatin

For inhibition of myosin II motors walking along actin filaments, the acanthamoebae were treated with (-)-Blebbistatin, a motor inhibiting substance. In Figure 5-7 an image of a blebbistatin treated acanthamoeba is shown (A) as well as the trajectories of particles inside the acanthamoeba right after addition.

The experiments showed that the trophozoite had a rough shape with long membrane extensions, which were not present in the intact case. The intracellular structures appeared less defined than before the treatment. Right after addition the overall motion of the cell was nearly stopped, and also the intracellular dynamics were reduced drastically, which is represented by the particle tracks shown in Figure 5-7 B. The tracks of the particles differed strongly from the intact acanthamoeba, as intracellular motion came to a complete stop.

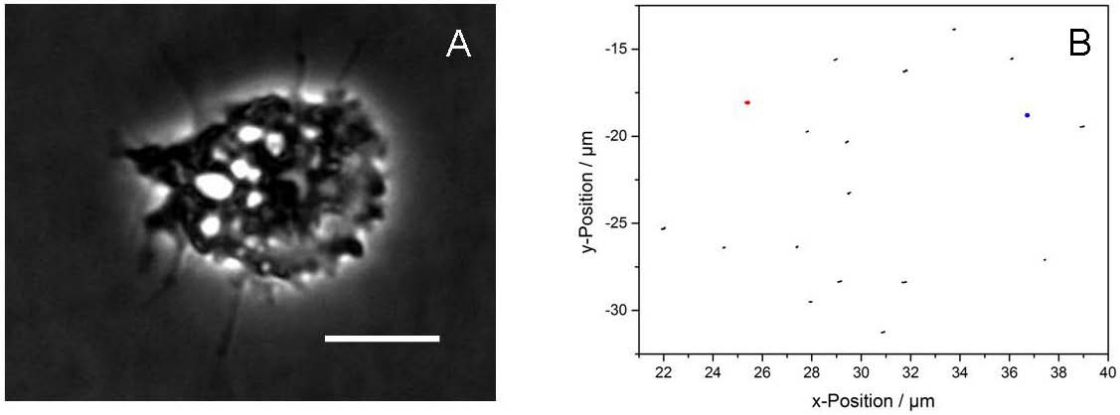

Figure 5-7 *A. castellanii* treated with (-)-Blebbistatin, which inhibits the myosin II motors (A). The acanthamoeba shows long acanthopodia and a rough surface. From the sequences it could be observed that the acanthamoeba stopped moving. The trajectories (B) indicate that also intracellular motions are drastically reduced.

20 min to 40 min after addition the intracellular movement started again. In Figure 5-8, a blebbistatin treated acanthamoeba (A) as well as the corresponding particle trajectories (B) are shown 20 min after addition. The acanthamoeba still looked different from the intact case. Long acanthopodia were visible around the whole cell, which had a relatively round shape. While the whole cell was immobile, intracellular motion started again, although the mode of motion strongly differed compared to intact acanthamoeba (Figure 5-8 B). The trajectories also appear different than those of the center of mass corrected particle trajectories.

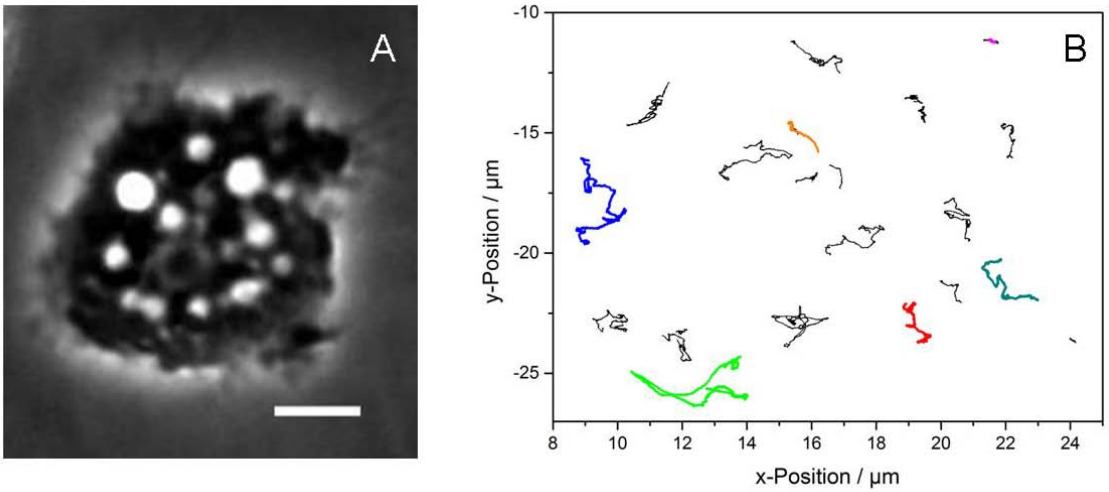

Figure 5-8 Blebbistatin treated *A. castellanii* 20 min after addition. The shape of the acanthamoeba is similar as directly after the addition of Blebbistatin, i.e. still with long membrane extensions. From the particle trajectories it becomes obvious that the particles started to move again although the cell itself does not move much. Scalebar = 5 µm

In Figure 5-9, the TA MSD for particles in a blebbistatin treated acanthamoeba right after addition is plotted over time. It became obvious that the diffusive exponent was significantly below 1 with $\alpha \sim 0.3$ at lag times of $\Delta \leq 1$ s. This revealed a severe change of the intracellular dynamics. After lag times of $\Delta \geq 1$ s nearly normal diffusion behavior with $\alpha \sim 1$ could be identified. This behavior was also remarkably different from the intact case. In the blebbistatin treated acanthamoebae no superdiffusion and therefore no active motion could be observed.

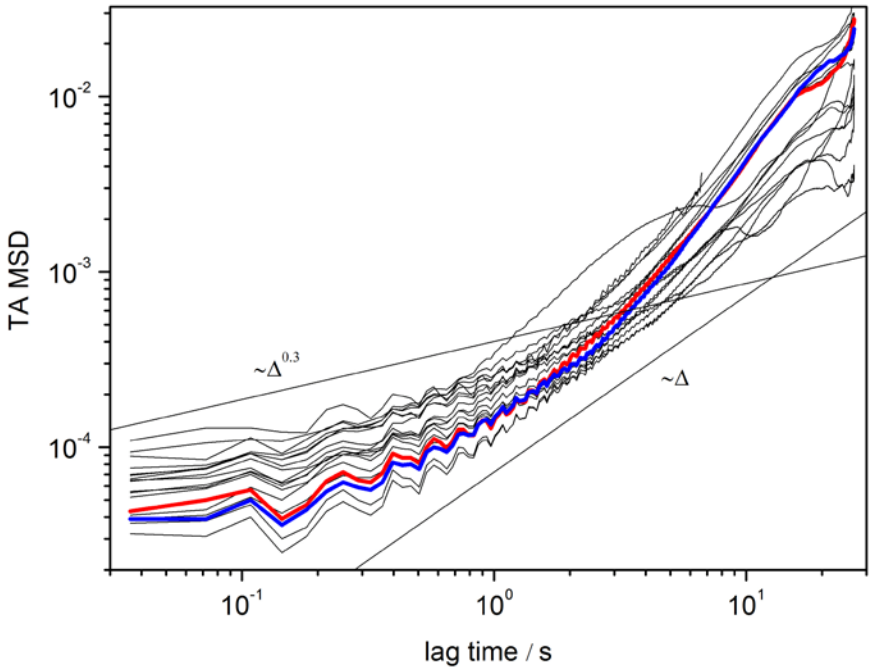

Figure 5-9 Time averaged MSD of intracellular particles and vacuoles in a blebbistatin treated acanthamoeba. Most of the particles show subdiffusive behavior at lag times of $\Delta \leq 1$ s, while it becomes normal diffusive or superdiffusive after lag times of $\Delta \geq 1$ s. The coloured lines belong to the tracks marked in the same colour in Figure 5-7.

In Figure 5-10, the TA MSD for vacuoles (A) and granules (B) (see Figure 5-1) in a blebbistatin treated acanthamoeba 20 min after addition are plotted over time.
For granules (B) it could be observed that after lag times of $\Delta \sim 0.1$ s most of the granules showed superdiffusive behavior. The diffusive exponent was almost $\alpha = 2$. In case of the MSD there was no strong difference between the blebbistatin treated acanthamoebae after 20 min, and the non-treated acanthamoebae. In case of larger vacuoles, the diffusive exponent was mostly between 1 and 2.

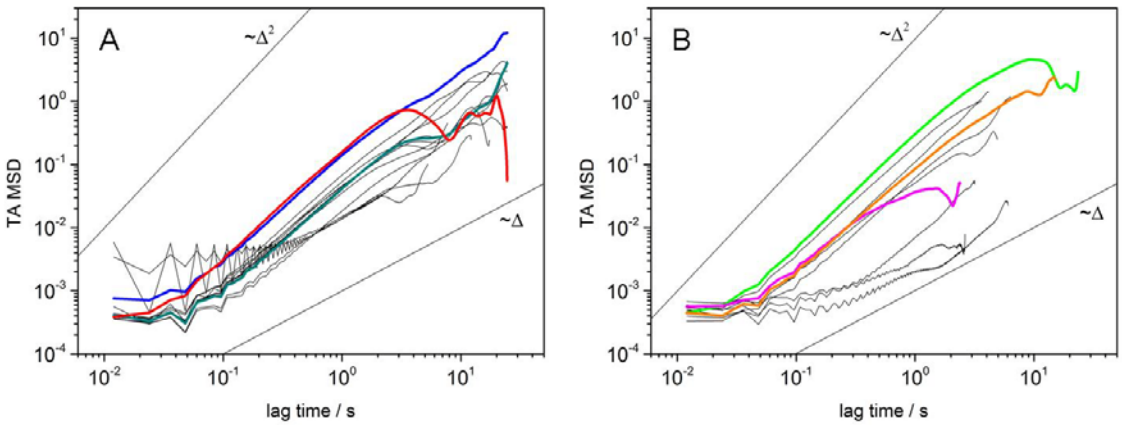

Figure 5-10 Time averaged MSD 20 min after blebbistatin addition. Most particles and vacuoles show superdiffusive motion in the long term, for small granules at short lag time scales the diffusive exponent is α < 1. Coloured lines belong to the marked traces in Figure 5-8 B.

5.2.3. Depolymerization of Actin Filaments by Latrunculin A

In Figure 5-11, a latrunculin A treated acanthamoeba (A) is shown as well as the corresponding trajectories of intracellular particles (B). The phase contrast image of the acanthamoeba shows that after latrunculin A treatment it had a round shape compared to the intact case. Small acanthopodia could be identified at the edge of the acanthamoeba, but the movement of the acanthamoeba was significantly reduced and nearly stopped. The whole cell seemed to be relatively flat and smaller granules could be identified more clearly at the acanthamoeba edge than in the intact case. The trajectories make clear that the particles inside the cell still moved in different directions but without drift.

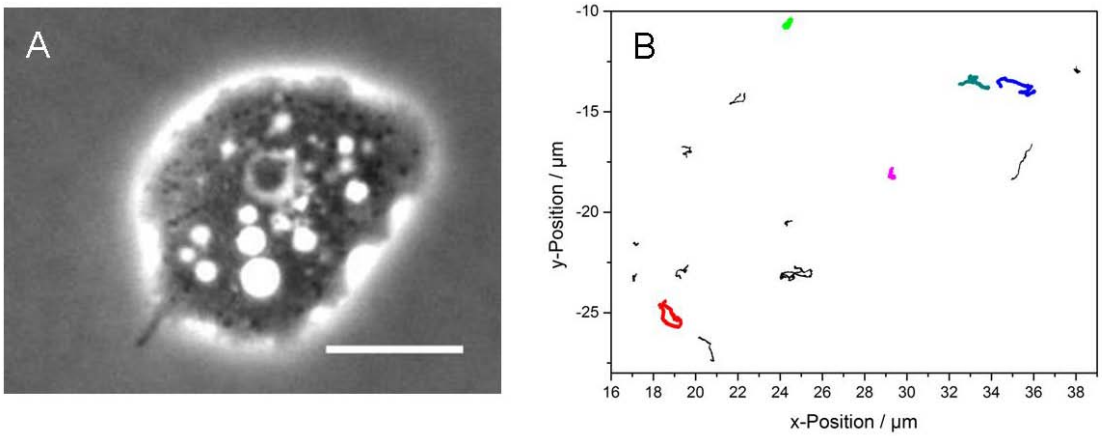

Figure 5-11 Latrunculin A treated *A. castellanii* (A) and corresponding particle trajectories (B). The acanthamoeba has a round shape and vacuoles and granules are better visible than in the intact case presumably due to a reduced actin content in the regions near the acanthamoeba edge. The trajectories indicate slight movements of intracellular particles but no strong drift. Scalebar = 10 µm.

In Figure 5-12 the TA MSDs for large and small particles inside the latrunculin A treated acanthamoeba are shown. The colours mark the particles, which were shown in the same colour in Figure 5-11.
From the 2D plot of the MSD over time it becomes obvious that the diffusive exponent was $\alpha \sim 1.7$ in nearly all cases for the larger particles (A), which indicated a superdiffusive kind of motion. For the small particles (B), the diffusive exponent was $\alpha < 1$ for short lag times, after $\Delta \geq 0.2$ s lag time the curve approached a slope of $\alpha \sim 1$ or slightly higher values, indicating brownian motion.

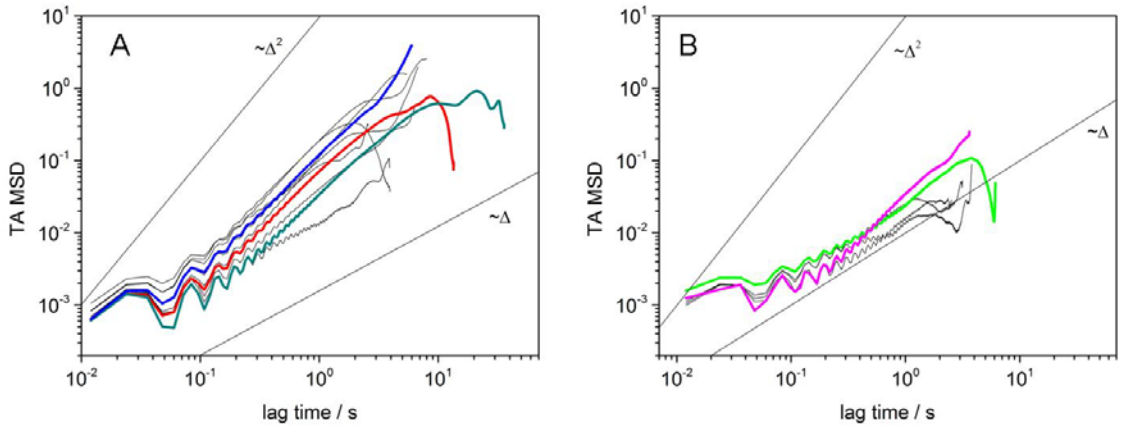

Figure 5-12 Time averaged MSD curves for latrunculin A treated *A. castellanii* for large (A) and small (B) particles. Most vacuoles (A) show superdiffusive motion with diffusive exponents close to $\alpha \sim 1.7$. Small granules have a diffusive exponent of $\alpha < 1$ for short lag times, for lag times of $\Delta \geq 0.2$ s it approaches $\alpha \sim 1$ or slightly higher values. Coloured lines belong to the marked traces in Figure 5-11 B.

5.2.4. Depolymerization of Microtubules by Nocodazole

In case of acanthamoebae treated with nocodazole for microtubule depolymerization, the acanthamoebae had a comparably rough shape (Figure 5-13 A) and the motion of the acanthamoebae was drastically reduced compared to the intact case, and nearly completely stopped.
Small acanthopodia as well as membrane protrusions are visible in Figure 5-13 A. The motion of the acanthamoeba stopped nearly completely. Also the intracellular motion was changed significantly by nocodazole. This can also be observed from the particle trajectories in Figure 5-13 B. The particles moved in diverse directions, indicating that the fluid flow inside the acanthamoeba was drastically reduced.
Comparable to latrunculin A, the TA MSD lead to diffusive exponents of $\alpha \sim 1.7$ for nearly all particles (Figure 5-14) in nocodazole-treated acanthamoebae. The oscillations in the TA MSD were less pronounced compared to the latrunculin A case.

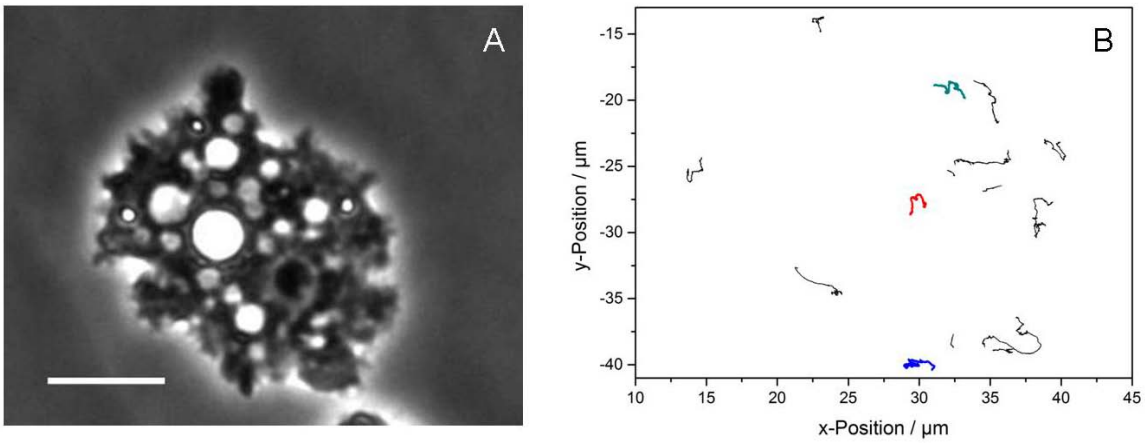

Figure 5-13 Nocodazole treated *A. castellanii* (A) and corresponding trajectories of intracellular particles (B). The shape of the acanthamoeba is rougher than in the intact case. The vacuoles and some smaller particles are clearly visible. The trajectories show that the particles move in different directions, which indicates that the fluid flow in one direction inside the acanthamoeba is drastically reduced. Scalebar = 10 µm.

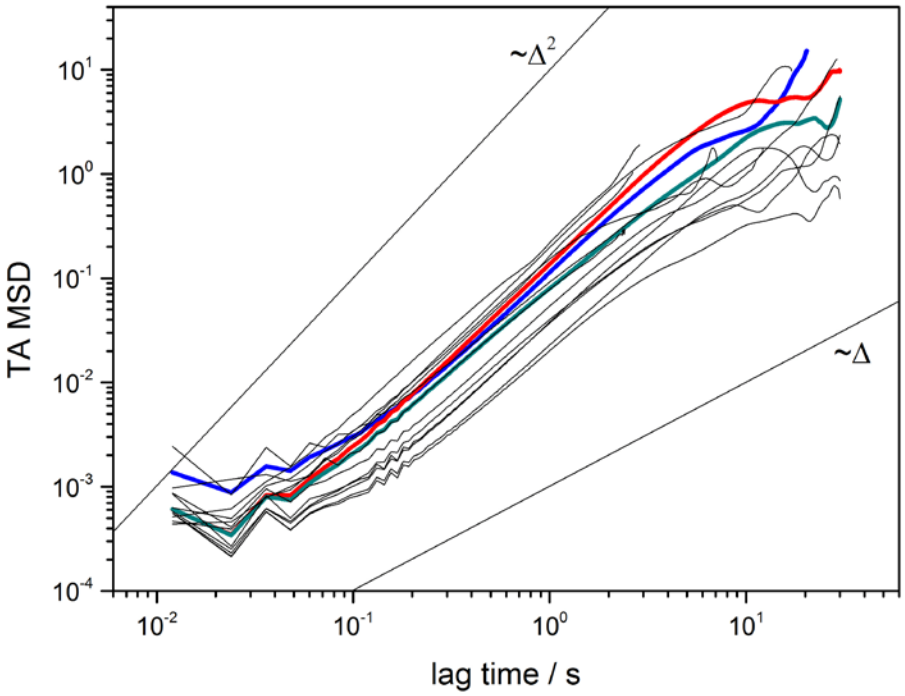

Figure 5-14 Time averaged MSD curves for nocodazole treated *A. castellanii*. All particles show superdiffusive motion with diffusive exponents close to $\alpha \sim 1.7$. Coloured lines belong to the marked traces in Figure 5-13 B.

5.2.5. Comparison of the Results after Different Treatments

The results of the different treatments are given in the boxplots in Figure 5-15 and Figure 5-16. In all regarded cases the diffusive exponent as well as the directionality

was determined. These values differ strongly, when comparing the different treatments to the intact case.

In Figure 5-15 the diffusive exponents for the intact acanthamoebae as well as for the different treatments are shown. The largest median was determined for the intact cells with a median of about 1.7 (small square in the boxplot). The center of mass corrected data gave lower diffusive exponents, but the values were larger than $\alpha > 1$ indicating superdiffusive motion. This result could also be observed for the blebbistatin treated acanthamoebae 20 min after addition and for the latrunculin A and nocodazole treated acanthamoebae. For blebbistatin treated acanthamoeba right after addition significantly lower values for the diffusive exponent could be observed.

Concerning the directionality (Figure 5-16), strong differences between the intact acanthamoebae and the acanthamoebae after the different drug-treatments were observed

The largest directionality could be observed for the intact acanthamoebae with a median value slightly larger than 0.2. For all other treatments the median of the directionality was between 0 and 0.1.

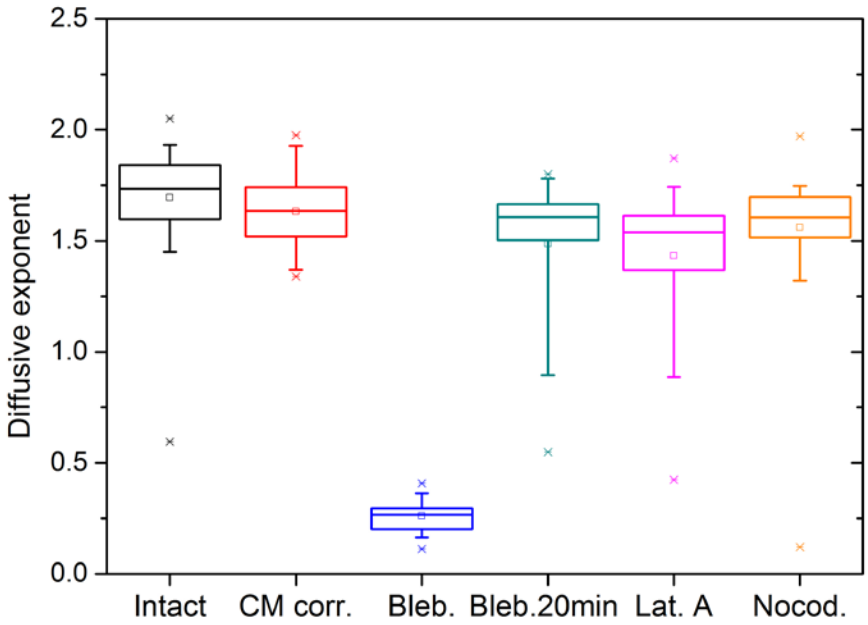

Figure 5-15 Boxplots of diffusive exponents of several treatments. Explanation of the boxplot: 1 % / 99 % = ×, min / max = -, average = □, median = line in the box (50 % of the values are above and 50 % are below this value), 25 % / 75 % = lower and upper edge of box; 10 % / 90 % = whisker. Maximum and minimum are nearly the same as 1 % and 99 %, respectively and therefore the symbols overlap. The intact acanthamoebae (black) show the largest values for the diffusive exponent, but also for blebbistatin 20 min after addition(dark cyan), for latrunculin A (pink) and for nocodazole (orange) diffusive exponents of $\alpha > 1$ are observed, indicating superdiffusive motion. Only for blebbistatin directly after addition (blue) values of $\alpha < 1$ are found.

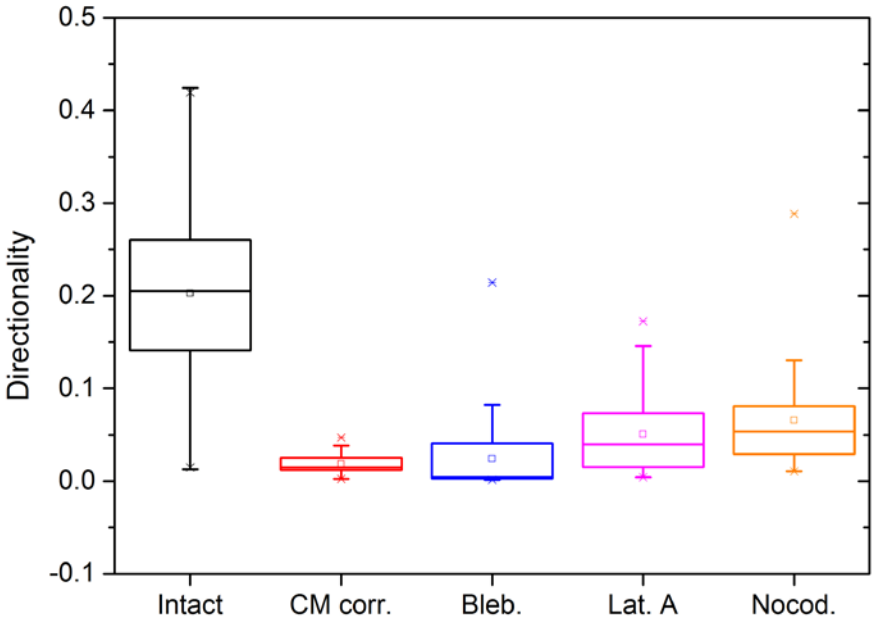

Figure 5-16 Directionality of particle motion in intact *A. castellanii* and after different drug treatments. The highest directionality can be observed for the intact acanthamoebae. All drug treatments lead to significantly decreased directionalities in the particle motions.

5.3.Discussion

In this chapter, several aspects of intracellular dynamics in acanthamoebae were investigated using particle tracking and mean squared displacement analysis. By applying different drugs, such as motor inhibiting substances, actin filament and microtubuli depolymerizing drugs, processes involved in intracellular transport mechanisms were identified.

Intact acanthamoebae showed typical amoeboid crawling motion. Also most intracellular particles followed this motion towards the leading edge of the acanthamoebae, resulting in a strong directionality of their motion (Figure 5-16). This directionality of particle motion in intact acanthamoebae was significantly larger than for acanthamoebae treated with depolymerizing or motor inhibiting substances. Furthermore, in intact acanthamoebae predominantly actively driven motion with diffusive exponents between 1.6 and 1.9 with a median of about 1.7 was observed. The nearly exclusively active nature of the intracellular transport in acanthamoebae is an unusual behavior compared to other cell systems [142]. It may be caused through two processes: either by active transport of particles with molecular motors along cytoskeletal filaments, or by fluid flow of the cytosol due to motion of the whole cell. As the intracellular space of the acanthamoeba trophozoites is extremely crowded, intracellular motion is comparable to movements in a ball pit. This means that the motion of one ball causes motion of other balls. If one particle inside the acanthamoebae is actively transported, others have to move in order to enable the motion of the actively moving particle. In order to study the influence of the motion

of the whole acanthamoeba on intracellular particle motion, the center of mass of the acanthamoebae was determined and subtracted from the particle trajectories of intact acathamoebae. This lead to a significant decrease in particle directionality, showing that the particles were moving in the same direction as the acanthamoeba itself before the subtraction of center of mass motion. In addition, also the diffusive exponent was decreased by the subtraction of the center of mass, but it was still larger than $\alpha > 1$. This shows that the particles after subtraction of the drift motion still exhibit actively driven motion, presumably caused by molecular motors.

By applying different drugs, the diffusive exponent and the directionality of the intracellular particles were significantly reduced. Blebbistatin, a myosin II inhibiting agent, completely abolished motion of the whole cell including all intracellular motion right after its addition. This lead to a significantly reduced diffusive exponent with a median of slightly less than $\alpha = 0.3$. Also the directionality of intracellular particle motion was reduced to nearly zero. This complete stop of all motion was very surprising as in the acanthamoeba besides actin filaments also microtubuli are present, on which cargo can by transported by molecular motors. This is, e.g., well-known for the transport of mitochondria, which co-localize with microtubuli [135]. A possible explanation why the whole cell stops moving and why also the intracellular processes are nearly stopped, might be that myosin II is present in the whole cytoplasm and in the cell cortex [132].

20 to 40 min after addition of blebbistatin, intracellular motion in acanthamoebae started again. At the same time, the movement of the whole cell was still strongly inhibited. This indicates that the cells were not significantly damaged or killed. The intracellular particle trajectories showed that the motion of the particles was restricted to a small area and also the directionality of the particle tracks was significantly reduced compared to the intact case. Nevertheless, the results for the diffusive exponent, which was slightly lower than for the intact case, showed that active transport mechanisms were predominant (median $\alpha \sim 1.5$). As acanthamoebae were in this situation still immobile, the superdiffusive motion of the small particles was not related to fluid flow or the movement of the whole cell. Since the myosin II motors are blocked by the blebbistatin, the reason for the superdiffusive behavior may be most likely attributed to molecular motors on microtubuli, such as kinesins and dyneins, which are known to transport cargo inside cells [17, 135].

Another way of disrupting intracellular transport on actin filaments was the treatment of acanthamoebae with latrunculin A, which inhibits the polymerization of actin filaments. In latrunculin A-treated *A. castellanii* the investigated particles showed superdiffusive behavior although the cell itself was not moving. A reason for the reduced motion of the latrunculin A-treated acanthamoebae might be that myosin and therefore also actin filaments are mainly present in the pseudopodia and acanthopodia [23-24]. Since the actin polymerization was stopped, the production of pseudopodia, which are needed for active motion of the acanthamoebae, is also reduced. The fact that despite actin disruption superdiffusive motion remained dominant shows that

another route of active transport was still available. Here, the movement of molecular motors along microtubules was presumably also involved. As actin is needed for the contraction of the contractile vacuole [132-134], the dose of the latrunculin A was always low enough to ensure that the acanthamoebae survived the treatment. For that reason actin might to some extent still have been involved in the active transport processes of latrunculin A-treated acanthamoebae. As discussed above, the dense packing of vesicles in the cytosolic space induced a ripple effect of active transport. Cargo transported along microtubules caused also other vesicles and particles to move, which yielded actively driven movement of the different particles. Although molecular motors were still active, stopping the motion of the acanthamoebae lead to a significantly reduced directionality.

A similar rationale can be applied in case of nocodazole treated acanthamoebae. Also here the motion of the acanthamoeba itself was drastically reduced, but intracellular particles were still moving and actively driven motions of intracellular particles with diffusive exponents slightly lower than in the intact case were observed. The directionality was significantly reduced compared to the intact case. Nocodazole is known to stop the polymerization of microtubules but does not influence the actin filaments. Thus, transport by molecular motors along actin filaments was still possible after nocodazole treatment. According to the ball pit phenomenon, the motion of particles by myosin motors on actin influenced the motion of other particles due to the extremely crowded space inside acanthamoebae.

In recent years high effort was made to understand movements in crowded systems. Such transport phenomena have recently been studied by using crowded fluids. In passive systems of nanoparticles in fluids, subdiffusive motions caused by viscoelasticity of the fluid due to crowding have been observed [143-144]. In living crowded systems all different types of diffusive motion have been observed [145-146]. In yeast cells predominattly subdiffusive transport processes have been detected [146], while in *Dictyostelium discoideum* subdiffusive motion but also superdiffusive motion have been identified [145, 147-148]. A recent study gave new hints, why cell systems still remain active although crowding hinders the motion of particles; most probably not only a single motor, but several motors of the same type attach to the cargo and in such a way overcome "traffic jams" [149]. In order to understand the intracellular motion, besides the methods shown here, diverse statistical approaches have been applied and are still developed [150]. The nearly exclusively superdiffusive motion in acanthamoebae, also after treatment with depolymerizing substances, appears to be quite unusual.

Overall, it can be concluded that active transport mechanisms inside acanthamoebae are strongly influenced by the motion of the cells themselves. This motion leads to a significant directionality of intracellular particle motion. Nevertheless, the actively driven nature of intracellular transport in the experiments presented in this chapter was also influenced by molecular motors, as all depolymerizing and motor inhibiting substances lead to a drastically decreased mobility of the cells. In general, transport

processes induced by such molecular motors leads to changes in the normal fluid flow as the particles have to move through the narrow space between all other organelles and have to push vacuoles and granules out of their path. The experiments showed new and surprising results that are not understood completely yet, but provide a foundation for future studies, in particular regarding studies on transport in extremely crowded systems.

6. Conclusions and Summary

The focus of this thesis was to investigate two steps (adhesion and intracellular dynamics) that are involved in the infection pathway of acanthamoeba keratitis. Most patients suffering from acanthamoeba keratitis are contact lens users, who are infected with acanthamoeba due to bad hygiene or wrong cleaning procedures. Therefore, in the first part of this thesis (chapter 3), different contact lens materials were investigated concerning dependencies between contamination with pathogenic *A. castellanii* and material parameters. The experiments revealed that an important parameter in this context is the water content. With increasing water content, the number of acanthamoebae present on the lenses increased. From these results it can be concluded that the risk of an infection with acanthamoebae is reduced for lenses with low water content. Besides this influence, the cleaning and disinfecting procedure plays a significant role. The experiments showed that the use of a multipurpose solution for cleaning the lenses is not sufficient, because it influences the adhesion of the acanthamoebae, but does not kill them. In addition, or instead of a multipurpose solution, a peroxide solution with neutralizing tablet should be used in order to ensure that acanthamoebae present in the storage cases or on the lenses are killed effectively.

If contact lenses are contaminated with pathogenic acanthamoebae, the amoebae get into the eye, where the extracellular killing process is initiated in the corneal epithelium and in underlying cell layers. This process starts with the formation of a close contact between acanthamoebae and target-cells that is mostly mediated by mannose. Therefore, in chapter 4 the mannose-specific binding of acanthamoebae was investigated in detail. In investigations on the adhesion of *A. castellanii* to extracellular matrix proteins it was observed that the number of adhering acanthamoebae was larger on protein coatings such as fibronectin, and matrigel than on reference samples. This effect was partly mediated by mannose. Furthermore, the experiments revealed that pathogenic acanthamoebae showed increased adhesion to mannose-coated agarose surfaces with increasing time, while there was nearly no adhesion to carbohydrate surfaces without mannose. For the non-pathogenic strain of acanthamoebae (*A.comandoni*), only unspecific binding could be observed. Mannose-specific adhesion was further investigated using gold nanostructured surfaces. The gold dots were biofunctionalized with carbohydrates and the interparticle space was passivated against adhesion of acanthamoebae by a PEG layer. On mannose-functionalized nanostructures without passivation of the inter-particle space, the spreading of the acanthamoebae increased with increasing densities of mannose-functionalized gold nanodots. For the nanostructures with passivated inter-particle space, spacings even larger than 100 nm between the mannose-functionalized gold dots lead to spreading areas of the acanthamoebae comparable to glass reference samples. This is a surprising effect as on these samples a huge part of the adhesion substrate was passivated and therefore only single binding sites were available for adhesion compared to the glass slides, where the acanthamoebae could attach to the

whole surface. This shows that already low concentrations of mannose on the surface lead to strong contact formation of the acanthamoebae. In contrast, adhesion experiments of acanthamoebae to glucose-functionalized nanostructures showed that there is no glucose specific binding involved.

In order to investigate the forces, which are involved in the adhesion process to target-cells and to further investigate the time course of adhesion at short contact times, AFM force spectroscopy measurements on *A. castellanii* to mannose-functionalized cantilevers were conducted. The experiments showed that the contact time between acanthamoeba and cantilever as well as the mode of operation of the AFM influenced the maximum adhesion force and the adhesion energy of *A. castellanii* binding to mannose. With increasing contact time, both the adhesion energy and the maximum adhesion force tend to increase. When operated in constant height mode, the values for those two parameters are larger than for constant force mode. In case of mannose-coated cantilevers, the binding of acanthamoebae could be inhibited by adding mannose to the medium, which leads to a saturation of the MBP in the amoebic membrane and therefore to a decrease in the mannose-specific binding. The experiments lead to the conclusion that the binding of acanthamoebae to target-cells is mannose-specific and that the interaction forces are in the nN-range. Besides mannose, also mannitol and glucose were used for functionalization of the cantilever. In case of mannitol the adhesion energy and maximum adhesion force increased after the addition of mannose, indicating that some binding processes are enhanced by mannose. Moreover, against our expectations, the acanthamoebae also showed binding to glucose-functionalized cantilevers. As this effect was not observed in the long-term adhesion experiments of *A. castellanii* on mannose, this might be a short-time effect.

After contact formation, intracellular processes are involved in the target-cell killing by acanthamoebae as cytolytic factors have to be transported to the target-cell. Therefore, in chapter 5 experiments on intracellular dynamics inside the acanthamoebae were carried out by statistically evaluating sequences of moving *A. castellanii*. In the intact case, the acanthamoebae are extremely mobile. The intracellular granules and vacuoles are predominantly moving actively. By inhibiting molecular motors and by depolymerizing parts of the cytoskeleton distinct active processes were inhibited. The different treatments could decrease the drift inside the cell, but actively driven motion could not be stopped completely. The reason for this behavior might be a kind of ball pit phenomenon. When one particle inside the crowded cell starts to move actively, others have to follow in order to enable active movement. Therefore, single particle motions are coupled to motion of other particles.

Overall, the experiments carried out in this thesis could answer open questions concerning the pathway of acanthamoeba infections and contribute to a better understanding of the involved biophysical mechanisms, in particular regarding the time-course of adhesion and intracellular dynamics.

List of Figures

Bibliography

1. Marciano-Cabral, F. and G. Cabral, *Acanthamoeba spp. as Agents of Disease in Humans.* Clinical Microbiology Reviews, 2003. **16**(2): p. 273-307.
2. Larkin, D.F.P., S. Kilvington, and D.L. Easty, *Contamination of Contact-Lens Storage Cases by Acanthamoeba and Bacteria.* British Journal of Ophthalmology, 1990. **74**(3): p. 133-135.
3. Lorenzo-Morales, J., et al., *Acanthamoeba keratitis: an emerging disease gathering importance worldwide?* Trends in Parasitology, 2013. **29**(4): p. 181-187.
4. Illingworth, C.D. and S.D. Cook, *Acanthamoeba keratitis.* Survey of Ophthalmology, 1998. **42**(6): p. 493-508.
5. Garate, M., et al., *Cloning and characterization of a novel mannose-binding protein of Acanthamoeba.* Journal of Biological Chemistry, 2004. **279**(28): p. 29849-29856.
6. Panjwani, N., *Pathogenesis of Acanthamoeba Keratitis.* Ocular Surface, 2010. **8**(2): p. 70-79.
7. Cao, Z., D.M. Jefferson, and N. Panjwani, *Role of Carbohydrate-mediated Adherence in Cytopathogenic Mechanisms of Acanthamoeba.* The Journal of Biological Chemistry, 1998. **273**(25): p. 15838-15845.
8. Garate, M., et al., *In Vitro Pathogenecity of Acanthamoeba is Associated with the Expression of the Mannose-Binding Protein.* Investigative Ophthalmology & Visual Science, 2006. **47**(3): p. 1056-1062.
9. Sharma, S., P. Garg, and G.N. Rao, *Patient characteristics, diagnosis, and treatment of non-contact lens related Acanthamoeba keratitis.* British Journal of Ophthalmology, 2000. **84**(10): p. 1103-1108.
10. Vanklink, F., et al., *The Role of Contact-Lenses, Trauma, and Langerhans Cells in a Chinese-Hamster Model of Acanthamoeba Keratitis.* Investigative Ophthalmology & Visual Science, 1993. **34**(6): p. 1937-1944.
11. Moore, M.B., et al., *In Vitro Penetration of Human Corneal Epithelium by Acanthamoeba castellanii: A Scanning and Transmission Electron Microscopy Study.* Cornea, 1991. **10**(4): p. 291-298.
12. Garner, A., *Pathogenesis of Acanthamoebic Keratitis - Hypothesis Based on a Histological Analysis of 30 Cases.* British Journal of Ophthalmology, 1993. **77**(6): p. 366-370.
13. Siddiqui, R. and N.A. Khan, *Biology and pathogenesis of Acanthamoeba.* Parasites & Vectors, 2012. **5**(6).
14. Khan, N.A., *Acanthamoeba Biology and Pathogenesis*. 2009: Caister Academic Press. 290.
15. Greub, G. and D. Raoult, *Microorganisms resistant to free-living amoebae.* Clinical Microbiology Reviews, 2004. **17**(2): p. 413-+.
16. Khan, N.A., *Acanthamoeba: biology and increasing importance in human health.* Fems Microbiology Reviews, 2006. **30**(4): p. 564-595.
17. Alberts, B., et al., *Molecular Biology of the Cell*. Fourth Edition ed. 2002: Garland Science.
18. Baron, R. and J.A. McCammon, *Molecular Recognition and Ligand Association.* Annual Review of Physical Chemistry, Vol 64, 2013. **64**: p. 151-175.

19. Helm, C.A., W. Knoll, and J.N. Israelachvili, *Measurement of Ligand Receptor Interactions.* Proceedings of the National Academy of Sciences of the United States of America, 1991. **88**(18): p. 8169-8173.
20. Madigan, M.T. and J.M. Martinko, *Brock Mikrobiologie*. 11 ed. 2009: Pearson Studium.
21. Preston, T.M., *A prominent microtubule cytoskeleton in Acanthamoeba.* Cell Biology International Reports, 1985. **9**(4): p. 307-314.
22. Elzinga, M., et al., *Complete Amino-Acid Sequence of Actin of Rabbit Skeletal Muscle.* PNAS, 1973. **70**(9): p. 2687-2691.
23. Kong, H.-H. and T.D. Pollard, *Intracellular localization and dynamics of myosin-II and myosin-IC in live Acanthamoeba by transient transfection of EGFP fusion proteins.* Journal of Cell Science, 2002. **115**: p. 4993-5002.
24. Yonemura, S. and T.D. Pollard, *The localization of myosin I and myosin II in Acanthamoeba by fluorescence microscopy.* Journal of Cell Science, 1992. **102**: p. 629-642.
25. Vale, R.D. and R.A. Milligan, *The Way Things Move: Looking Under the Hood of Molecular Motor Proteins.* Science, 2000. **288**(88): p. 88-95.
26. Pollard, T.D. and E.D. Korn, *Acanthamoeba Myosin .1. Isolation from Acanthamoeba-Castellanii of an Enzyme Similar to Muscle Myosin.* Journal of Biological Chemistry, 1973. **248**(13): p. 4682-4690.
27. Collins, J.H. and E.D. Korn, *Actin Activation of Ca2+-Sensitive Mg2+-Atpase Activity of Acanthamoeba Myosin-Ii Is Enhanced by Dephosphorylation of Its Heavy-Chains.* Journal of Biological Chemistry, 1980. **255**(17): p. 8011-8014.
28. Pollard, T.D., et al., *Ultrastructural Characterization of F-Actin Isolated from Acanthamoeba-Castellanii and Identification of Cytoplasmic Filaments as F-Actin by Reaction with Rabbit Heavy Meromyosin.* Journal of Molecular Biology, 1970. **50**(1): p. 91-&.
29. Aszodi, A., et al., *What mouse mutants teach us about extracellular matrix function.* Annual Review of Cell and Developmental Biology, 2006. **22**: p. 591-621.
30. Mammen, M., S.K. Choi, and G.M. Whitesides, *Polyvalent interactions in biological systems: Implications for design and use of multivalent ligands and inhibitors.* Angewandte Chemie-International Edition, 1998. **37**(20): p. 2755-2794.
31. Kiessling, L.L., J.E. Gestwicki, and L.E. Strong, *Synthetic multivalent ligands as probes of signal transduction.* Angewandte Chemie-International Edition, 2006. **45**(15): p. 2348-2368.
32. Geiger, B. and A. Bershadsky, *Assembly and mechanosensory function of focal contacts.* Current Opinion in Cell Biology, 2001. **13**(5): p. 584-592.
33. Zaidel-Bar, R., et al., *Hierarchical assembly of cell-matrix adhesion complexes.* Biochemical Society Transactions, 2004. **32**: p. 416-420.
34. Albelda, S.M. and C.A. Buck, *Integrins and Other Cell-Adhesion Molecules.* Faseb Journal, 1990. **4**(11): p. 2868-2880.
35. Pankov, R. and K.M. Yamada, *Fibronectin at a glance.* Journal of Cell Science, 2002. **115**(20): p. 3861-3863.
36. Kleinman, H.K. and G.R. Martin, *Matrigel: Basement membrane matrix with biological activity.* Seminars in Cancer Biology, 2005. **15**(5): p. 378-386.
37. Preston, T.M. and C.A. King, *Ameboid Locomotion of Acanthamoeba-Castellanii with Special Reference to Cell-Substratum Interactions.* Journal of General Microbiology, 1984. **130**(Sep): p. 2317-2323.

38. Paul, R., et al., *Propagation of mechanical stress through the actin cytoskeleton toward focal adhesions: Model and experiment.* Biophysical Journal, 2008. **94**(4): p. 1470-1482.
39. Harwood, C.R., et al., *Isolation of Acanthamoeba from a Cerebral Abscess.* Medical Journal of Australia, 1988. **148**(1): p. 47-49.
40. Gonzalez, M.M., et al., *Acquired-Immunodeficiency-Syndrome Associated with Acanthamoeba Infection and Other Opportunistic Organisms.* Archives of Pathology & Laboratory Medicine, 1986. **110**(8): p. 749-751.
41. Dart, J.K.G., F. Stapleton, and D. Minassian, *Contact-Lenses and Other Risk-Factors in Microbial Keratitis.* Lancet, 1991. **338**(8768): p. 650-653.
42. Moffat, J.F. and L.S. Tompkins, *A Quantitative Model of Intracellular Growth of Legionella-Pneumophila in Acanthamoeba-Castellanii.* Infection and Immunity, 1992. **60**(1): p. 296-301.
43. Cirillo, J.D., et al., *Intracellular Growth in Acanthamoeba castellanii Affects Monocyte Entry Mechanisms and Enhances Virulence of Legionella pneumophila.* Infection and Immunity, 1999. **67**(9): p. 4427-4434.
44. Cirillo, J.D., S. Falkow, and L.S. Tompkins, *Growth of Legionella-Pneumophila in Acanthamoeba-Castellanii Enhances Invasion.* Infection and Immunity, 1994. **62**(8): p. 3254-3261.
45. Aksozek, A., et al., *Resistance of Acanthamoeba castellanii cysts to physical, chemical, and radiological conditions.* Journal of Parasitology, 2002. **88**(3): p. 621-623.
46. Turner, N.A., et al., *Emergence of resistance to biocides differentiation of Acanthamoeba castellanii.* Journal of Antimicrobial Chemotherapy, 2000. **46**(1): p. 27-34.
47. Niederkorn, J.Y., et al., *The pathogenesis of Acanthamoeba keratitis.* Microbes and Infection, 1999. **1**: p. 437-443.
48. Bowers, B., *Comparison of Pinocytosis and Phagocytosis in Acanthamoeba-Castellanii.* Experimental Cell Research, 1977. **110**(2): p. 409-417.
49. Pettit, D.A.D., et al., *In vitro destruction of nerve cell cultures by Acanthamoeba spp: A transmission and scanning electron microscopy study.* Journal of Parasitology, 1996. **82**(5): p. 769-777.
50. Narayanan, S., *Analysis of Acanthamoeba's Adhesion to Host Cells Via Mannose Binding Protein*, in *Department of Molecular Genetics*. 2010, The Ohio State University: Ohio. p. 31.
51. Leher, H., et al., *Mannose Induces the Release of Cytopathic Factors from Acanthamoeba castellanii.* Infection and Immunity, 1998. **66**(1): p. 5-10.
52. Alsam, S., et al., *Acanthamoeba Interactions with Human Brain Microvascular Endothelial Cells.* Microbial Pathogenesis, 2003. **35**: p. 235-241.
53. Hurt, M., et al., *Pathogenic Acanthamoeba spp. Secrete a Mannose-Induced Cytolytic Protein that Correlates with the Ability to Cause Disease* Infection and Immunity, 2003. **71**(11): p. 6243-6255.
54. Michalek, M., et al., *Structure and function of a unique pore-forming protein from a pathogenic acanthamoeba.* Nature Chemical Biology 2012.
55. Leippe, M., *Amoebapores.* Parasitology Today, 1997. **13**(5): p. 178-183.
56. Mortimer, L. and K. Chadee, *The immunopathogenesis of Entamoeba histolytica.* Experimental Parasitology, 2010. **126**(3): p. 366-380.

57. *WHO/PAHO/UNESCO report. A consultation with experts on amoebiasis. Mexico City, Mexico 28-29 January, 1997.* Epidemiol Bull, 1997. **18**(1): p. 13-4.
58. Astorga, B., et al., *Acanthamoeba Belonging to T3, T4, and T11: Genotypes Isolated from Air-Conditioning Units in Santiago, Chile.* Journal of Eukaryotic Microbiology, 2011. **58**(6): p. 542-544.
59. Chan, L.L., et al., *Isolation and characterization of Acanthamoeba spp. from air-conditioners in Kuala Lumpur, Malaysia.* Acta Tropica, 2011. **117**(1): p. 23-30.
60. Kao, P.M., et al., *Isolation and identification of Acanthamoeba species from thermal spring environments in southern Taiwan.* Experimental Parasitology, 2012. **130**(4): p. 354-358.
61. Caumo, K. and M.B. Rott, *Acanthamoeba T3, T4 and T5 in swimming-pool waters from Southern Brazil.* Acta Tropica, 2011. **117**(3): p. 233-235.
62. Mahmoudi, M.R., et al., *Isolation of Acanthamoeba species in surface waters of Gilan province-north of Iran.* Parasitology Research, 2012. **110**(1): p. 473-477.
63. Wanachiwanawin, D., W. Booranapong, and P. Kosrirukvongs, *Clinical Features of Acanthamoeba Keratitis in Contact Lens Wearers and Non-Wearers (Vol 43, Pg 549, 2012).* Southeast Asian Journal of Tropical Medicine and Public Health, 2012. **43**(4): p. 1065-1065.
64. Lalitha, P., et al., *Acanthamoeba Keratitis in South India: A Longitudinal Analysis of Epidemics.* Ophthalmic Epidemiology, 2012. **19**(2): p. 111-115.
65. Yoder, J.S., et al., *Acanthamoeba keratitis: The Persistence of Cases Following a Multistate Outbreak.* Ophthalmic Epidemiology, 2012. **19**(4): p. 221-225.
66. Yoo, K.T. and S.Y. Jung, *Effects of Mannose on Pathogenesis of Acanthamoeba castellanii.* Korean Journal of Parasitology, 2012. **50**(4): p. 365-369.
67. Kim, J.H., et al., *Functional roles of mannose-binding protein in the adhesion, cytotoxicity and phagocytosis of Acanthamoeba castellanii.* Experimental Parasitology, 2012. **132**(2): p. 287-292.
68. Soto-Arredondo, K.J., et al., *Biochemical and cellular mechanisms regulating Acanthamoeba castellanii adherence to host cells.* Parasitology, 2013: p. 1-11.
69. Furukawa, A., K. Nakada-Tsukui, and T. Nozaki, *Novel transmembrane receptor involved in phagosome transport of lysozymes and beta-hexosaminidase in the enteric protozoan Entamoeba histolytica.* Plos Pathogens, 2012. **8**(2): p. e1002539.
70. Schlierf, M., F. Berkemeier, and M. Rief, *Direct observation of active protein folding using lock-in force spectroscopy.* Biophysical Journal, 2007. **93**(11): p. 3989-3998.
71. Churnside, A.B., et al., *Routine and Timely Sub-picoNewton Force Stability and Precision for Biological Applications of Atomic Force Microscopy.* Nano Letters, 2012. **12**(7): p. 3557-3561.
72. Nazirizadeh, Y., et al., *Photonic crystal slabs for surface contrast enhancement in microscopy of transparent objects.* Optics Express, 2012. **20**(13): p. 14451-14459.
73. Glass, R., M. Moller, and J.P. Spatz, *Block copolymer micelle nanolithography.* Nanotechnology, 2003. **14**(10): p. 1153-1160.

74. Romeis, B., M. Mulisch, and U. Welsch, *Romeis Mikroskopische Technik*, ed. U. Welsch. Vol. 18. 2010, Heidelberg, Germany: Heidelberg : Spektrum, Akad. Verl. .
75. Zernike, F., *Phase contrast, a new method for the microscopic observation of transparent objects part II.* Physica, 1942. **9**(10): p. 974-980.
76. Zernike, F., *How I Discovered Phase Contrast.* Science, 1955. **121**(3141): p. 345-349.
77. Nazirizadeh, Y., et al., *Material-based three-dimensional imaging with nanostructured surfaces.* Applied Physics Letters, 2013. **102**(1).
78. Binnig, G., C.F. Quate, and C. Gerber, *Atomic Force Microscope.* Physical Review Letters, 1986. **56**(9): p. 930-933.
79. Butt, H.J., B. Cappella, and M. Kappl, *Force measurements with the atomic force microscope: Technique, interpretation and applications.* Surface Science Reports, 2005. **59**(1-6): p. 1-152.
80. Jalili, N. and K. Laxminarayana, *A review of atomic force microscopy imaging systems: application to molecular metrology and biological sciences.* Mechatronics, 2004. **14**(8): p. 907-945.
81. Lal, R. and S.A. John, *Biological Applications of Atomic-Force Microscopy.* American Journal of Physiology, 1994. **266**(1): p. C1-&.
82. Benoit, M., et al., *Discrete interactions in cell adhesion measured by single-molecule force spectroscopy.* Nature Cell Biology, 2000. **2**(6): p. 313-317.
83. Friedrichs, J., et al., *A practical guide to quantify cell adhesion using single-cell force spectroscopy.* Methods, 2013. **60**(2): p. 169-178.
84. Borgia, A., P.M. Williams, and J. Clarke, *Single-molecule studies of protein folding.* Annual Review of Biochemistry, 2008. **77**: p. 101-125.
85. Helenius, J., et al., *Single-cell force spectroscopy.* Journal of Cell Science, 2008. **121**(11): p. 1785-1791.
86. Zlatanova, J., S.M. Lindsay, and S.H. Leuba, *Single molecule force spectroscopy in biology using the atomic force microscope.* Progress in Biophysics & Molecular Biology, 2000. **74**(1-2): p. 37-61.
87. Baró, A.M. and R.G. Reifenberger, *Atomic Force Microscopy in Liquid*, ed. A.M. Baró and R.G. Reifenberger. 2012, Weinheim, Germany: Wiley-VCH Verlag & Co. KGaA.
88. Wojcikiewicz, E.P., X.H. Zhang, and V.T. Moy, *Force and Compliance Measurements on Living Cells Using Atomic Force Microscopy (AFM).* Biological Procedures Online, 2004. **6**(1): p. 1-9.
89. Schilcher, K., et al., *A non-invasive method for the tight anchoring of cells for scanning force microscopy.* Cell Biology International, 1997. **21**(11): p. 769-778.
90. Parot, P., et al., *Past, present and future of atomic force microscopy in life sciences and medicine.* Journal of Molecular Recognition, 2007. **20**(6): p. 418-431.
91. Radmacher, M., et al., *Measuring the viscoelastic properties of human platelets with the atomic force microscope.* Biophysical Journal, 1996. **70**(1): p. 556-567.
92. Goldmann, W.H., et al., *Differences in elasticity of vinculin-deficient F9 cells measured by magnetometry and atomic force microscopy.* Experimental Cell Research, 1998. **239**(2): p. 235-242.

93. Selhuber-Unkel, C., et al., *Cell Adhesion Strength Is Controlled by Intermolecular Spacing of Adhesion Receptors.* Biophysical Journal, 2010. **98**(4): p. 543-551.
94. Spatz, J.P., et al., *Ordered deposition of inorganic clusters from micellar block copolymer films.* Langmuir, 2000. **16**(2): p. 407-415.
95. Arnold, M., et al., *Activation of integrin function by nanopatterned adhesive interfaces.* Chemphyschem, 2004. **5**(3): p. 383-388.
96. VandeVondele, S., J. Voros, and J.A. Hubbell, *RGD-Grafted poly-l-lysine-graft-(polyethylene glycol) copolymers block non-specific protein adsorption while promoting cell adhesion.* Biotechnology and Bioengineering, 2003. **82**(7): p. 784-790.
97. Cavalcanti-Adam, E.A., et al., *Lateral spacing of integrin ligands influences cell spreading and focal adhesion assembly.* European Journal of Cell Biology, 2006. **85**(3-4): p. 219-224.
98. Allen, P.G. and E.A. Dawidowicz, *Phagocytosis in Acanthamoeba: I. A Mannose Receptor is Responsible for the Binding and Phagocytosis of Yeast.* Journal of Cellular Physiology, 1990. **145**(3): p. 508-513.
99. Yang, Z., Z. Cao, and N. Panjwani, *Pathogenesis of Acanthamoeba Keratitis: Carbohydrate-Mediated Host-Parasite Interactions.* Infection and Immunity, 1997. **65**(2): p. 439-445.
100. Yang, Z.T., Z.Y. Cao, and N. Panjwani, *A mannose-binding protein of Acanthamoeba: Potential role in the pathogenesis of Acanthamoeba keratitis.* Glycobiology, 1996. **6**(7): p. 413-413.
101. Moore, M.B., et al., *Acanthamoeba Keratitis - a Growing Problem in Soft and Hard Contact-Lens Wearers.* Ophthalmology, 1987. **94**(12): p. 1654-1661.
102. Reverey, J.F., et al., *In vitro adhesion of Acanthamoeba castellanii to soft contact lenses depends on water content and disinfection procedure.* Contact Lens & Anterior Eye, 2013.
103. Stehrgreen, J.K., et al., *Acanthamoeba Keratitis in Soft Contact-Lens Wearers - a Case-Control Study.* Jama-Journal of the American Medical Association, 1987. **258**(1): p. 57-60.
104. Yang, Y.F., et al., *Persistence of acanthamoeba antigen following acanthamoeba keratitis.* British Journal of Ophthalmology, 2001. **85**(3): p. 277-280.
105. Seal, D.V., et al., *Differential Adherence of Acanthamoeba to Contact-Lenses - Effects of Material Characteristics.* Optometry and Vision Science, 1995. **72**(1): p. 23-28.
106. Gorlin, A.I., et al., *Binding of Acanthamoeba to hydrogel contact lenses.* Current Eye Research, 1996. **15**(2): p. 151-155.
107. Beattie, T.K., et al., *Enhanced attachment of Acanthamoeba to extended-wear silicone hydrogel contact lenses - A new risk factor for infection.?* Ophthalmology, 2003. **110**(4): p. 765-771.
108. Beattie, T.K., A. Tomlinson, and A.K. McFadyen, *Attachment of Acanthamoeba to first- and second-generation silicone hydrogel contact lenses.* Ophthalmology, 2006. **113**(1): p. 117-125.
109. Ramachandran, L., et al., *Effect of Time and Washing on the Adhesion of Acanthamoeba to Extended Wear Disposable Hydrogel Contact Lenses.* CLAO Journal, 1997. **23**(2): p. 113-116.
110. Discher, D.E., P. Janmey, and Y.L. Wang, *Tissue cells feel and respond to the stiffness of their substrate.* Science, 2005. **310**(5751): p. 1139-1143.

111. Ren, Y.X., et al., *Mechanosensing through Cooperative Interactions between Myosin II and the Actin Crosslinker Cortexillin I.* Current Biology, 2009. **19**(17): p. 1421-1428.
112. Pramanik, M.K., et al., *PTEN is a mechanosensing signal transducer for myosin II localization in Dictyostelium cells.* Genes to Cells, 2009. **14**(7): p. 821-834.
113. Uno, T., et al., *Effects of Multipurpose Contact Lens Care Solutions on the Adhesion of Acanthamoeba to Silicone Hydrogel Contact Lenses.* Cornea, 2012. **31**(10): p. 1170-1175.
114. Kilvington, S. and J. Lonnen, *A comparison of regimen methods for the removal and inactivation of bacteria, fungi and Acanthamoeba from two types of silicone hydrogel lenses* Contact Lens & Anterior Eye, 2009. **32**(6): p. 73-77.
115. Hughes, R. and S. Kilvington, *Comparison of hydrogen peroxide contact lens disinfection systems and solutions against Acanthamoeba polyphaga.* Antimicrobial Agents and Chemotherapy, 2001. **45**(7): p. 2038-2043.
116. Hiti, K., et al., *Viability of Acanthamoeba after exposure to a multipurpose disinfecting contact lens solution and two hydrogen peroxide systems.* British Journal of Ophthalmology, 2002. **86**(2): p. 144-146.
117. McDonald, J.H., *Handbook of Biological Statistics*. 2 ed. 2009: Sparky House Publishing, Baltimore, Maryland.
118. Gordon, V.R., et al., *Acanthamoeba Binds to Extracellular Matrix Proteins in Vitro.* Investigative Ophthalmology & Visual Science, 1993. **34**(3): p. 658-662.
119. Rocha-Azevedo, B.d., et al., *Acanthamoeba culbertsoni: Analysis of amoebic adhesion and invasion on extracellular matrix components collagen I and laminin-1*. Experimental Parasitology, 2010. **126**(1): p. 79-84.
120. Rocha-Azevedo, B.d., et al., *Acanthamoeba Interaction with Extracellular Matrix Glycoproteins: Biological and Biochemical Characterization and Role in Cytotoxicity and Invasiveness.* Journal of Eukaryotic Microbiology, 2009. **56**(3): p. 270-278.
121. Jin, F., et al., *Structure and Function of Laminin-1 Glycans - Glycan Profiling.* Glycobiology, 1995. **5**(2): p. 157-158.
122. Sekiguchi, K., M. Fukuda, and S.I. Hakomori, *Domain-Structure of Hamster Plasma Fibronectin - Isolation and Characterization of 4 Functionally Distinct Domains and Their Unequal Distribution between 2 Subunit Polypeptides.* Journal of Biological Chemistry, 1981. **256**(12): p. 6452-6462.
123. Garate, M., et al., *Biochemical characterization and functional studies of Acanthamoeba mannose-binding protein.* Infection and Immunity, 2005. **73**(9): p. 5775-5781.
124. Morton, L.D., G.L. McLaughlin, and H.E. Whiteley, *Effects of Temperature, Amebic Strain, and Carbohydrates on Acanthamoeba Adherence to Corneal Epithelium in vitro.* Infection and Immunity, 1991. **59**(10): p. 3819-3822.
125. Seu, K.J., et al., *Effect of surface treatment on diffusion and domain formation in supported lipid bilayers.* Biophysical Journal, 2007. **92**(7): p. 2445-2450.
126. Hinterdorfer, P. and Y.F. Dufrene, *Detection and localization of single molecular recognition events using atomic force microscopy.* Nature Methods, 2006. **3**(5): p. 347-355.

127. Khan, N.A., E.L. Jarroll, and T.A. Paget, *Acanthamoeba can be differentiated by the polymerase chain reaction and simple plating assays.* Current Microbiology, 2001. **43**(3): p. 204-208.
128. Butt, H.J. and M. Jaschke, *Calculation of Thermal Noise in Atomic-Force Microscopy.* Nanotechnology, 1995. **6**(1): p. 1-7.
129. Friedrichs, J., J. Helenius, and D.J. Muller, *Quantifying cellular adhesion to extracellular matrix components by single-cell force spectroscopy.* Nature Protocols, 2010. **5**(7): p. 1353-1361.
130. Sackmann, E., *Physical basis of self-organization and function of membranes: Physics of vesicles*, in *Structure and Dynamics of Mambranes*, R. Lipowsky and E. Sackmann, Editors. 1995, Elsevier Amsterdam. p. 213-304.
131. Selhuber-Unkel, C., et al., *Cooperativity in Adhesion Cluster Formation during Initial Cell Adhesion.* Biophysical Journal, 2008. **95**(11): p. 5424-5431.
132. Baines, I.C. and E.D. Korn, *Localization of Myosin IC and Myosin II in Acanthamoeba castellanii by Indirect Immunofluorescence and Immunogold Electron Microscopy.* The Journal of Cell Biology, 1990. **111**: p. 1895-1904.
133. Baines, I.C., A. Corigliano-Murphy, and E.D. Korn, *Quantification and localization of phosphorylated myosin I isoforms in Acanthamoeba castellanii.* The Journal of Cell Biology, 1995. **130**(3): p. 591-603.
134. Doberstein, S.K., et al., *Inhibition of contractile vacuole function in vivo by antibodies against myosin-I.* Nature, 1993. **365**: p. 841-843.
135. Baumann, O. and D.B. Murphy, *Microtubule-Assiciated Movement of Mitochondria and Small Particles in Acanthamoeba castellanii.* Cell Motility and the Cytoskeleton, 1995. **32**(4): p. 205-317.
136. Tolic-Norrelykke, I.M., et al., *Anomalous diffusion in living yeast cells.* Physical Review Letters, 2004. **93**(7).
137. Rogers, S.S., T.A. Waigh, and J.R. Lu, *Intracellular Microrheology of Motile Amoeba proteus.* Biophysical Journal, 2008. **94**(8): p. 3313-3322.
138. Selhuber-Unkel, C., et al., *Variety in intracellular diffusion during the cell cycle.* Physical Biology, 2009. **6**(2).
139. Kovács, M., et al., *Mechanism of Blebbistatin Inhibition of Myosin II.* The Journal of Biological Chemistry, 2004. **279**(34): p. 35557-35563.
140. Rogers, S.S., et al., *Precise particle tracking against a complicated background: polynomial fitting with Gaussian weight* Physical Biology, 2007. **4**(3): p. 220-227.
141. Tejedor, V., et al., *Quantitative Analysis of Single Particle Trajectories: Mean Maximal Excursion Method.* Biophysical Journal, 2010. **98**(7): p. 1364-1372.
142. Caspi, A., R. Granek, and M. Elbaum, *Enhanced Diffusion in Active Intracellular Transport.* Physical Review Letters, 2000. **85**(26): p. 5655-5658.
143. Weiss, M., *Single-particle tracking data reveal anticorrelated fractional Brownian motion in crowded fluids.* Physical Review E, 2013. **88**(1).
144. Ernst, D., et al., *Fractional Brownian motion in crowded fluids.* Soft Matter, 2012. **8**(18): p. 4886-4889.
145. Arcizet, D., et al., *Temporal Analysis of Active and Passive Transport in Living Cells.* Physical Review Letters, 2008. **101**(24): p. 248103.
146. Selhuber-Unkel, C., et al., *Intracellular Diffusion in Fission Yeast Cells Depends on Cell Cycle Stage.* Biophysical Journal, 2010. **98**(3): p. 368a-368a.
147. Otten, M., et al., *Local Motion Analysis Reveals Impact of the Dynamic Cytosceleton on Intracellular Subdiffusion.* Biophysical Journal, 2012. **102**(4): p. 758-767.

148. Mahowald, J., D. Arcizet, and D. Heinrich, *Impact of External Stimuli and Cell Micro-Architecture on Intracellular Transport States.* Chemphyschem, 2009. **10**(9-10): p. 1559-1566.
149. Conway, L., et al., *Motor transport of self-assembled cargos in crowded environments.* Proceedings of the National Academy of Sciences of the United States of America, 2012. **109**(51): p. 20814-20819.
150. Hofling, F. and T. Franosch, *Anomalous transport in the crowded world of biological cells.* Reports on Progress in Physics, 2013. **76**(4).
151. Snedecor, G.W. and W.G. Cochran, *Statistical Methods*. 8 ed. 1989: Iowa State University Press.
152. Martinez, A.J., *Infection of the Central-Nervous-System Due to Acanthamoeba.* Reviews of Infectious Diseases, 1991. **13**: p. S399-S402.
153. Martinez, A.J. and G.S. Visvesvara, *Free-living, amphizoic and opportunistic amebas.* Brain Pathology, 1997. 7(1): p. 583-598.

List of Publications

J. F. Reverey, R. Fromme, M. Leippe, C. Selhuber-Unkel. *In vitro* adhesion of *Acanthamoeba castellanii* to soft contact lenses depends on water content and disinfection procedure. Contact lens & Anterior Eye, published online Dec 20, 2013, doi: 10.1016/j.clae.2013.11.010

J. F. Reverey, J.-H. Jeon, M. Leippe, R. Metzler, C. Selhuber-Unkel. Intracellular Motion in the Extremely Crowded Space of *Acanthamoeba castellanii*. In Manuscript.

Y. Nazirizadeh, T. Becker, J. F. Reverey, C. Selhuber-Unkel, D. H. Rapoport, U. Lemmer, M. Gerken. Photonic crystal slabs for surface contrast enhancement in microscopy of transparent objects. Optics Express (2012), 20(13), 14451-14459.

Y. Nazirizadeh, J. F. Reverey, U. Geyer, U. Lemmer, C. Selhuber-Unkel, M. Gerken. Material-based three-dimensional imaging with nanostructured surfaces. Applied Physics Letters (2013), 102, 011116.

Acknowledgements

First, I would like to thank Prof. Dr. Christine Selhuber-Unkel for giving me the opportunity to work in the Biocompatible Nanomaterials group and experience the buildup of this new group. She always had an open ear for my questions and I am very grateful for the fruitful discussions, for her support and for her nice supervision.

I am very thankful for the help of Prof. Dr. Matthias Leippe from the Zoological Institute of the Christian-Albrechts University of Kiel (CAU) concerning the biological questions in my work. Furthermore, I appreciate that he provided me the acanthamoebae and gave me the opportunity to carry out experiments in his lab during times, when our lab was not complete yet.

I would also like to thank Heidrun Liessegang for her helping hand and her friendly advice during my time in the Zoological Institute.

I would like to thank Dr. Vijayanand Chandrasekaran from the Organic Chemistry department of the CAU for the nice and friendly co-work and for providing the carbohydrate-disulfides for the adhesion experiments on gold nanostructures.

I am very grateful for the cooperation with WÖHLK Contactlinsen GmbH. The contact lens experiments would not have been possible without the kind co-work with Roland Fromme from WÖHLK.

For the cooperation and support in the intracellular diffusion analysis, I would like to thank Dr. Jae-Hyung Jeon (Tampere University of Technology, Finland) and Prof. Dr. Ralf Metzler (University of Potsdam).

I am especially thankful for the funding of the project by the Emmy Noether program of the Deutsche Forschungsgemeinschaft (DFG).

Furthermore, I would like to thank all my colleagues from the Biocompatible Nanomaterials group for the nice working atmosphere and for becoming real friends. I am very grateful to Manuela Lieb for her friendly help during the lab work and for the nice conversations. I would like to thank Ellen Riemer for the office work and especially for the funny breaks. The work in our group would not have been the same without the support and the friendly teamwork with my dear colleagues, Dr. Constanze Lamprecht, Dr. Saskia Viebig, Dr. Carsten Grabosch, Sören Gutekunst, Laith Kadem, Qian Li, and Gunnar Zoch. Special thanks to my room mates for the nice company and for the fun.

I am very thankful to all my colleagues at the faculty of engineering, who were always with me during the time of my studies and the PhD. Especially, I would like to thank Arnim Schuchardt, Ingo Paulowicz, Christian Ohrt, Bodo Henkel, Tönjes Koschine, and Mark-Daniel Gerngroß for the nice company during all the time. I am happy that I met these guys and that we became good friends.

It is very important for me to thank my whole family for being with me all the time, for their emotional and financial support, and for their caring advices.

Last but not least I would like to thank Holger Jedtberg for his unconditional support, his patience and for the time we could spend together.

Appendix

1. Abbreviations

A. astronyxix	*Acanthamoeba astronyxix*
A. castellanii	*Acanthamoeba castellanii*
A. comandoni	*Acanthamoeba comandoni*
A. culbertsoni	*Acanthamoeba culbertsoni*
A. polyphaga	*Acanthamoeba polyphaga*
ADP	Adenosine Diphosphate
AFM	Atomic Force Microscope
AIDS	Acquired Immune Deficiency Syndrome
ATCC	American Type Culture Collection
ATP	Adenosine Triphosphate
CCD	Charge-coupled Device
cmc	Critical Micelle Concentration
DMEM	Dulbecco's Modified Eagle's Medium; cell medium
ECM	Extracellular Matrix
Hy	Hydrogel
IPD	Inter-Particle Distance
MBP	Mannose Binding Protein in acanthamoeba membrane
MIP	Mannose Induced Protein
mPEG-Si	Methoxy PEG-Silane
NA	Numerical Aperture
P2VP	Poly-2-vinylpyridine
PBS	Phosphate Buffered Saline
PCS	Photonic Crystal Slab
PEG	Polyethyleneglycol
PLL	Poly-L-lysine
PLL-g-PEG	PLL-grafted-PEG, for passivating surfaces
PS	Polystyrene
REF 52 WT	Rat Embryonic Fibroblast, wild type
RGD	R=arginine (arg), G=glycine (gly), D=asparagine(asp); Integrin binding sequence in fibronectin
RT	Room Temperature
SCM	Surface Contrast Microscopy
SEM	Scanning Electron Microscope
SH-SY5Y	Cell line
SiHy	Silicone Hydrogel
TA MSD	Time Averaged Mean Square Displacement
UV	Ultra Violet

2. Symbols

d	resolution of microscope
λ	wavelength
m	magnification
$f_{tube\ lens}$	focal length of tube lens
$f_{objective}$	focal length of objective
$N_{adhAmoebae}$	number of acanthamoebae adhering to bead
$N_{totalAmoebae}$	total number of acanthamoebae
$N_{totalBeads}$	total number of beads
MW	molecular weight
d_{dots}	distance between gold dots on gold nanostructures
n	number of gold dots per area
δ^2	mean square displacement
T	measurement time for calculation of TAMSD
Δ	lag time for calculation of TAMSD
x	intracellular trajectory
α	diffusive exponent

3. Two Sample T-Test

In order to determine the significance of the evaluated results, a two sample t-test was applied [117, 151]. In this case, the t-test compares the mean values of two sample groups (x and y) according to the null hypothesis

$$H_0 : \bar{x} - \bar{y} = 0$$

and the alternative hypothesis

$$H_1 : \bar{x} - \bar{y} \neq 0$$

and gives a significance level depending on the number of evaluated samples per group (n and m).

The t-value is determined according to

$$t = \sqrt{\frac{nm}{n+m}} \frac{\bar{x} - \bar{y}}{s} \tag{6}$$

where n is the number of x-samples, m is the number of y-samples and $\bar{x}$ and $\bar{y}$ are the average values of the sample groups x and y, respectively. s is calculated according to

$$s = \sqrt{\frac{(n-1)s_x^2 + (m-1)s_y^2}{n+m-2}} \tag{7}$$

with s_x and s_y being the standard deviations of the two sample groups. It becomes obvious that the number of evaluated samples is a key factor.

The null hypothesis is rejected in support of the alternative hypothesis if

$$|t| > t\left(1-\frac{1}{2}\alpha, n+m-2\right)$$

with α being the significance level. The t-values are listed in tables and can be checked according to the number of samples.
The *p*-value (from: probability) given for the different experiments in this thesis is compared to the significance level α. If *p* is smaller than α, the null hypothesis is rejected. In case of * the *p*-value is smaller than the significance level $\alpha = 0.05$ (5 %) and the null hypothesis is rejected. This means that there is a significant difference in the mean values of the two sample groups. ** mark the case that the *p*-value is smaller than $\alpha = 0.01$ (1 %) and for *** the *p*-value is smaller than $\alpha = 0.001$ (0.1 %).

4. Phosphate Buffered Saline Solution (PBS)

For the experiments home-made phosphate buffered saline solution (PBS) was used.
In order to prepare a 10× PBS solution, 1.37 MM NaCl, 27 MM KCl, 124.2 MM $Na_2HPO_4 \times 2H_2O$, and 14.7 MM KH_2PO_4 (all from Carl Roth GmbH & Co. KG, Karlsruhe, Germany) were solved in destilled water and adjusted to a pH of 7.2. For 1× PBS the prepared solution is 10× diluted. Subsequently, the solution was autoclaved for 15 min at 121 °C.

5. Experimental Procedure of Coculture of *A. castellanii* with Human SHSY5Y Cells

The SHSY5Y cells were cultured in Dulbecco's Modified Eagle's Medium (DMEM) (Biochrom) supplemented with 10 % FCS (Biochrom) and 1% Penecillin Streptomycin at 37°C and 5% CO_2. For the experiments the cells were washed twice with Phosphate Buffered Saline (PBS) and trypsinated. Afterwards the cells were counted by using a hemocytometer (Neubauer counting chamber) and 10^5 cells were seeded on objective glasses with a diameter of 24 mm or on 6-well plates (Sarstedt AG & Co., Nümbrecht, Germany). After 24 h of incubation at 37 °C and 5 % CO_2 the living cells were washed once in PBS. The *A. castellanii* were counted and 2.5×10^4 acanthamoebae and 1 ml of PYG Medium were added to the adherent SHSY5Y cells.
Subsequently, high-speed sequences were recorded by using an inverted phase contrast microscope (Olympus CKX41) equipped with a high speed camera (Hamamatsu C9300).

5.1. Contact Formation between *A. castellanii* and SHSY5Y Cells

In the coculture the contact formation between *A. castellanii* and target-cells could be observed. In most of the cases the acanthamoebae started the contact formation at the extensions like axons and dendrites of the nerve cells. This is also shown in figure Appendix A1.

As soon as the trophozoites reach the extensions of the nerve cells, they move in the direction of the cell body, where they can build a larger contact area. In the further progress they move away from the cell body again along axons or dendrites. This also agrees with previous studies about the entry of acanthamoebae to the central nervous system. The acanthamoebae move along the nerve cells, which act as a kind of guideline for the acanthamoebae [152-153].

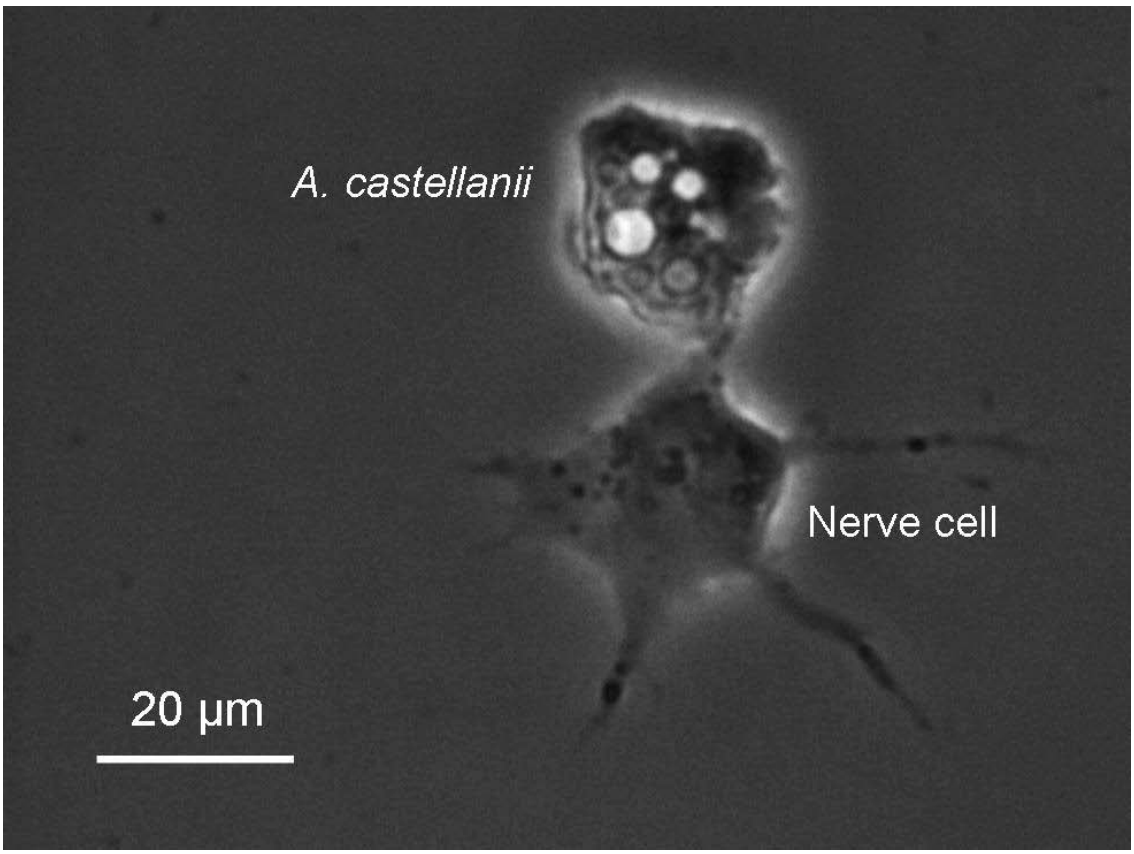

Figure Appendix A1 *A. castellanii* and an adhering nerve cell of the type SHSY5Y. The acanthamoebae move along the axons or dendrites of the nerve cells.